UNIVERSITY OF CALIFORNIA SAN DIEGO

Discovery and Characterization of Novel Bioactive Lipids and Enzymes Involved in their Regulation

A dissertation submitted in partial satisfaction of the requirements for the degree
Doctor of Philosophy

in

Biomedical Sciences

by

Matthew John Kolar

Committee in charge:

Professor Alan Saghatelian, Chair
Professor Steven Dowdy, Co-Chair
Professor Mohit Jain
Professor Oswald Quehenberger
Professor Alan Saltiel
Professor Dionicio Siegel

2018

The Dissertation of Matthew John Kolar is approved, and is acceptable in quality and form for publication on microfilm and electronically:

Co-Chair

Chair

University of California San Diego

2018

TABLE OF CONTENTS

LIST OF ABBREVIATIONS

ABPP	activity-based protein profiling
ADTRP	androgen-dependent TFPI regulating protein
AIG1	androgen-induced gene 1
AG4OX	adipose-specific GLUT4 overexpressor
DAG	diacylglycerol
CEL	carboxyl ester lipase
CE	cholesterol ester
FAHFA	fatty acid ester of hydroxy fatty acid
FFA	free (non-esterified) fatty acid
FP	fluorophosphonate
HHDA	hydroxy heptadecanoic acid
HLA	hydroxylinoleic acid
HSA	hydroxystearic acid
LA	linoleic acid
LAHLA	linoleic acid ester of hydroxy linoleic acid
LC–MS	liquid chromatography–mass spectrometry
LC–MS/MS	liquid chromatography–tandem mass spectrometry
m/z	mass-to-charge ratio
MODY	maturity-onset diabetes of the young
NaTC	sodium taurocholate
OAHSA	oleic acid ester of hydroxy stearic acid
PA	palmitic acid
PAHSA	palmitic acid ester of hydroxy stearic acid
PGWAT	perigonadal white adipose tissue

PO	palmitoleic acid
POHSA	palmitoleic acid ester of hydroxy stearic acid
OA	oleic acid
SA	stearic acid
SAHSA	stearic acid ester of hydroxy stearic acid
SQWAT	subcutaneous white adipose tissue
SH	serine hydrolase
TAG	triacylglycerol
TFPI	tissue factor pathway inhibitor
WAT	white adipose tissue

LIST OF FIGURES, TABLES, AND SCHEMES

Chapter 1

Chapter 2

Chapter 3

ACKNOWLEDGEMENTS

During my academic career I have been extremely fortunate to be surrounded by such great mentors and role models. Without the support of my true first mentor, Dr. Gregory Verdine, I would not be where I am today. It was during my time in the Verdine lab, where I found my passion for research and where my interest in chemical biology was sparked.

I am especially grateful to have Dr. Alan Saghatelian as my dissertation advisor. Not only is Alan an extraordinary scientist, but he is a fair and kind advisor who wishes the best for everyone in his lab. I have never met a scientist who is as understanding and supportive of one's immediate and future goals. His guidance and support is insurmountable and I could not have asked for a better mentor for my Ph.D.

I am also thankful to have worked closely with our collaborators Dr. Barbara Kahn and Dr. Benjamin Cravatt. Without the support of lab members in the Saghatelian, Kahn, and Cravatt lab, none of this could have been possible, as the members of these labs have provided me with invaluable advice.

I am grateful to my dissertation committee members: Dr. Steven Dowdy, Dr. Mohit Jain, Dr. Oswald Quehenberger, Dr. Alan Saltiel, and Dr. Dionicio Siegel, for their time, support, and scientific advice.

Chapter 2, in full, is a reprint with minor modifications as it appears in Branched Fatty Acid Esters of Hydroxy Fatty Acids Are Preferred Substrates of the MODY8 Protein Carboxyl Ester Lipase, *Biochemistry* 55, 4636-4641 (2016). The dissertation author was the primary investigator and author of this paper. Other authors include Siddhesh S. Kamat, William H. Parsons, Edwin A. Homan, Timothy Maher, Odile D. Peroni, Ismail Syed, Karianne Fjeld, Anders Molven, Barbara B. Kahn, Benjamin .F Cravatt, and Alan Saghatelian.

Chapter 3, in full, is a reprint with slight modifications as it appears in AIG1 and ADTRP are atypical integral membrane hydrolases that degrade bioactive FAHFAs, *Nature Chemical*

Biology 12, 367-372 (2016). The dissertation author was the co-primary investigator and author of this paper along with William H. Parsons. Other authors include Siddhesh S. Kamat, Armand B. Cognetta III, Jonathan J. Hulce, Enrique Saez, Barbara B. Kahn, Alan Saghatelian, and Benjamin F. Cravatt.

Chapter 4, in full, is a reprint with minor modification as it appears in Stereochemistry of Endogenous Palmitic Acid Ester of 9-Hydroxystearic Acid and Relevance of Absolute Configuration to Regulation, *Journal of the American Chemical Society* 139, 4943-4947 (2017). The dissertation author was the co-primary investigator and author of this paper along with Andrew T. Nelson. Other authors include Qian Chu, Ismail Syed, Barbara B. Kahn, Alan Saghatelian, and Dionicio Siegel.

Chapter 5, in full, is a reprint with minor changes as it appears in A Faster Protocol for Endogenous FAHFA Measurements, *Analytical Chemistry*. The dissertation author was the primary investigator and author of this paper. Other authors include Andrew T. Nelson, Tina Chang, Meric E. Ertunc, Mitchell P. Christy, Lena Ohlsson, Magnus Härröd, Barbara B. Kahn, Dionicio Siegel, and Alan Saghatelian.

VITA

2009	Bachelor of Science, University of North Carolina at Chapel Hill
2009-2012	Research Assistant, Harvard University
2012-	Medical Scientist Training Program, University of California San Diego
2018	Doctor of Philosophy, University of California San Diego

PUBLICATIONS

1. **Kolar M. J.**, Nelson A. T., Chang T., Ertunc M. E., Christy M. P., Ohlsson L., Harrod M., Kahn B. B., Siegel D. & Saghatelian A. Faster Protocol for Endogenous Fatty Acid Esters of Hydroxy Fatty Acid (FAHFA) Measurements. *Analytical Chemistry* (2018).

2. Syed I., Lee J., Moraes-Vieira P. M., Donaldson C. J., Sontheimer A., Aryal P., Wellenstein K., **Kolar M. J.**, Nelson A. T., Siegel D., Mokrosinski J., Farooqi I. S., Zhao J. J., Yore M. M., Peroni O. D., Saghatelian A. & Kahn B. B. Palmitic Acid Hydroxystearic Acids Activate GPR40, Which Is Involved in Their Beneficial Effects on Glucose Homeostasis. *Cell Metabolism* 27, 419-427 (2018).

3. Mesci P., Macia A., Moore S.M., Shiryaev S.A., Pinto A., Huang C.T., Tejwani L., Fernandes I.R., Suarez N.A., **Kolar M.J.**, Montefusco S., Rosenberg S.C., Herai R.H., Cugola F.R., Russo F.B., Sheets N., Saghatelian A., Shresta S., Momper J.D., Siqueira-Neto J.L., Corbett K.D., Beltrão-Braga P.C.B., Terskikh A.V., Muotri A.R. Blocking Zika virus vertical transmission. *Scientific Reports* 8, 1218 (2018).

4. Sulli G., Rommel A., Wang X, **Kolar M.J.**, Puca F., Saghatelian A., Plikus M.V., Verma I.M., Panda S. Pharmacological activation of REV-ERBs is lethal in cancer and oncogene-induced senescence. *Nature* 553, 351-355 (2018).

5. Mitra, S., Montgomery, J. E., **Kolar M.J.**, Li, G., Jeong, K. J., Peng, B., Verdine, G. L., Mills, G. B., Moellering, R. E. Stapled peptide inhibitors of RAB25 target context-specific phenotypes in cancer, *Nature Communications* 8, 660 (2017).

6. Nelson A. T.[#], **Kolar M.J.**[#], Chu Q., Syed I., Kahn B. B., Saghatelian A., Siegel D. Stereochemistry of Endogenous Palmitic Acid Ester of 9-Hydroxystearic Acid and Relevance of Absolute Configuration to Regulation, *Journal of the American Chemical Society* 139, 4943-4947 (2017). [#] co-first authors

7. Howell J. J., Hellberg K., Turner M., Talbott G., **Kolar M.J.**, Ross D. S., Hoxhaj G., Saghatelian A., Shaw R. J., Manning B. D. Metformin Inhibits Hepatic mTORC1 Signaling via Dose-Dependent Mechanisms Involving AMPK and the TSC Complex, *Cell Metabolism* 25, 463-471 (2017).

8. Chen, P., Zuo, H., Xiong, H., **Kolar M.J.**, Chu, Q., Saghatelian, A., Siegwart, D. J., Wan, Y. Gpr132 sensing of lactate mediates tumor-macrophage interplay to promote breast cancer metastasis, *Proceedings of the National Academy of Sciences U S A* 114, 580-585 (2017).

9. Oishi Y., Spann N. J., Link V. M., Muse E. D., Strid T., Edillor C., **Kolar M.J.**, Matsuzaka T. Hayakawa, S., Tao J., Kaikkonen M. U., Carlin A. F., Lam M. T., Manabe I., Shimano H., Saghatelian A., Glass C. K. SREBP1 Contributes to Resolution of Pro-inflammatory TLR4 Signaling by Reprogramming Fatty Acid Metabolism, *Cell Metabolism* 25, 412-427 (2017).

10. Svensson R. U., Parker S. J., Eichner L. J., **Kolar M.J.**, Wallace M., Brun S. N., Lombardo P. S., Van Nostrand J. L., Hutchins A., Vera L., Gerken L., Greenwood J., Bhat S., Harriman G., Westlin W. F., Harwood H. J., Jr., Saghatelian A., Kapeller R., Metallo C. M., Shaw R. J. Inhibition of acetyl-CoA carboxylase suppresses fatty acid synthesis and tumor growth of non-small-cell lung cancer in preclinical models, *Nature Medicine* 22, 1108-1119 (2016).

11. **Kolar M.J.**, Kamat, S. S., Parsons W. H., Homan E. A., Maher T., Peroni O. D., Syed I., Fjeld K., Molven A., Kahn B. B., Cravatt B. F., Saghatelian A. Branched Fatty Acid Esters of Hydroxy Fatty Acids Are Preferred Substrates of the MODY8 Protein Carboxyl Ester Lipase, *Biochemistry* 55, 4636-4641 (2016).

12. Parsons W. H.[#], **Kolar M.J.**[#], Kamat S. S., Cognetta A. B., 3rd, Hulce J. J., Saez E., Kahn B. B., Saghatelian A., Cravatt B. F. AIG1 and ADTRP are atypical integral membrane hydrolases that degrade bioactive FAHFAs, *Nature Chemical Biology* 12, 367-372 (2016). [#] co-first authors

13. Zhang T., Chen S., Syed I., Stahlman, M., **Kolar M. J.**, Homan E. A., Chu Q., Smith U., Boren J., Kahn B. B., Saghatelian A. A LC-MS-based workflow for measurement of branched fatty acid esters of hydroxy fatty acids, *Nature Protocols* 11, 747-763 (2016).

ABTRACT OF THE DISSERTATION

Discovery and Characterization of Novel Bioactive Lipids and Enzymes Involved in their Regulation

by

Matthew John Kolar

Doctor of Philosophy in Biomedical Sciences

University of California San Diego, 2018

Professor Alan Saghatelian, Chair
Professor Steven Dowdy, Co-Chair

Fats or lipids are thought to be deleterious to human health, but recent research has begun to identify beneficial roles for these molecules. Branched fatty acid esters of hydroxy fatty acids, named FAHFAs, are a newly discovered group of lipids that are produced in mammalian tissues. Administration of purified FAHFAs to mice reverses diabetes and reduces inflammation, indicating that raising the levels of these lipids *in vivo* would be of therapeutic benefit. Indeed, analysis of FAHFA levels in humans revealed that people with type 2 diabetes had lower FAHFA levels than healthy individuals. One approach to raising FAHFA levels would be to inhibit the proteins that are responsible for degrading these lipids *in vivo*. As newly discovered lipids there are many questions that remain about these molecules, their regulation, structure, and biological roles. Here we make progress on all these fronts. First, we report the identification and characterization of the first FAHFA hydrolases: carboxyl ester lipase (CEL), androgen-induced gene 1 (AIG1) protein, and androgen-dependent TFPI regulating protein

(ADTRP). We have developed inhibitors of these enzymes and hypothesize that by inhibiting these enzymes, we can increase FAHFA levels which will result in reduced inflammation and better metabolic parameters. Second, we have characterized the structure and biological activity of a novel FAHFA family discovered in oats called linoleic acid esters of hydroxy linoleic acid (LAHLAs). LAHLAs are more potent than previously characterized FAHFAs in similar assays, and regulate key genes involved in inflammation. These findings open up the possibility of using LAHLAs or LAHLA analogs to modulate the immune system. In addition to these major findings, we have also refined the structure of FAHFAs through the identification of the stereochemistry of these lipids in cells and tissues of mice. The identification of a preferred stereoisomer *in vivo* indicates that FAHFAs are produced by unidentified enzymes because non-enzymatic production of the hydroxy fatty acid would result a racemic mixture of FAHFAs. Finally, we optimized the methods for FAHFA analysis, which will increase the rate that labs can study FAHFAs and open up the possibility to analyze hundreds of samples for clinical applications.

Chapter 1:

Introduction

1.1 Discovery of FAHFAs

Though some beneficial lipids such as omega-3 fatty acids are known[1-3], lipids are generally considered deleterious since rodents and humans on high-fat diets become obese, display insulin resistance, and develop type 2 diabetes[4-6]. However, several studies have linked increased adipose tissue de novo lipogenesis with improved metabolic health[7,8], a seemingly paradoxical observation because of the impact of high-fat diets on metabolic health. Mice that overexpress the glucose transporter Glut4 in their adipose tissue (AG4OX mice), for example, were shown to have greatly improved metabolic health while also displaying a robust increase in de novo lipogenesis in adipose tissues[9,10]. This data led to a hypothesis that the increased de novo lipogenesis might lead elevated levels of a beneficial lipid(s), such as palmitoleic acid[11] or omega-3 fatty acids[1-3].This idea was tested via lipidomics of adipose tissue from WT and AG4OX mice.

Lipidomics revealed highly elevated levels of structurally novel class of mammalian lipids in AG4OX mice that were revealed to be fatty acid esters of hydroxy fatty acids (FAHFAs) through a combination of mass spectrometry and chemical synthesis[12].Targeted analysis of FAHFAs revealed the existence of at least 16 different FAHFA families—a family is defined as a specific combination of fatty acid and hydroxy fatty acid. Palmitic Acid esters of Hydroxy Stearic Acids (PAHSAs) and Oleic Acid esters of Hydroxy Stearic Acids (OAHSAs) are examples of two different FAHFA families (**Figure 1.1a**). Furthermore, each family has multiple regioisomers which differ by the branched ester position on the hydroxy-fatty acid (**Figure 1.1b**). For instance, there are eight different PAHSA regioisomers in adipose tissue (13-, 12-, 11-, 10-, 9-, 8-, 7-, and 5-PAHSA), and each of these regioisomers is more concentrated in adipose tissue from AG4OX mice. We later discovered that stereochemistry of the FAHFAs might play a factor in the regulation of these lipids. Specifically, we synthesized both enantiomers of 9-PAHSA, *R*-9-PAHSA and *S*-9-PAHSA, and found that *R*-9-PAHSA is the predominant stereoisomer that accumulated in the adipose tissue of AG4OX mice (**Figure 1.1c**)[13]. This could be due to

increased synthesis of this stereoisomer or decreased degradation, but the fact that we find only a single stereoisomer in tissues is supportive of the enzymatic introduction of the oxygen of the ester group and makes it unlikely that FAHFAs are produced from spurious non-enzymatic lipid oxidation.

1.2 Beneficial Effects of PAHSAs

Because of limitations in the number of FAHFA families that could be detected by mass spectrometry, subsequent analysis focused on a single family, the PAHSAs. PAHSAs are most abundant in white adipose tissue (WAT), brown adipose tissue (BAT) and liver, and fasting or placement on a high-fat diet (HFD) results in regulation of endogenous PAHSA levels in mice. To ensure that FAHFAs are not limited to mice, the lab compared endogenous PAHSA levels in serum and WAT of insulin-sensitive and insulin-resistant people. These experiments revealed that PAHSA levels correlate strongly with insulin sensitivity (**Figure 1.2a**), and that higher PAHSA levels indicate better insulin sensitivity[12]. This suggested that raising PAHSA levels may improve metabolic health. Indeed, PAHSA administration to HFD-fed mice rapidly improves glucose tolerance and reduces pro-inflammatory macrophages in WAT[14]. The anti-inflammatory PAHSAs was later shown to extend to a mouse model of colitis where PAHSAs protected against inflammatory damage of the colon (**Figure 1.2b**)[15].

Mechanism of action studies with PAHSAs are underway, and preliminary results indicate that the activation of two G protein-coupled receptors (GPCRs), GPR120 and GRP40[12,16], mediates at least some of the biological activity of PAHSAs[12,16].*In vitro* mechanistic studies revealed that PAHSAs augment insulin-stimulated glucose transport in adipocytes by activating G protein-coupled receptor-120 (GPR120). GPR120 activation is also reported to inhibit inflammation, and PAHSAs showed potent anti-inflammatory effects in immune cells. A recent study has shown that PAHSAs augment glucose-stimulated insulin secretion via GPR40[16].

With the diverse actions PAHSAs exert on multiple tissues, it is not surprising that these lipids activate multiple GPCRs. Many GPCRs are known metabolic sensors that can be activated by metabolic substrates such as fatty acids, sugars, lactate, and ketone bodies. Due the central roles of these GPCRs in metabolism, they have become a lucrative target for pharmaceutical companies to treat metabolic diseases[17]. Since PAHSAs can activate both GPR40 and GPR120, which are both potential drug targets, these lipids provide an interesting opportunity to compare a dual GPR40/120 agonist versus compounds that target GRP40 or GRP120 individually. All together, these studies highlight FAHFAs as a new class of anti-diabetic and anti-inflammatory lipids, and my graduate work focused on furthering knowledge regarding FAHFA bioactivity and regulation using cutting-edge methods in chemical biology.

1.3 Discovery of FAHFA Hydrolases

Regulation of PAHSA levels can occur through changes in biosynthesis or degradation. Since FAHFAs are a structurally novel class of lipids, nothing is known about the genes that are responsible for FAHFA regulation. However, preliminary data demonstrated that tissue lysates are capable of FAHFA hydrolysis and FAHFA biosynthesis[12]. The identification of candidate FAHFA degrading enzymes is accomplished by measuring FAHFA hydrolysis in different tissue proteomes. After a known tissue is known to have FAHFA degrading potential, the active lipases of that tissue are identified and then tested for FAHFA hydrolysis activity.

To carry out this strategy, a FAHFA hydrolysis assay was used to measure hydroxy stearic acid (HSA) release from PAHSA after incubation of PAHSA with a tissue lysate (**Figure 1.3a**). To identify the lipases that are candidate FAHFA hydrolases, we used activity-based protein profiling (ABPP), a chemoproteomics technology that uses active-site directed chemical probes to detect lipases directly from cell or tissue proteomes by proteomics[18,19]. Probes have been developed to target individual classes of enzymes such including serine hydrolases (SHs), a class that contains most of the known lipases[20,21]. SHs make up approximately 1% of the

proteome with more than 100 known serine proteases and more than 100 metabolic SHs in the human genome[22]. The metabolic SH family includes many lipases such as pancreatic lipase (PNLIP), monacylglycerol lipase (MGLL), and lipoprotein lipase (LPL). The probe used to target serine hydrolases is fluorophosphonate (FP), which covalently reacts with the serine nucleophile of these enzymes (**Figure 1.2b**). Comparing the lipase profiles of the pancreatic membrane proteome to other, less active proteomes, revealed carboxyl ester lipase (CEL) as a FAHFA hydrolase[23].

FP probes can also react with the much smaller class of threonine hydrolases, such as the proteasome, and this is important for as two of the FAHFA hydrolases end up belonging to the threonine hydrolase family[24]. We found these threonine hydrolases, using a second strategy that can be used to identify in combination with ABPP to find FAHFA hydrolases relies on an experiment called competitive ABPP (**Figure 1.3c**)[19]. In a competitive ABPP experiment, the ABPP probe "competes" with an inhibitor for a serine hydrolase active site. If an enzyme binds an inhibitor it is no longer labeled by the ABPP probe, and by analyzing proteomes treated with different inhibitors and then labeled with the ABPP probe it becomes possible to map the all of the enzymes that are inhibited by a particular molecule. The Cravatt lab had already mapped the targets for many serine hydrolase inhibitors using competitive ABPP. Using the Cravatt lab inhibitors along with the known enzymes that each inhibitor blocks it is possible to use this information to discover the enzyme(s) responsible for the hydrolysis of a specific substrates. For example, if a one or more inhibitors prevents the hydrolysis of a FAHFA while other compounds have no effect, comparison of the enzyme targets of the active versus inactive compounds can reveal candidate FAHFA-degrading enzymes.

Utilizing this inhibitor screening strategy in combination with our FAHFA substrate hydrolysis assay, we have discovered two additional FAHFA hydrolases: androgen-induced gene 1 (AIG1) and androgen-dependent TFPI regulation protein (ADTRP)[25]. The characterization of CEL, and AIG1 and ADTRP as FAHFA hydrolases are described in Chapters

2 and 3, respectively. These are the first FAHFA hydrolases identified and animals lacking these enzymes have been generated and are being used to study the role of endogenous FAHFA regulation on physiology.

1.4 Other Beneficial FAHFAs

The initial discovery of FAHFAs in 2014, revealed the presence of 16 FAHFA families, each of which contains multiple regioisomers. Due to the high abundance of stearic, palmitic, palmitoleic, and oleic acid in mammalian tissues, FAHFAs containing all combinations of these as the fatty acids and hydroxy fatty acids were analyzed for using a targeted mass spectrometry approach and were all found to be present. Additional methods have led to the discovery of additional FAHFAs. For example, an *in silico* MS/MS library for FAHFAs was generated and resulted in more than 1000 theoretical FAHFAs[26]. This library was generated using 33 of the most common fatty acids in mammalian cells spanning from 14:1 to 24:6, and subsequent mass spectrometry experiments analyzing egg yolk revealed the existence of previously unidentified FAHFAs. Another approach to identify FAHFAs employed by Kuda et al, was to test whether FAHFAs can be derived from known beneficial free fatty acids. Supplementation of n-3 polyunsaturated fatty acids (PUFAs, EPA and DHA) in mice resulted in DHA-derived FAHFAs in their WAT and serum[27]. They went on to show that one of the these FAHFAs, 13-docosahexaenoic acid hydroxy linoleic acid (DHAHLA), like 9-PAHSA, exerted potent anti-inflammatory effects when tested *in vitro*[27]. The detection of this lipid and other lipids such as docosahexaenoic acid hydroxy docosahexaenoic acid (DHAHDHA) after n-3 PUFA supplementation, reveals that these FAHFAs may be contributing to the established beneficial effects of n-3 PUFAs. Furthermore, this study demonstrates the role of dietary lipids on levels of endogenous FAHFA levels.

To date, only three FAHFAs have been tested for their biological activities. Given that multiple members of many lipid families have biological activity, it begs the question whether

other, more active FAHFAs remain to be discovered. As previously discussed, one possible approach to increase endogenous FAHFA levels is through pharmacological inhibition of FAHFA hydrolases. Another means of increasing endogenous FAHFAs may be through consumption of FAHFA-dense foods. But do any foods have biologically active FAHFAs? Some lipids, like linoleic acid, cannot be biosynthesized in humans and must be acquired through the diet. These lipids are termed “essential” and have critical roles in signaling, as they are precursors to many downstream lipid mediators[28]. FAHFAs may be a class of lipids where some FAHFAs are endogenously biosynthesized, while other FAHFAs or their components are obtained through the diet. In Chapter 6, we explain how we characterized linoleic acid esters of linoleic acids (LAHLAs) from oat oil as a novel family of biologically active FAHFAs. Our findings demonstrate that at least some of the beneficial effects of oat oil in human studies might be attributed to LAHLAs, a routinely consumed and apparently safe FAHFA.

1.5 Scope of this Work

The work presented in this thesis is centrally focused on discovering and characterizing biologically active FAHFAs and the first FAHFA hydrolases. In Chapter 2, we show the CEL is a pancreatic FAHFA hydrolase that preferentially hydrolyzed FAHFAs compared to other lipids. In addition, mutations of CEL have been like to maturity-onset diabetes of the young, type 8 (MODY8) and chronic pancreatitis. We show that the CEL MODY8 variant has a modest increase in FAHFA hydrolase activity compared to the normal enzyme. In Chapter 3, we used ABPP to discover the poorly characterized proteins AIG1 and ADTRP as atypical hydrolytic enzymes. We show that these enzymes are threonine hydrolases and preferably hydrolyze FAHFAs over other major lipid classes. In Chapter 4, we show that the stereochemistry of 9-PAHSA is important to its regulation. Specifically, we developed a method that resolves PAHSA stereoisomers and show that CEL selectively hydrolyzes *S*-9-PAHSA while HEK cells preferably biosynthesize *R*-9-PAHSA. Chapter 5 shows the development of a faster protocol for

endogenous FAHFA measurements. The time to analyze FAHFAs was shortened by greater than 70% compared to our previous method, which will allow higher throughput of FAHFA analysis for basic and clinical applications. Chapter 6 shows the discovery and characterization of novel FAHFA family, LAHLAs, that were discovered in oat oil. We show that LAHLAs are the highest abundant FAHFAs in oat oil and correlate with the beneficial metabolic effects seen in humans ingesting oat oil extract. In addition, we show that mice and humans have endogenous 13-LAHLA within their fat. We also synthesized 13-LAHLA and a 13-aza-LAHLA, a non-hydrolyzable version of 13-LAHLA, and show that these lipids have potent anti-inflammatory effects *in vitro*.

1.6 Conclusion and Future Directions

Understanding how FAHFAs are biochemically regulated and determining the role of these lipids *in vivo* are critical questions, which could have an important impact on developing new strategies to prevent or treat type 2 diabetes and inflammatory pathologies. With current research showing the beneficial effects of FAHFAs on metabolism and inflammation, increasing the levels of FAHFAs either through inhibition of FAHFA hydrolases or FAHFA supplementation has great promise.

Many mouse tissues have FAHFA hydrolase activity but only a couple of these hydrolytic enzymes have been discovered. We have discovered herein three FAHFAs hydrolases CEL, AIG1, and ADTRP. These enzymes have specific tissue distribution and may mediate local inflammation in the respective tissues where they are expressed. For example, AIG1 is the principal FAHFA hydrolase in the brain and CEL is predominantly expressed in the pancreas. Although the role these enzymes play in disease is unknown, we hypothesize the inhibition of some of these enzymes may afford beneficial effects through the upregulation of FAHFA levels. To elucidate the biology these enzymes have *in vivo*, we have generated tailored inhibitors to these hydrolases in addition to generating AIG1 and ADTRP knockout (KO) mice. Prior work

has established the correlation between insulin sensitivity and increased serum PAHSA levels in humans, and we hope that through the pharmacological inhibition of FAHFA hydrolases we can increase systemic FAHFA levels. Although the study of FAHFAs and their roles in biology is incomplete, we now have invaluable tools in studying this field.

Since the discovery of FAHFAs in 2014, additional FAHFA families have been discovered[26,27]. To streamline the process of discovering bioactive FAHFAs we looked to natural sources, specifically oat oil. This was not a random effort in searching different food sources for FAHFAs. Like FAHFAs, oat oil is known to have beneficial metabolic and anti-inflammatory effects[29-31]. Also, oat oil contains a large amount DGDG which has a FAHFA moiety[32], therefore, we hypothesized oat oil may also have a large abundance of free FAHFAs. We discovered a novel FAHFA family called LAHLAs in oat oil. Plasma levels of LAHLAs correlate with the beneficial metabolic effects seen in humans after ingesting oat oil. We synthesized 13-LAHLA and showed that this FAHFA has greater anti-inflammatory effects *in vitro* compared to 9-PAHSA, revealing the potential of better therapeutic FAHFAs in existence. Understanding the structure-relationship activity of FAHFAs will also allow us to design synthetic FAHFAs for use in therapies.

We also describe herein the analytical tools to efficiently measure and properly characterize FAHFAs. With serum FAHFAs known to be correlated with metabolic status, these have potential to be biomarkers. We have developed a faster analytical method to analyze FAHFAs, thus being amenable to a large number of clinical samples.

Although there are many known FAHFA family members, each FAHFA family contains many positional isomers that must be addressed in elucidating what FAHFAs are most relevant to human physiology. It has been reported that certain PAHSA regioisomers have better anti-inflammatory effects compared to others in their family. For example, of the 8-PAHSA regioisomers discovered to date, 9- and 5-PAHSA have been shown to have the best therapeutic potential. However, we do not know if the activity of these PAHSAs is due to *R* or *S*,

or even both stereoisomers. We do not understand why some FAHFAs are more active than others in our activity assays, and further structure activity relationship (SAR) studies will need to be established. Understanding the importance of carbon length, degrees of unsaturation, position of the ester group, and stereoisomerism will be important to understand when developing synthetic FAHFAs with increased potency and bioavailability.

Overall, this dissertation explores many aspects of FAHFA biology from their regulation to discovery of new FAHFAs. In addition, we discuss novel analytical tools to identifying and characterizing FAHFAs more efficiently. We hope that that the scientific knowledge gained from this work can eventually be used to develop next-generation anti-inflammatory and anti-diabetic drugs.

1.7 Figures

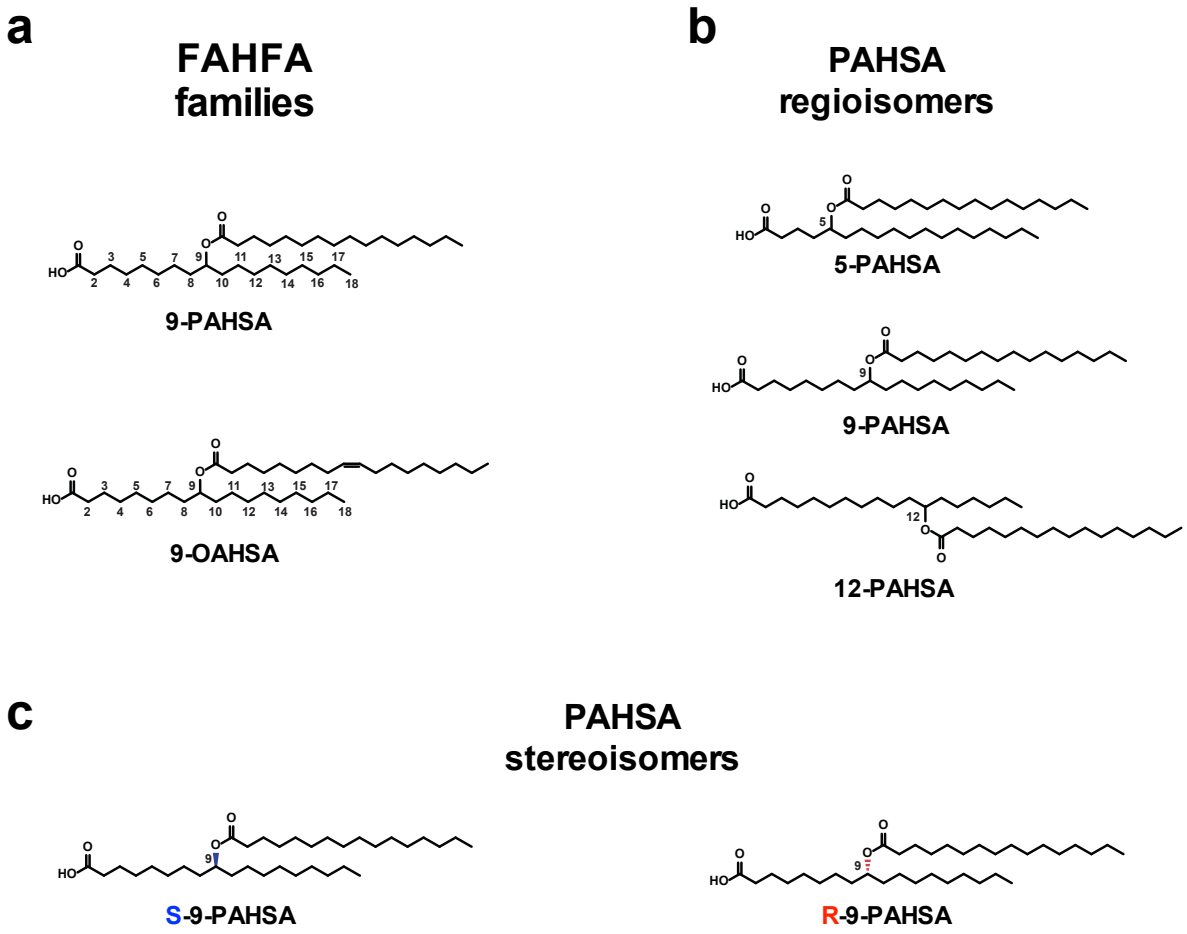

Figure 1.1. Classification of FAHFAs. (**a**) Two different FAHFA families, PAHSA and OAHSA are shown. (**b**) Structures of three different PAHSA regioisomers (5-, 9-, and 12-PAHSA). Numbering is determined by the position of the ester bond relative to the carboxyl carbon. (**c**) Chemical structures of 9-PAHSA stereoisomers (*S* and *R*).

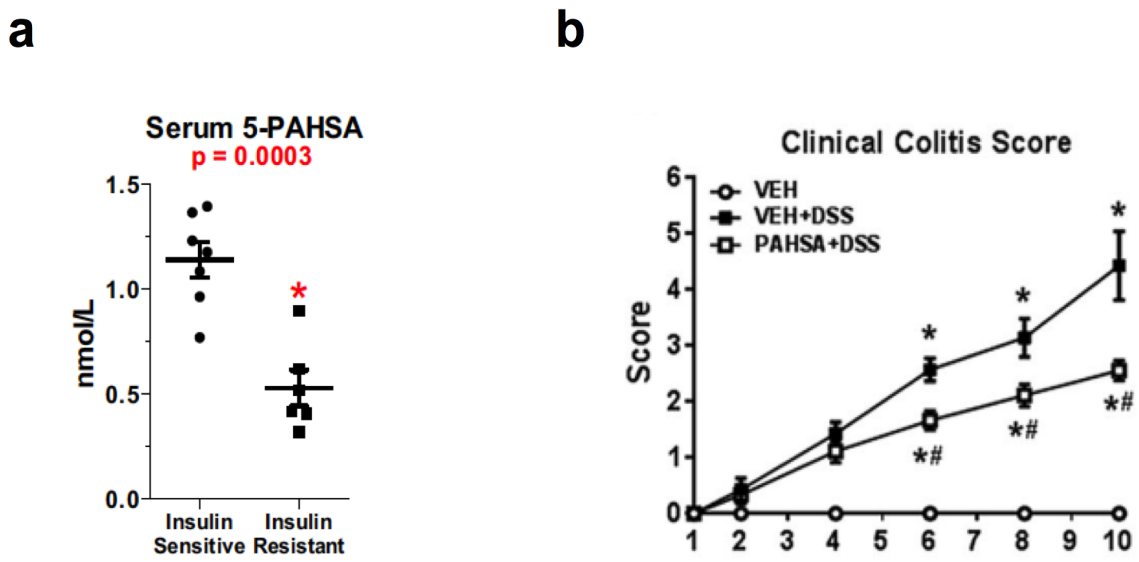

Figure 1.2. Beneficial effects of PAHSAs. (**a**) Quantification of 5-PAHSA in serum of insulin-sensitive and insulin-resistant nondiabetic humans shows that insulin-resistant humans have lower 5-PAHSA serum levels[12]. (**b**) PAHSA treatments improves clinical colitis score throughout 10 days of DSS treatment[15].

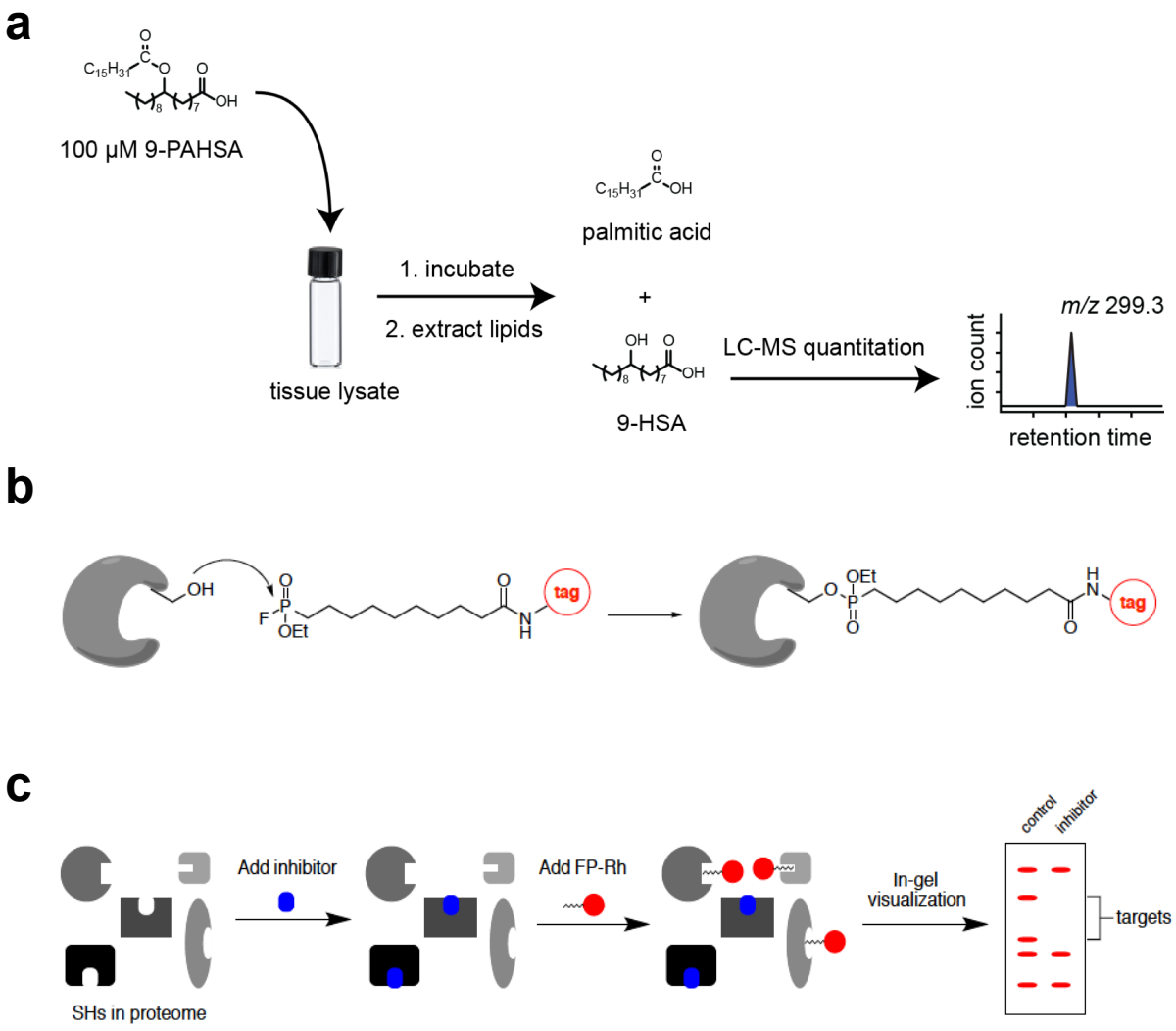

Figure 1.3. Tools and assays used to identify FAHFA hydrolases**.** (**a**) Schematic of the FAHFA substrate hydrolysis assay. (**b**) Schematic of ABPP. FP activity-based probe reacting with a serine hydrolase. (**c**) Schematic of competitive ABPP.

1.8 References:

1 Kris-Etherton, P. M., Harris, W. S., Appel, L. J. & American Heart Association. Nutrition, C. Fish consumption, fish oil, omega-3 fatty acids, and cardiovascular disease. *Circulation* **106**, 2747-2757 (2002).

2 Popp-Snijders, C., Schouten, J. A., Heine, R. J., van der Meer, J. & van der Veen, E. A. Dietary supplementation of omega-3 polyunsaturated fatty acids improves insulin sensitivity in non-insulin-dependent diabetes. *Diabetes Res* **4**, 141-147 (1987).

3 Simopoulos, A. P. Omega-3 fatty acids in health and disease and in growth and development. *Am J Clin Nutr* **54**, 438-463 (1991).

4 Surwit, R. S., Kuhn, C. M., Cochrane, C., McCubbin, J. A. & Feinglos, M. N. Diet-induced type II diabetes in C57BL/6J mice. *Diabetes* **37**, 1163-1167 (1988).

5 Winzell, M. S. & Ahren, B. The high-fat diet-fed mouse: a model for studying mechanisms and treatment of impaired glucose tolerance and type 2 diabetes. *Diabetes* **53 Suppl 3**, S215-219 (2004).

6 Vessby, B., Uusitupa, M., Hermansen, K., Riccardi, G., Rivellese, A. A., Tapsell, L. C., Nalsen, C., Berglund, L., Louheranta, A., Rasmussen, B. M., Calvert, G. D., Maffetone, A., Pedersen, E., Gustafsson, I. B., Storlien, L. H. & Study, K. Substituting dietary saturated for monounsaturated fat impairs insulin sensitivity in healthy men and women: The KANWU Study. *Diabetologia* **44**, 312-319 (2001).

7 Roberts, R., Hodson, L., Dennis, A. L., Neville, M. J., Humphreys, S. M., Harnden, K. E., Micklem, K. J. & Frayn, K. N. Markers of de novo lipogenesis in adipose tissue: associations with small adipocytes and insulin sensitivity in humans. *Diabetologia* **52**, 882-890 (2009).

8 Herman, M. A., Peroni, O. D., Villoria, J., Schon, M. R., Abumrad, N. A., Bluher, M., Klein, S. & Kahn, B. B. A novel ChREBP isoform in adipose tissue regulates systemic glucose metabolism. *Nature* **484**, 333-338 (2012).

9 Shepherd, P. R., Gnudi, L., Tozzo, E., Yang, H., Leach, F. & Kahn, B. B. Adipose cell hyperplasia and enhanced glucose disposal in transgenic mice overexpressing GLUT4 selectively in adipose tissue. *J Biol Chem* **268**, 22243-22246 (1993).

10 Carvalho, E., Kotani, K., Peroni, O. D. & Kahn, B. B. Adipose-specific overexpression of GLUT4 reverses insulin resistance and diabetes in mice lacking GLUT4 selectively in muscle. *Am J Physiol Endocrinol Metab* **289**, E551-561 (2005).

11 Cao, H., Gerhold, K., Mayers, J. R., Wiest, M. M., Watkins, S. M. & Hotamisligil, G. S. Identification of a lipokine, a lipid hormone linking adipose tissue to systemic metabolism. *Cell* **134**, 933-944 (2008).

12 Yore, M. M., Syed, I., Moraes-Vieira, P. M., Zhang, T., Herman, M. A., Homan, E. A., Patel, R. T., Lee, J., Chen, S., Peroni, O. D., Dhaneshwar, A. S., Hammarstedt, A., Smith, U., McGraw, T. E., Saghatelian, A. & Kahn, B. B. Discovery of a class of endogenous mammalian lipids with anti-diabetic and anti-inflammatory effects. *Cell* **159**, 318-332 (2014).

13 Nelson, A. T., Kolar, M. J., Chu, Q., Syed, I., Kahn, B. B., Saghatelian, A. & Siegel, D. Stereochemistry of Endogenous Palmitic Acid Ester of 9-Hydroxystearic Acid and Relevance of Absolute Configuration to Regulation. *J Am Chem Soc* **139**, 4943-4947 (2017).

14 Wang, D., Capehart, S. L., Pal, S., Liu, M., Zhang, L., Schuck, P. J., Liu, Y., Yan, H., Francis, M. B. & De Yoreo, J. J. Hierarchical assembly of plasmonic nanostructures using virus capsid scaffolds on DNA origami templates. *ACS Nano* **8**, 7896-7904 (2014).

15 Lee, J., Moraes-Vieira, P. M., Castoldi, A., Aryal, P., Yee, E. U., Vickers, C., Parnas, O., Donaldson, C. J., Saghatelian, A. & Kahn, B. B. Branched Fatty Acid Esters of Hydroxy Fatty Acids (FAHFAs) Protect against Colitis by Regulating Gut Innate and Adaptive Immune Responses. *J Biol Chem* **291**, 22207-22217 (2016).

16 Syed, I., Lee, J., Moraes-Vieira, P. M., Donaldson, C. J., Sontheimer, A., Aryal, P., Wellenstein, K., Kolar, M. J., Nelson, A. T., Siegel, D., Mokrosinski, J., Farooqi, I. S., Zhao, J. J., Yore, M. M., Peroni, O. D., Saghatelian, A. & Kahn, B. B. Palmitic Acid Hydroxystearic Acids Activate GPR40, Which Is Involved in Their Beneficial Effects on Glucose Homeostasis. *Cell Metab* **27**, 419-427 e414 (2018).

17 Blad, C. C., Tang, C. & Offermanns, S. G protein-coupled receptors for energy metabolites as new therapeutic targets. *Nat Rev Drug Discov* **11**, 603-619 (2012).

18 Willems, L. I., Overkleeft, H. S. & van Kasteren, S. I. Current developments in activity-based protein profiling. *Bioconjug Chem* **25**, 1181-1191 (2014).

19 Niphakis, M. J. & Cravatt, B. F. Enzyme inhibitor discovery by activity-based protein profiling. *Annu Rev Biochem* **83**, 341-377 (2014).

20 Bachovchin, D. A. & Cravatt, B. F. The pharmacological landscape and therapeutic potential of serine hydrolases. *Nat Rev Drug Discov* **11**, 52-68 (2012).

21 Nomura, D. K., Dix, M. M. & Cravatt, B. F. Activity-based protein profiling for biochemical pathway discovery in cancer. *Nat Rev Cancer* **10**, 630-638 (2010).

22 Simon, G. M. & Cravatt, B. F. Activity-based proteomics of enzyme superfamilies: serine hydrolases as a case study. *J Biol Chem* **285**, 11051-11055 (2010).

23 Kolar, M. J., Kamat, S. S., Parsons, W. H., Homan, E. A., Maher, T., Peroni, O. D., Syed, I., Fjeld, K., Molven, A., Kahn, B. B., Cravatt, B. F. & Saghatelian, A. Branched Fatty Acid Esters of Hydroxy Fatty Acids Are Preferred Substrates of the MODY8 Protein Carboxyl Ester Lipase. *Biochemistry* **55**, 4636-4641 (2016).

24 Jessani, N., Niessen, S., Wei, B. Q., Nicolau, M., Humphrey, M., Ji, Y., Han, W., Noh, D. Y., Yates, J. R., 3rd, Jeffrey, S. S. & Cravatt, B. F. A streamlined platform for high-content functional proteomics of primary human specimens. *Nat Methods* **2**, 691-697 (2005).

25 Parsons, W. H., Kolar, M. J., Kamat, S. S., Cognetta, A. B., 3rd, Hulce, J. J., Saez, E., Kahn, B. B., Saghatelian, A. & Cravatt, B. F. AIG1 and ADTRP are atypical integral membrane hydrolases that degrade bioactive FAHFAs. *Nat Chem Biol* **12**, 367-372 (2016).

26 Ma, Y., Kind, T., Vaniya, A., Gennity, I., Fahrmann, J. F. & Fiehn, O. An in silico MS/MS library for automatic annotation of novel FAHFA lipids. *J Cheminform* **7**, 53 (2015).

27 Kuda, O., Brezinova, M., Rombaldova, M., Slavikova, B., Posta, M., Beier, P., Janovska, P., Veleba, J., Kopecky, J., Jr., Kudova, E., Pelikanova, T. & Kopecky, J. Docosahexaenoic Acid-Derived Fatty Acid Esters of Hydroxy Fatty Acids (FAHFAs) With Anti-inflammatory Properties. *Diabetes* **65**, 2580-2590 (2016).

28 Simopoulos, A. P. The importance of the ratio of omega-6/omega-3 essential fatty acids. *Biomed Pharmacother* **56**, 365-379 (2002).

29 Ohlsson, L., Rosenquist, A., Rehfeld, J. F. & Harrod, M. Postprandial effects on plasma lipids and satiety hormones from intake of liposomes made from fractionated oat oil: two randomized crossover studies. *Food Nutr Res* **58** (2014).

30 Meydani, M. Potential health benefits of avenanthramides of oats. *Nutrition Reviews* **67**, 731-735 (2009).

31 Michelle Garay, M., Judith Nebus, M. & Menas Kizoulis, B. Anti-inflammatory activities of colloidal oatmeal (Avena sativa) contribute to the effectiveness of oats in treatment of itch associated with dry, irritated skin. *Journal of Drugs in Dermatology* **14**, 43-48 (2015).

32 Hamberg, M., Liepinsh, E., Otting, G. & Griffiths, W. Isolation and structure of a new galactolipid from oat seeds. *Lipids* **33**, 355-363 (1998).

Chapter 2:

Branched Fatty Acid Esters of Hydroxy Fatty Acids are Preferred Substrates of the MODY8 Protein

Abstract

A recently discovered class of endogenous mammalian lipids, branched fatty acid esters of hydroxy fatty acids (FAHFAs), possess anti-diabetic and anti-inflammatory activities. Here, we identified and validated carboxyl ester lipase (CEL), a pancreatic enzyme hydrolyzing cholesteryl esters and other dietary lipids, as a FAHFA hydrolase. Variants of CEL have been linked to maturity-onset diabetes of the young, type 8 (MODY8) and to chronic pancreatitis. We tested FAHFA hydrolysis activity of the CEL MODY8 variant and found a modest increase in activity as compared with the normal enzyme. Together, the data suggest that CEL might break down dietary FAHFAs.

2.1 Introduction

Lipids serve structural, energetic, and signaling roles in biology[1]. These activities are regulated by the action of lipid-modifying enzymes in the proteome[2]. The proper characterization of these enzymes, however, depends on knowing the composition of the lipidome, or, the complete set of lipids in a cell, tissue, or organism[3-5]. The recent discovery of new lipids[3,6,7] indicates gaps in the current knowledge of lipid biochemistry.

Transgenic mice overexpressing the GLUT4 glucose transporter in adipose tissue have proven to be an important model for understanding the role of adipose tissue in systemic insulin resistance[8,9]. These animals are obese, yet have improved glucose tolerance, and increased adipose tissue lipogenesis, which is important in maintaining insulin sensitivity[10]. The link between adipose lipogenesis and insulin sensitivity in mice and humans led to the hypothesis that the adipose tissue might be producing a metabolically beneficial lipid.

Lipidomic profiling of adipose tissue from the GLUT4 overexpressing mice revealed increased levels of a novel endogenous lipid family[7]. Structural characterization of these lipids using a combination of mass spectrometry and chemical synthesis identified them, as branched chain fatty acid esters of hydroxy fatty acids (FAHFAs). Subsequent analysis revealed 16 FAHFA families, which differ by the composition of their fatty acid chains. Prominent families include palmitic, oleic, and palmitoleic acid esters of hydroxy stearic acid, referred to as PAHSAs, OAHSAs, and POHSAs, respectively.

Analysis of the PAHSAs also revealed the existence of multiple positional isomers within each family. For instance, 5-PAHSA and 9-PAHSA are two isomers that have the conjoining ester bond at either 5- or 9- position (numbering from the carboxylate). A total of eight PAHSA isomers were identified (13-, 12-, 11-, 10-, 9-, 8-, 7-, and 5-PAHSA) and tissues have different distributions of these isomers[7].

Human studies revealed that serum PAHSA concentrations were highly correlated with insulin sensitivity[7] and insulin resistant people had low levels. This suggested that raising

PAHSA levels *in vivo* might be beneficial. Indeed, administration of PAHSAs to mice improved glucose tolerance and reduced inflammation, demonstrating that increased FAHFA concentrations are anti-diabetic and anti-inflammatory[7].

The discovery of FAHFAs has led to many questions, including what are the enzymes and metabolic pathways responsible for the production and catabolism of these lipids? Efforts towards this goal have already revealed two atypical FAHFA hydrolases[11], AIG1 and ADTRP. Here we describe the discovery that the pancreatic enzyme carboxyl ester lipase (CEL), can utilize FAHFAs as substrates.

2.2 Results and Discussion

We utilized a previously described liquid chromatography-mass spectrometry (LC-MS) assay for measuring FAHFA hydrolysis activity[11]. Addition of 9-PAHSA to liver lysates resulted in the production 9-hydroxystearic acid (9-HSA), which we use to quantify hydrolysis. Denaturation of the proteome by heat led to loss of 9-PAHSA hydrolysis activity (**Figure 2.1**).

We then profiled the activity of different tissue lysates using the 9-PAHSA hydrolysis assay. The tissue with the greatest amount of 9-PAHSA hydrolysis activity (per mg of lysate) was pancreas (**Figure 2.2a**). The pancreas produces a number of lipases that are secreted into the gastrointestinal (GI) tract to facilitate digestion of lipids from diet[12]. FAHFAs have been detected in a number of foods[7], indicating the need for FAHFA hydrolyzing enzyme(s) in the GI tract. Fractionation of pancreatic tissue into soluble and membrane proteomes revealed that 9-PAHSA hydrolysis activity was specifically associated with the membrane fraction (**Figure 2.2b**). Since the addition of the AIG1 and ADTRP inhibitor KC01 did not affect 9-PAHSA hydrolysis (**Figure 2.3a**), we hypothesized that the pancreatic FAHFA hydrolase activity originated from another enzyme(s).

The addition of fluorophosphonate rhodamine (FP-Rh), a broad serine hydrolase inhibitor blocked 9-PAHSA hydrolysis, which indicated that the FAHFA hydrolyzing enzyme(s) in

the pancreas membrane fraction is a serine lipase (**Figure 2.3b**). We searched a tissue database of serine hydrolases generated using activity-based protein profiling (ABPP) with a fluorophosphonate biotin (FP-biotin)[13]. Briefly, a FP-biotin probe was used to label serine hydrolase enzymes, which were thereafter enriched by avidin chromatography, digested by trypsin and the peptides were subsequently subjected to LC-MS/MS analysis[13,14]. The similar inhibition activity of FP-Rh and FP-biotin indicated that the enzyme we sought was likely present in the serine hydrolase database[13]. We identified three candidate lipases within this dataset with preferential expression in the pancreatic membrane: carboxyl ester lipase (CEL), pancreatic lipase (PNLIP), and pancreatic lipase related protein 2 (PNLIPRP2).

CEL is also known as bile salt-stimulated lipase[15], and its activity has been reported to increase in the presence of the bile salt taurocholate[16,17]. By contrast, PNLIP and PNLIPRP2 are reportedly inhibited by taurocholate[18,19]. Therefore, we reasoned that we might be able to distinguish between CEL, PNLIP, or PNLIPRP2 as a candidate FAHFA hydrolase by measuring 9-PAHSA hydrolysis in the presence of taurocholate. Addition of sodium taurocholate (NaTC) to pancreatic membrane lysates increased FAHFA hydrolysis activity in a concentration-dependent manner suggesting that CEL is a putative FAHFA-degrading enzyme (**Figure 2.2c**).

Expression of CEL in HEK293T cells resulted in more than a 50-fold increase in FAHFA hydrolysis activity compared to lysate from control (mock) cells transfected with an empty vector (**Figure 2.4a**), demonstrating that CEL has FAHFA hydrolysis activity. Treatment of CEL-transfected lysates with a CEL inhibitor WWL92[13], completely blocked FAHFA hydrolysis activity (**Figure 2.4a)**. The addition of WWL92 to pancreatic membrane proteome also abrogated 9-PAHSA activity (**Figure 2.4b**), indicating that CEL is a principal FAHFA hydrolase in the pancreas. Also in support of this conclusion, 9- PAHSA hydrolysis activity was substantially reduced in pancreas tissue membrane from CEL–/– mice compared to control pancreatic tissue from CEL+/+ mice (**Figure 2.4c**). Together, these data provide strong evidence that CEL is a FAHFA hydrolase and the main source of 9-PAHSA hydrolysis activity in the pancreatic lysates.

CEL is expressed in the acinar cells of the exocrine pancreas[20]. Upon feeding, CEL, along with a variety of other lipases, are released into the gut to break down complex lipids and aid with their absorption. Several lipids, including triglycerides, retinyl esters, phospholipids, and cholesteryl esters are reported as CEL substrates based on *in vitro* studies. *In vivo*, however, CEL has no impact on triglyceride[21] or retinyl ester absorption[22], but is reported to influence cholesteryl ester hydrolysis[23].

To ascertain the relative activity of CEL against different lipids, including FAHFAs, we performed a broad substrate analysis (**Figure 2.5**). This assay used a total of 31 total lipids, including 15 FAHFAs, a triacylglycerol (TAG), a diacylglycerol (DAG), a cholesteryl ester (CE), along with a variety of phospholipids and lysophospholipids. Activity was monitored by the release of fatty acids from the different substrates upon hydrolysis by CEL. The substrate hydrolysis activity profile was generated using HEK293T membrane lysates overexpressing mouse CEL using a previously established LC-MS assay[11]. As reported previously, we found that CEL can hydrolyze TAGs, DAGs, and CEs (**Figure 2.5**). However, CEL hydrolyzed FAHFAs at much greater rates than these reported substrates under the reaction conditions employed.

Analysis of the hydrolysis data also revealed that CEL had preferences among different FAHFAs. FAHFAs are divided into families and isomers. Families are comprised of different acyl chains (i.e. oleic acid or palmitic acid) and isomers describe the same acyl chain combination with the ester bond at different positions (**Figure 2.5**). Two clear preferences emerged from the substrate hydrolysis activity profile with different FAHFAs. First, and most dramatically, CEL preferentially hydrolyzed FAHFAs with the ester bond further away from the carboxylate (12-PAHSA > 9-PAHSA >> 5-PAHSA). A similar trend was observed for all the FAHFA families tested. Second, unsaturated FAHFAs were hydrolyzed more quickly than saturated FAHFAs (POHSAs/OAHSAs > PAHSAs/SAHSAs). The physiological significance of these trends is

unclear, but they do suggest that individual FAHFA isomers can be metabolized at different rates.

CEL has been linked to diabetes, exocrine pancreatic dysfunction and chronic pancreatitis[24,25]. As such, rare variants of the CEL gene can cause maturity-onset diabetes of the young (MODY), a hereditary, autosomal dominant form of diabetes[26]. The MODY type caused by CEL mutations is denoted MODY8. Considering further the metabolic and anti-inflammatory activities of FAHFAs, we tested the effect of a MODY8-associated human CEL mutant (1686delT) on 9-PAHSA and 9-OAHSA hydrolysis activity. The human CEL mutant exhibited a 2-fold increase in FAHFA hydrolysis compared with human CEL protein (**Figure 2.6**). We also tested the effect of NaTC on these two normal and disease-associated variants and both were bile-salt sensitive, with mutant CEL having slightly higher 9-PAHSA hydrolysis activity (**Figure 2.6**). Current evidence indicates that MODY8 mutations result in CEL variants that are prone to protein aggregation in the pancreas, which could induce tissue damage leading to the symptoms of pancreatic dysfunction[27,28]. While there is no dramatic enzymatic difference between normal CEL and the MODY8 mutant, aggregation of the latter could nevertheless lead to physiological changes in CEL activity, which again might affect endogenous FAHFA levels.

2.3 Conclusion

Knowing the substrates of an enzyme is a critical piece of information needed to understand its endogenous functions of the protein. In this study, we have utilized an unbiased approach that combines biochemistry and ABPP to characterize CEL as a FAHFA hydrolase. The complementary tissue distribution of CEL compared to other recently discovered FAHFA hydrolases – AIG1 and ADTRP – indicates the metabolism of FAHFAs may be differentially regulated across the body. Future studies with knockout mice and *in vivo*-active inhibitors of individual FAHFA hydrolases should enrich our understanding of the respective roles that these

enzymes and their lipid substrates play in mammalian biology and disease. In this regard, our results provide new hypothesis about the biochemical function of CEL that extends beyond previously established TAG/DAG and CE substrates to include the regulation of bioactive FAHFAs. Our findings may help to explain some of the endogenous phenotypes seen in CEL-/- mice, such as how CEL influences lipoprotein assembly and secretion[29] and how loss of CEL promotes atherosclerosis[30].

2.4 Figures

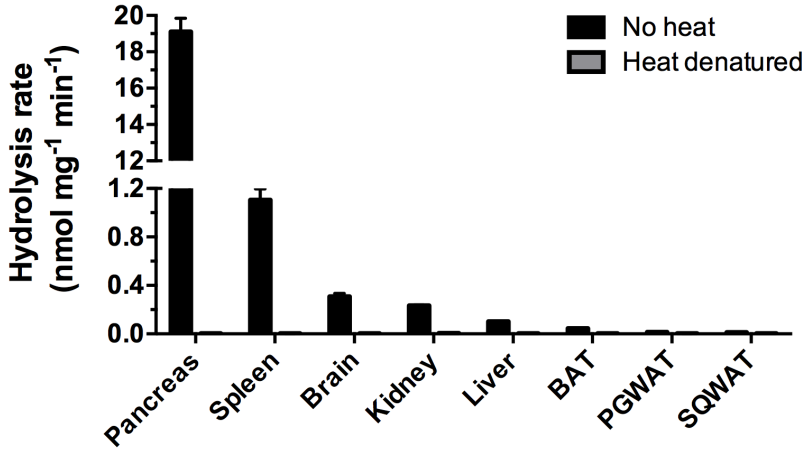

Figure 2.1. *In vitro* 9-PAHSA substrate hydrolysis assay for various murine tissues. Heat-denatured controls show loss of 9-PAHSA hydrolytic activity. Hydrolysis rate was determine by measuring comparing 9-HSA to the internal standard 9-HHDA and normalizing this to the weight of tissue and reaction time. Data represents mean ± s.e.m. for three biological replicates.

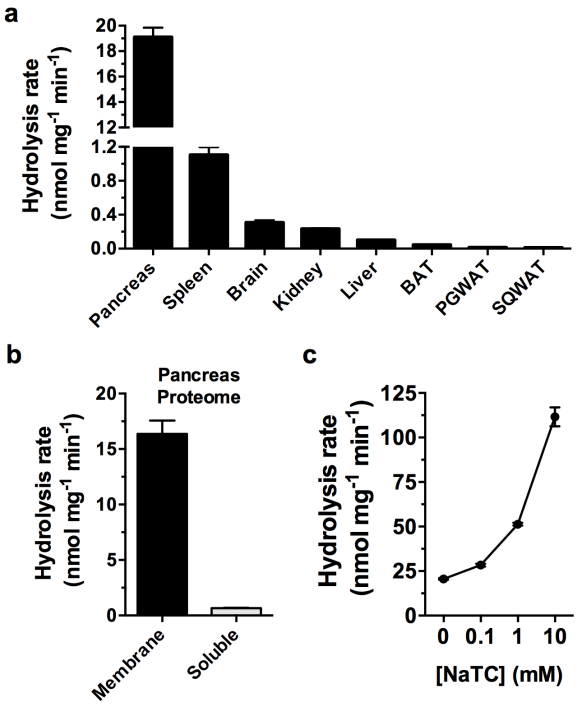

Figure 2.2. Identification of a bile salt-stimulated pancreatic FAHFA hydrolase. (**a**) Measurement of 9-PAHSA hydrolysis activity using tissue lysates from various tissues showed varying levels of FAHFA hydrolysis, with the pancreas having the highest activity. (**b**) Fractionation of the pancreas lysate into membrane and soluble proteomes revealed that the 9-PAHSA hydrolysis activity is largely membrane associated. (**c**) Addition of the bile salt sodium taurocholate (NaTC) increased 9-PAHSA hydrolysis identifying CEL as the most likely FAHFA hydrolase. Data represents mean ± s.e.m values for three biological replicates.

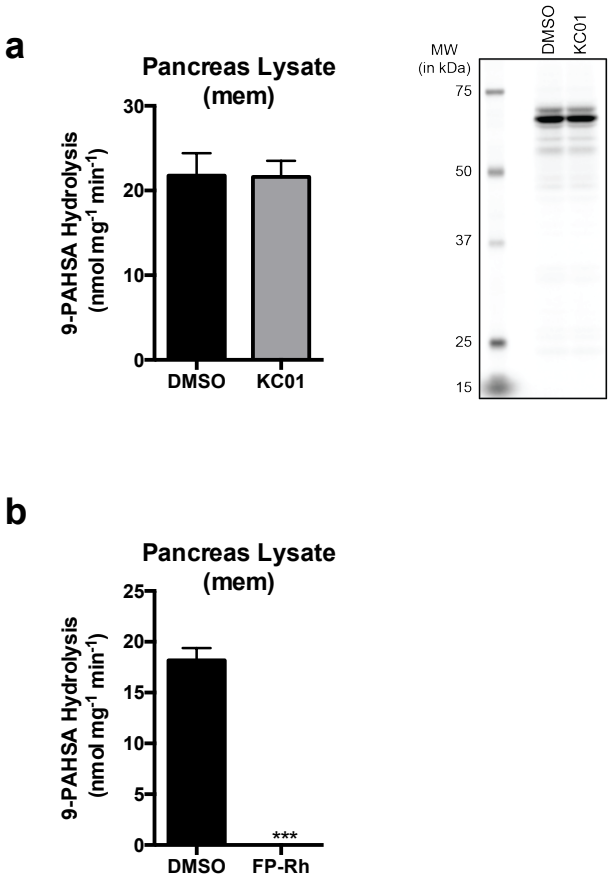

Figure 2.3. Pancreatic FAHFA hydrolysis is sensitive to FP-Rh but not KC01. (**a**) *In vitro* 9-PAHSA hydrolysis activity and full ABPP gel image for pancreas membrane lysates treated with DMSO and KC01 (10 μM). (**b**) *In vitro* 9-PAHSA hydrolysis activity for pancreas membrane lysates treated with DMSO and FP-Rh (10 μM). Data represents mean ± s.e.m for three biological replicates. ***$p < 0.001$ by Student's t-test

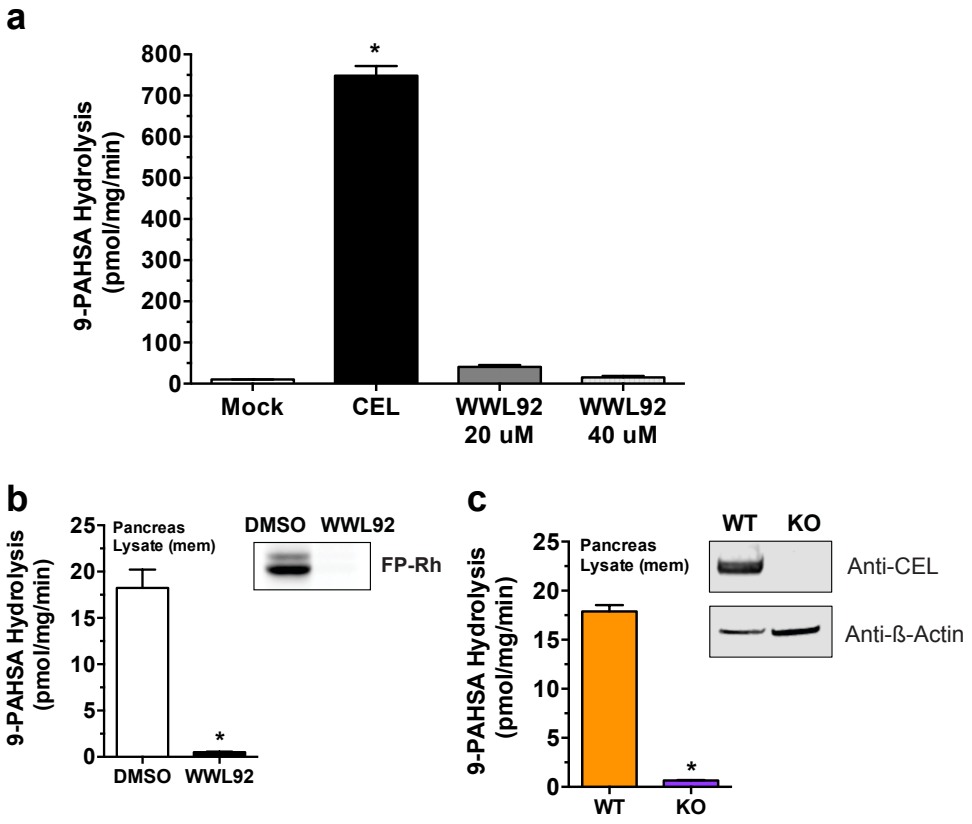

Figure 2.4. Identification of CEL as a FAHFA hydrolase. (**a**) 9-PAHSA hydrolysis activity for membrane lysates from mock-transfected and CEL-transfected HEK293T cells, and CEL-transfected membrane lysates treated with WWL92 (20 μM and 40 μM). Data represents mean ± s.d for two replicates. ***$p < 0.001$ by ANOVA. (**b**) 9-PAHSA hydrolysis and gel-based ABPP (inset) for WT pancreatic membrane lysates treated with DMSO or WWL92 (10 μM). (**c**) 9-PAHSA hydrolysis and western blot analysis (inset) of of $CEL^{+/+}$ and $CEL^{-/-}$ pancreatic membrane lysates. Data represents mean ± s.e.m. for three biological replicates. ***$p < 0.001$ by Student's t-test. Full images of gel and western blots are provided in **Figure 2.7**.

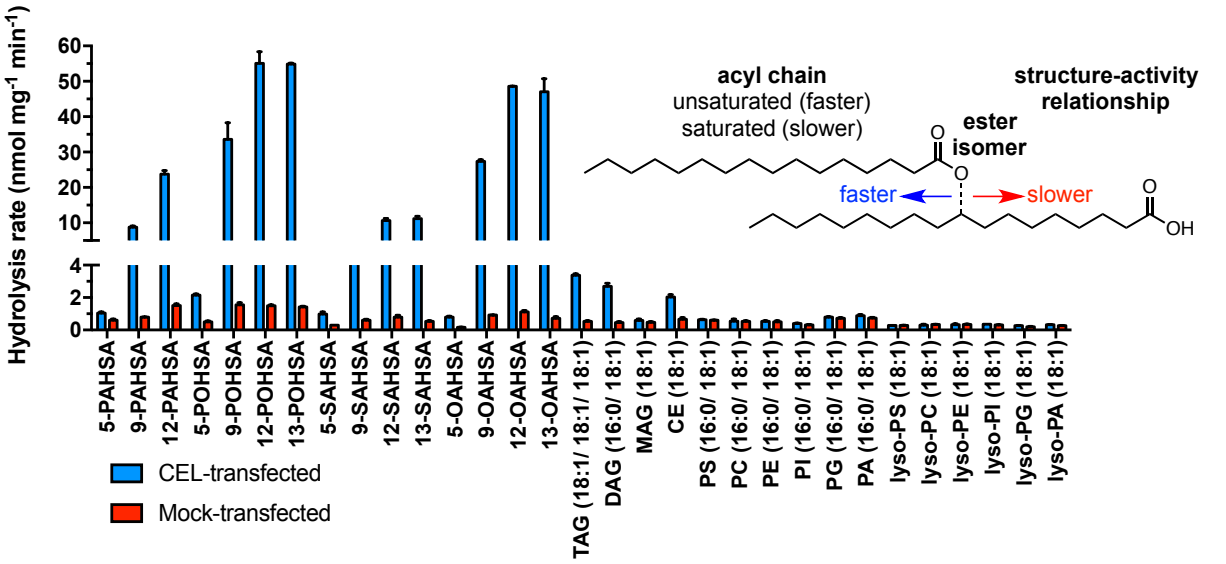

Figure 2.5. *In vitro* lipid substrate hydrolysis assay for cellular lysates of CEL- and mock-transfected HEK293T cells. PAHSA, palmitic acid ester of hydroxy-stearic acid; POHSA, palmitoleic acid ester of hydroxy-stearic acid; SAHSA, stearic acid ester of hydroxy-stearic acid; OAHSA, oleic acid ester of hydroxy-stearic acid; TAG, triacylglycerol (tri-C18:1); DAG, diacylglycerol (C16:0/C18:1); MAG, monoacylglycerol (C18:1); CE, cholesterol ester (C18:1); PS, phosphatidylserine (18:0, 18:2); PC, phosphatidylcholine (C17:0, C20:4); PE, phosphatidylethanolamine (C17:0, C20:4); PI, phosphatidylinositol (C16:0, C18:1); PG, phosphatidylglycerol (C16:0, C18:1); PA, phosphatidic acid (C17:0, C20:4); lyso-phospholipids (all C18:1). For each assay, 20 µg of mock or CEL-transfected proteome was incubated with 100 µM substrate for 30 min at 37 °C. Data represents mean ± s.d. for two replicates.

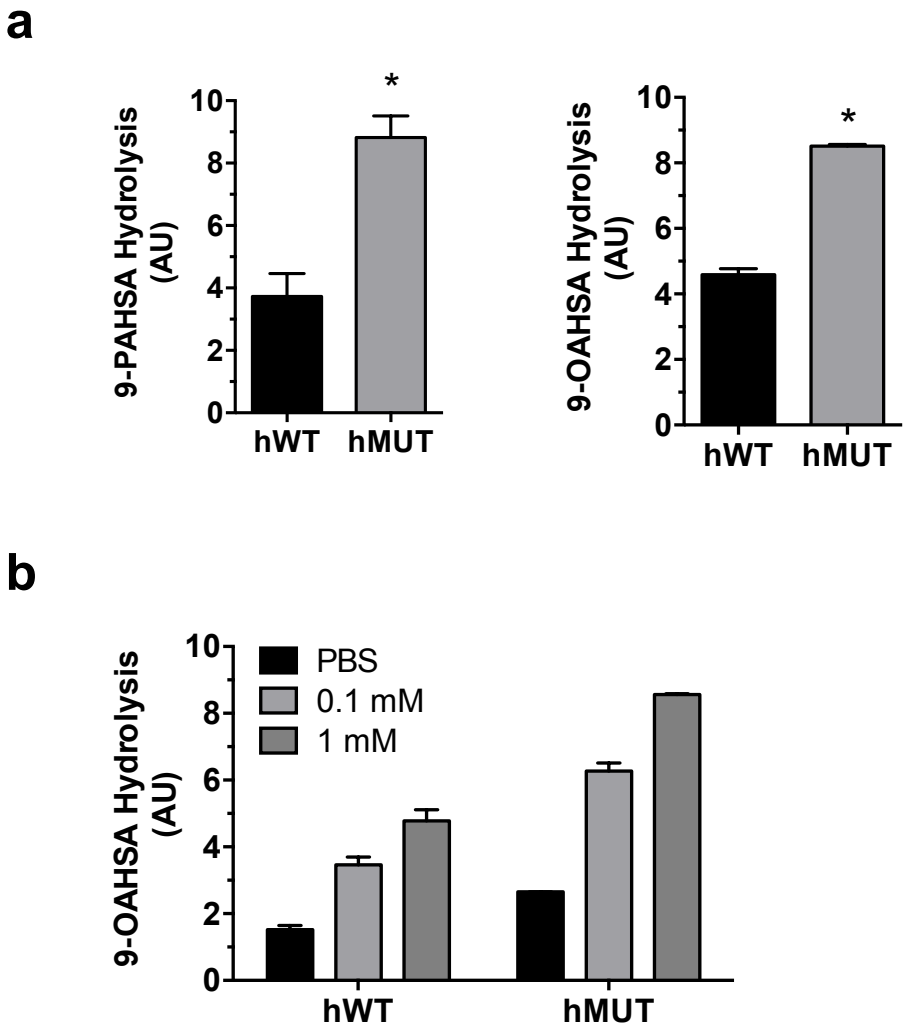

Figure 2.6. WT and MUT CEL hydrolysis of PAHSA and OAHSA (**a**) *In vitro* 9-PAHSA and 9-OAHSA hydrolysis activity comparing human normal wild type (hWT) CEL-transfected HEK293T cells and human MODY8 mutant (hMUT) CEL-transfected HEK293T cells. (**b**) The effect of NaTC on 9-PAHSA hydrolysis activity for hWT CEL and hMUT CEL-transfected membrane lysates. Hydrolysis rate was normalized to western blot expression of each construct, which was monitored by immunostaining for their V5 tag. AU (arbitrary units). Data represents mean ± s.d. for two biological replicates. *$p < 0.05$ by two-sided Student's *t*-test for hMUT.

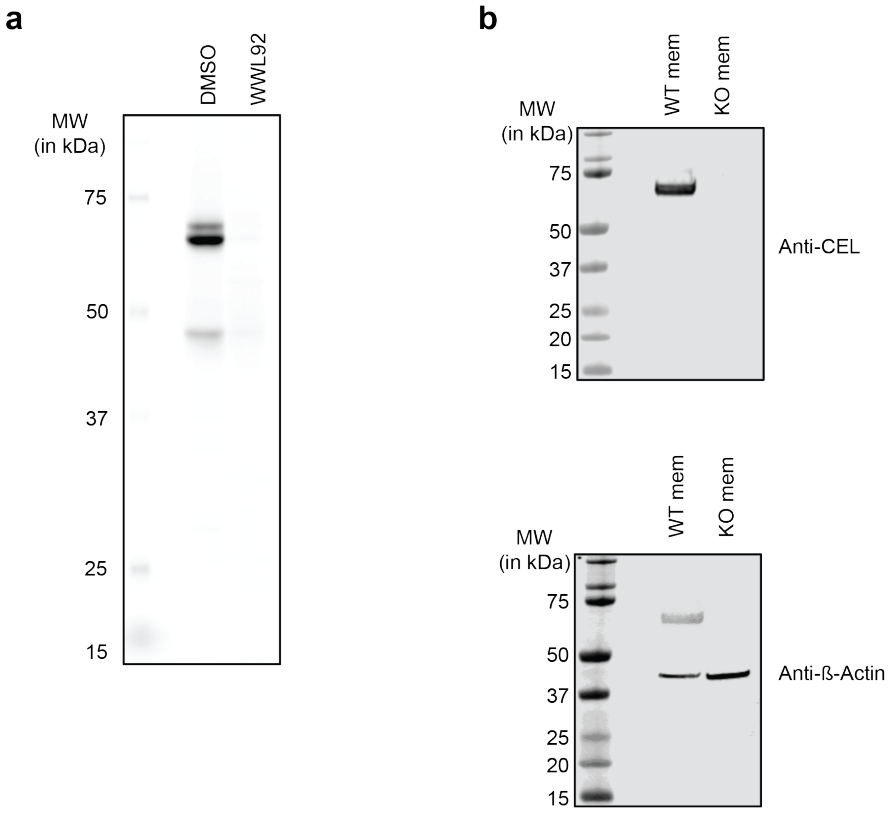

Figure 2.7. (**a**) Full ABPP gel image and (**b**) Western blots for **Figures 2.4b,c**.

2.5 Experimental Section

Chemicals. FAHFAs were purchased from Cayman Chemical and other lipids were purchased from Avanti Polar Lipids or Sigma-Aldrich. FP-rhodamine[31], WWL92[13], and 9-hydroxyheptadecanoic acid[32] were synthesized as reported.

Tissue lysate preparation. Wild-type C57BL/6J mice were purchased from Jackson Laboratories. All animals were housed in groups on a 14-h light, 10-h dark schedule at the Salk. All animal care and experimental procedures were in accordance with the standing committee on the Use of Animals in Research and Teaching at Salk and Institutional Animal Care and Use Committee (IACUC), and the National Institutes of Health Guidelines for the Humane Treatment of Laboratory Animals. Tissues were collected immediately after euthanasia and snap frozen using liquid nitrogen. Tissue lysates were prepared on ice by dounce homogenizing tissues in PBS. Homogenized lysates were centrifuged at 1,000 g for 10 min at 4 °C to pellet cell debris. The supernatant was then used as the total lysate for some assays. To prepare membrane and soluble fractions, the supernatant was separated by ultra-centrifugation at 100,000 x g for 45 min at 4 °C. Protein concentrations were measured using QuickStart Bradford 1x Dye Reagent (Bio-Rad). Aliquots were flash-frozen and stored at -80 °C for further use.

Gel-based ABPP analysis. Tissue and HEK293T cell proteomes (100 μL) were treated with FP-rhodamine (1 μM) for 30 min at 37 °C. Reactions were quenched by the addition of 4x SDS-PAGE loading buffer (40 μL). Competitive gel-based ABPP experiments were performed as previously described[33]. Samples were visualized in-gel using ChemiDoc MP imaging system (Bio-Rad). The fluorescence from rhodamine is presented in gray scale. 1 s and 5 s exposure times were used for native proteomes and CEL-transfected cell proteomes, respectively.

9-PAHSA and 9-OAHSA substrate hydrolysis assay and analysis. Tissue lysates/proteomes (20 μg) were incubated with lipid substrate (100 μM) in PBS (200 μL) at 37 °C with constant shaking. After 10 minutes, the reaction was stopped by addition of 2:1 mixture

of $CHCl_3$:MeOH (400 μL). 9-hydroxyheptadecanoic (9-HHDA) (50 pmol) was premixed into the $CHCl_3$:MeOH mixture as an internal standard. The mixture was vortexed and centrifuged at 2200 x g for 5 min. The bottom organic layer was collected and dried under a stream of nitrogen. The extract was then dissolved in MeOH (200 μL) and a portion of this sample (10 μL) analyzed by LC-MS using a Thermo TSQ Quantiva LC-MS fitted with an Acquity UPLC BEH C18 (1.7 μM; 2.1 mm x 100 mm; Waters). The LC solvents were as follows: buffer A, H_2O + 0.01% NH_4OH + 5 mM ammonium acetate; buffer B, 95:5 ACN:H_2O + 0.01% NH_4OH + 5 mM ammonium acetate. A typical LC run was 15 min long at 0.2 mL/min with a binary gradient consisting of the following steps: 50-90% buffer B over 6 min, 90-100% B over 0.1 min, 100% buffer B for 3 min, 100-50% buffer B over 0.1 min, and 50% buffer B for 6 minutes. MS analyses were performed using electrospray ionization (ESI) in negative ion mode with source parameters of 3kV spray voltage, ion transfer tube temperature of 325 °C, and a vaporizer temperature of 275 °C. Pseudo-MRM (collision energy (CE) of 9 V, RF lens set at 97 V) was used to detect 9-HSA (m/z 299.3 → 299.3) and 9-HHDA (m/z 285.3 → 285.3). Hydrolysis was quantified by measuring 9-HSA peak area and diving this by 9-HHDA peak area. The ratio of 9-HSA/9-HHDA was then multiplied by 50 pmol (internal standard amount) and then divided by the amount of proteome (20 μg) and reaction time (10 min) to afford hydrolysis rates. Data represents mean values for 2-3 independent replicates.

Broad substrate hydrolysis assay. 20 μg of proteome was incubated with 100 μM lipid substrate in a reaction volume of 250 μL PBS at 37 °C with constant shaking. After 30 minutes the reaction was quenched with 400 μL of 2:1 (vol/vol) $CHCl_3$: MeOH doped with internal standard (0.5 nmol C17:1 heptadecenoic acid (C17:1 FFA) and 0.05 nmol 9-hydroxyheptadecanoic acid (9-HHDA)). The mixture was vortexed and centrifuged at 2800 x g for 5 min to separate the aqueous (top) and organic (bottom) phase. The organic phase was collected and dried under a stream of N_2, re-solubilized in 100 μL of 2:1 (vol/vol) $CHCL_3$: MeOH,

and subjected to LC-MS analysis. A fraction of the organic extract (~15 μL) was injected onto an Agilent 6520 quadrupole-time-of-flight (QTOF) LC-MS and analyzed as described previously[34]. Data represents mean values for 2-3 replicates.

Western blotting. SDS-PAGE gels were transferred to PVDF membranes by iBlot2 Dry Blotting System (Life Technologies) according to manufacturer's protocol. Immunoblots were blocked with Odyssey blocking buffer (LI-COR). The primary antibodies and dilutions are as follows: anti-CEL (Rabbit, Proteintech, 15384-1-AP, 1:1,000), anti-V5 (Mouse, Invitrogen, R96025, 1:2,000), and anti-β Actin (Rabbit, LI-COR, 926-42210, 1:1000). Secondary antibodies anti-rabbit IRDye 800CW (goat, 926-32211, LI-COR) and anti-mouse (goat, 925-32210, LI-COR) were applied at a dilution of 1:10,000 in blocking buffer for visualization.

Cloning and recombinant expression of CEL constructs. Full-length cDNA encoding mouse CEL (GE Dharmacon, in pCMV-SPORT6) was cloned into the pcDNA3.1/V5-His (B) vector. Human CEL wild-type in pcDNA3.1/V5-His (B), Human CEL mutant (1686delT) in pcDNA3.1/V5-His (B), and empty vector pcDNA3.1/V5-His were the same a previously published[27,28]. To recombinantly express these CEL constructs, HEK293T cells were grown to 50% confluence in 10 cm tissue culture plates and transiently transfected with 12 μg of the desired construct using Lipofectamine 2000 (ThermoFisher Scientific) as the transfection reagent per the manufacturer's protocol. "Mock" transfected cells were transfected with 12 μg of empty vector. Thirty-six hours after transfection, cells were washed with PBS (3x), harvested by scraping, and lysed by sonication in PBS. Membrane and soluble fractions were separated by ultra-centrifugation at 100,000 x g for 45 min at 4 °C. Protein concentrations were measured using QuickStart Bradford 1x Dye Reagent (Bio-Rad).

2.6 Acknowledgements

Chapter 2, in full, is a reprint with minor modifications as it appears in Branched Fatty Acid Esters of Hydroxy Fatty Acids Are Preferred Substrates of the MODY8 Protein Carboxyl Ester Lipase, *Biochemistry* 55, 4636-4641 (2016). The dissertation author was the primary investigator and author of this paper. Other authors include Siddhesh S. Kamat, William H. Parsons, Edwin A. Homan, Timothy Maher, Odile D. Peroni, Ismail Syed, Karianne Fjeld, Anders Molven, Barbara B. Kahn, Benjamin F. Cravatt, and Alan Saghatelian.

2.7 References

1 Berg, J. M., Tymoczko, J. L. & Stryer, L. *Biochemistry*. (W. H. Freeman, 2010).

2 Vance, J. E. & Vance, D. E. *Biochemistry of Lipids, Lipoproteins and Membranes*. (Elsevier Science, 2008).

3 Saghatelian, A., Trauger, S. A., Want, E. J., Hawkins, E. G., Siuzdak, G. & Cravatt, B. F. Assignment of endogenous substrates to enzymes by global metabolite profiling. *Biochemistry* 43, 14332-14339 (2004).

4 Wenk, M. R. The emerging field of lipidomics. *Nature Reviews Drug Discovery* 4, 594-610 (2005).

5 Shevchenko, A. & Simons, K. Lipidomics: coming to grips with lipid diversity. *Nature reviews Molecular cell biology* 11, 593-598 (2010).

6 Saghatelian, A., McKinney, M. K., Bandell, M., Patapoutian, A. & Cravatt, B. F. A FAAH-regulated class of N-acyl taurines that activates TRP ion channels. *Biochemistry* 45, 9007-9015 (2006).

7 Yore, M. M., Syed, I., Moraes-Vieira, P. M., Zhang, T., Herman, M. A., Homan, E. A., Patel, R. T., Lee, J., Chen, S., Peroni, O. D., Dhaneshwar, A. S., Hammarstedt, A., Smith, U., McGraw, T. E., Saghatelian, A. & Kahn, B. B. Discovery of a class of endogenous mammalian lipids with anti-diabetic and anti-inflammatory effects. *Cell* 159, 318-332 (2014).

8 Carvalho, E., Kotani, K., Peroni, O. D. & Kahn, B. B. Adipose-specific overexpression of GLUT4 reverses insulin resistance and diabetes in mice lacking GLUT4 selectively in muscle. *Am J Physiol Endocrinol Metab* 289, E551-561 (2005).

9 Shepherd, P. R., Gnudi, L., Tozzo, E., Yang, H., Leach, F. & Kahn, B. B. Adipose cell hyperplasia and enhanced glucose disposal in transgenic mice overexpressing GLUT4 selectively in adipose tissue. *J Biol Chem* 268, 22243-22246 (1993).

10 Herman, M. A., Peroni, O. D., Villoria, J., Schon, M. R., Abumrad, N. A., Bluher, M., Klein, S. & Kahn, B. B. A novel ChREBP isoform in adipose tissue regulates systemic glucose metabolism. *Nature* 484, 333-338 (2012).

11 Parsons, W. H., Kolar, M. J., Kamat, S. S., Iii, A. B., Hulce, J. J., Saez, E., Kahn, B. B., Saghatelian, A. & Cravatt, B. F. AIG1 and ADTRP are atypical integral membrane hydrolases that degrade bioactive FAHFAs. *Nat Chem Biol* (2016).

12 Carey, M. C., Small, D. M. & Bliss, C. M. Lipid digestion and absorption. *Annual Review of Physiology* 45, 651-677 (1983).

13 Bachovchin, D. A., Ji, T., Li, W., Simon, G. M., Blankman, J. L., Adibekian, A., Hoover, H., Niessen, S. & Cravatt, B. F. Superfamily-wide portrait of serine hydrolase inhibition achieved by library-versus-library screening. *Proc Natl Acad Sci U S A* 107, 20941-20946 (2010).

14 Speers, A. E. & Cravatt, B. F. Activity-Based Protein Profiling (ABPP) and Click Chemistry (CC)–ABPP by MudPIT Mass Spectrometry. *Current protocols in chemical biology*, 29-41 (2009).

15 Blackberg, L. & Hernell, O. The bile-salt-stimulated lipase in human milk. Purification and characterization. *Eur J Biochem* 116, 221-225 (1981).

16 Chen, Q., Sternby, B. & Nilsson, A. Hydrolysis of triacylglycerol arachidonic and linoleic acid ester bonds by human pancreatic lipase and carboxyl ester lipase. *Biochim Biophys Acta* 1004, 372-385 (1989).

17 Hernell, O. Human milk lipases. III. Physiological implications of the bile salt-stimulated lipase. *Eur J Clin Invest* 5, 267-272 (1975).

18 Roussel, A., Yang, Y., Ferrato, F., Verger, R., Cambillau, C. & Lowe, M. Structure and activity of rat pancreatic lipase-related protein 2. *Journal of Biological Chemistry* 273, 32121-32128 (1998).

19 Morgan, R. & Huffman, N. The interacion of lipase, lipase cofactor and bile salts in triglyceride hydrolysis. *Biochimica et Biophysica Acta (BBA)-Lipids and Lipid Metabolism* 248, 143-148 (1971).

20 Aho, H. J., Sternby, B., Kallajoki, M. & Nevalainen, T. J. Carboxyl ester lipase in human tissues and in acute pancreatitis. *International Journal of Pancreatology* 5, 123-134 (1989).

21 Vesterhus, M., Raeder, H., Kurpad, A. J., Kawamori, D., Molven, A., Kulkarni, R. N., Kahn, C. R. & Njolstad, P. R. Pancreatic function in carboxyl-ester lipase knockout mice. *Pancreatology* 10, 467-476 (2010).

22 Weng, W., Li, L., van Bennekum, A. M., Potter, S. H., Harrison, E. H., Blaner, W. S., Breslow, J. L. & Fisher, E. A. Intestinal absorption of dietary cholesteryl ester is decreased but retinyl ester absorption is normal in carboxyl ester lipase knockout mice. *Biochemistry* 38, 4143-4149 (1999).

23 Howles, P. N., Carter, C. P. & Hui, D. Y. Dietary free and esterified cholesterol absorption in cholesterol esterase (bile salt-stimulated lipase) gene-targeted mice. *J Biol Chem* 271, 7196-7202 (1996).

24 Fjeld, K., Weiss, F. U., Lasher, D., Rosendahl, J., Chen, J. M., Johansson, B. B., Kirsten, H., Ruffert, C., Masson, E., Steine, S. J., Bugert, P., Cnop, M., Grutzmann, R., Mayerle, J., Mossner, J., Ringdal, M., Schulz, H. U., Sendler, M., Simon, P., Sztromwasser, P., Torsvik, J., Scholz, M., Tjora, E., Ferec, C., Witt, H., Lerch, M. M., Njolstad, P. R., Johansson, S. & Molven, A. A recombined allele of the lipase gene CEL and its pseudogene CELP confers susceptibility to chronic pancreatitis. *Nat Genet* 47, 518-522 (2015).

25 Raeder, H., Johansson, S., Holm, P. I., Haldorsen, I. S., Mas, E., Sbarra, V., Nermoen, I., Eide, S. A., Grevle, L., Bjorkhaug, L., Sagen, J. V., Aksnes, L., Sovik, O., Lombardo, D., Molven, A. & Njolstad, P. R. Mutations in the CEL VNTR cause a syndrome of diabetes and pancreatic exocrine dysfunction. *Nat Genet* 38, 54-62 (2006).

26 Molven, A. & Njølstad, P. R. Role of molecular genetics in transforming diagnosis of diabetes mellitus. *Expert review of molecular diagnostics* 11, 313-320 (2011).

27 Johansson, B. B., Torsvik, J., Bjorkhaug, L., Vesterhus, M., Ragvin, A., Tjora, E., Fjeld, K., Hoem, D., Johansson, S., Raeder, H., Lindquist, S., Hernell, O., Cnop, M., Saraste, J., Flatmark, T., Molven, A. & Njolstad, P. R. Diabetes and pancreatic exocrine dysfunction due to mutations in the carboxyl ester lipase gene-maturity onset diabetes of the young (CEL-MODY): a protein misfolding disease. *J Biol Chem* 286, 34593-34605 (2011).

28 Torsvik, J., Johansson, B. B., Dalva, M., Marie, M., Fjeld, K., Johansson, S., Bjorkoy, G., Saraste, J., Njolstad, P. R. & Molven, A. Endocytosis of secreted carboxyl ester lipase in a syndrome of diabetes and pancreatic exocrine dysfunction. *J Biol Chem* 289, 29097-29111 (2014).

29 Kirby, R. J., Zheng, S., Tso, P., Howles, P. N. & Hui, D. Y. Bile salt-stimulated carboxyl ester lipase influences lipoprotein assembly and secretion in intestine: a process mediated via ceramide hydrolysis. *J Biol Chem* 277, 4104-4109 (2002).

30 Kodvawala, A., Ghering, A. B., Davidson, W. S. & Hui, D. Y. Carboxyl ester lipase expression in macrophages increases cholesteryl ester accumulation and promotes atherosclerosis. *J Biol Chem* 280, 38592-38598 (2005).

31 Liu, Y., Patricelli, M. P. & Cravatt, B. F. Activity-based protein profiling: the serine hydrolases. *Proc Natl Acad Sci U S A* 96, 14694-14699 (1999).

32 Kahn, B. B., Herman, M. A., Saghatelian, A. & Homan, E. A. Lipids That Increase Insulin Sensitivity And Methods Of Using The Same. USA patent (2015).

33 Jessani, N., Niessen, S., Wei, B. Q., Nicolau, M., Humphrey, M., Ji, Y., Han, W., Noh, D. Y., Yates, J. R., 3rd, Jeffrey, S. S. & Cravatt, B. F. A streamlined platform for high-content functional proteomics of primary human specimens. *Nat Methods* 2, 691-697 (2005).

34 Kamat, S. S., Camara, K., Parsons, W. H., Chen, D. H., Dix, M. M., Bird, T. D., Howell, A. R. & Cravatt, B. F. Immunomodulatory lysophosphatidylserines are regulated by ABHD16A and ABHD12 interplay. *Nat Chem Biol* 11, 164-171 (2015).

Chapter 3:

AIG1 and ADTRP are Atypical Integral Membrane Hydrolases that Degrade Bioactive FAHFAs

Abstract

Enzyme classes may contain outlier members that share mechanistic, but not sequence or structural relatedness with more common representatives. The functional annotation of such exceptional proteins can be challenging. Here, we use activity-based profiling to discover that the poorly characterized multipass transmembrane proteins AIG1 and ADTRP are atypical hydrolytic enzymes that depend on conserved threonine and histidine residues for catalysis. Both AIG1 and ADTRP hydrolyze bioactive fatty-acid esters of hydroxy-fatty acids (FAHFAs), but not other major classes of lipids. We discover multiple cell-active, covalent inhibitors of AIG1 and show that these agents block FAHFA hydrolysis in mammalian cells. These results indicate that AIG1 and ADTRP are founding members of an evolutionarily conserved class of transmembrane threonine hydrolases involved in bioactive lipid metabolism. More generally, our findings demonstrate how chemical proteomics can excavate potential cases of convergent/parallel protein evolution that defy conventional sequence- and structure-based predictions.

3.1 Introduction

Activity-based protein profiling (ABPP) uses active site-directed chemical probes to study the functions of mechanistically and/or structurally related proteins in native biological settings[1-3]. ABPP probes are often broad-spectrum in their reactivity such that many members of an individual enzyme class can be characterized in parallel. A prominent example is the fluorophosphonate (FP) class of probes[4] that targets the serine (Ser) hydrolases, a large and diverse enzyme family that constitutes ~1% of all proteins in mammals and utilizes a conserved Ser nucleophile to hydrolyze amide, ester, and/or thioester bonds in biomolecules[5]. Prior work has demonstrated that FP probes provide extensive coverage of Ser hydrolases[6] and also react with some members of the much smaller class of threonine (Thr) hydrolases, such as the catalytic subunits of the proteasome[7]. FP probes do not cross-react with other classes of hydrolytic enzymes, including cysteine, aspartyl, and metallo-hydrolases, and this selectivity has facilitated the assignment of enzymes with established substrates to the Ser hydrolase class[8,9]. FP-probes can also be used in a competitive ABPP format, where biological samples are pre-treated with candidate small-molecule inhibitors that may compete for binding and/or reaction with targets of FP probes. Competitive ABPP has proven to be a robust platform for the discovery, optimization, and characterization of inhibitors of Ser hydrolases[2].

The Ser hydrolase family contains several sub-clans that are distantly, or even un-related to one another in terms of sequence, structure, and/or mechanism[5,10]. This remarkable diversity raises an intriguing question – might other, as-of-yet unassigned Ser (or Thr) hydrolases exist in the human proteome? Here, we hypothesized that reactivity with FP probes, being a near-universal feature of these enzymes, could provide a proteome-wide assay to discover cryptic members of the Ser/Thr hydrolase family that may have arisen by convergent or parallel evolution[11]. We evaluated human cell proteomes by quantitative, mass spectrometry (MS)-based ABPP, resulting in the discovery of a poorly characterized multipass transmembrane protein AIG1 as a highly FP-reactive protein. We show that AIG1, and the

sequence-related homologous protein ADTRP, possess conserved Thr and histidine (His) residues required for FP reactivity and find that both enzymes hydrolyze the fatty-acid esters of hydroxy-fatty acid (FAHFA) class of lipids *in vitro* and in human cells. Taken together, these data indicate that AIG1 and ADTRP represent a mechanistically novel class of Thr-dependent transmembrane hydrolases that regulate bioactive lipid metabolism in mammals.

3.2 Results

Discovery of AIG1 as an FP-reactive protein

We performed a series of competitive ABPP experiments where heavy and light amino acid-labeled proteomes from a human cancer cell line (SKOV3) were pre-treated with DMSO or an FP agent (FP-alkyne[12]) at a concentration (20 μM) and incubation time (1 h) that, based on previous studies[13], would be expected to fully label many serine hydrolases. We then exposed both DMSO-treated and FP-alkyne-blocked samples to a biotinylated FP probe (FP-biotin) and identified FP-biotin-labeled proteins by avidin enrichment and quantitative liquid chromatography (LC)-MS/MS analysis. Using this method, termed ABPP-SILAC[14], we identified a group of proteins that were blocked in their reactivity with FP-biotin by pre-treatment with FP-alkyne (defined as proteins that were highly enriched in DMSO-treated compared to FP-alkyne-treated proteomes). As expected, virtually all of these proteins were annotated Ser hydrolases (**Figure 3.1a**). However, within the group of FP-alkyne-sensitive proteins was one poorly characterized protein termed androgen-induced gene 1 protein (AIG1). Additional control experiments, as well as a review of legacy ABPP data sets performed in our lab, revealed that AIG1 was consistently enriched in studies that compared FP-biotin versus DMSO-treated proteomes (FP-probe-versus-no probe experiments) and showed a SILAC ratio of ~1 in probe-versus-probe control experiments where both heavy and light-labeled proteomes were treated with the same concentration of FP-biotin (**Figure 3.2**).

AIG1 is predicted to be a 28 kDa multipass transmembrane protein (with five-six predicted transmembrane domains; http://www.uniprot.org/uniprot/Q9NVV5) and was originally discovered as an androgen-induced gene product from human dermal papilla cells[15] and later found to interact with the E3 ligase Pirh2 by yeast two-hybrid screening[16]. The biochemical functions of AIG1, however, remain unknown. BLAST and HHpred searches failed to detect any sequence homology between AIG1 and known Ser/Thr hydrolases and also revealed that there are no proteins in the Protein Data Bank (PDB) with substantial sequence-relatedness to AIG1. These searches did, however, identify one protein in the human proteome that shares ~37% sequence identity with AIG1 – another poorly characterized protein termed ADTRP (androgen-dependent TFPI-regulating protein)[17]. We next set out to test whether AIG1 (and ADTRP) displayed biochemical properties consistent with those of a Ser hydrolase.

Conserved Thr and His residues in AIG1

We recombinantly expressed human AIG1 (hAIG1) as a C-terminal epitope-tagged protein in HEK293T cells and confirmed that this protein reacts with a rhodamine-conjugated FP probe (FP-Rh) by gel-based ABPP, which detected hAIG1 signals as 25 and 15 kDa bands in the membrane proteome of HEK293T cells (**Figure 3.3a**). FP-Rh-labeling of hAIG1 was time-dependent (**Figure 3.3b**), irreversible (**Figure 3.3c**), and competitively blocked by pre-treatment with FP-alkyne (**Figure 3.3a**). We also found that both the rat and mouse variants of AIG1 reacted with FP-Rh (**Figure 3.4**). Notably, when variants of AIG1 were expressed without a C-terminal epitope tag, we observed that they migrated as ~15-17 kDa proteins, which was substantially lower in molecular mass than that predicted from their full sequences (see below for further discussion). Recombinantly expressed human and mouse ADTRP were also labeled by FP-Rh and migrated as ~15 kDa proteins (**Figure 3.4**).

The protein sequence of hAIG1 contains 15 Ser residues, but, surprisingly, none of them were conserved across AIG1/ADTRP homologues from different species (**Figure 3.1b** and

Figure 3.5). On the other hand, we identified a single Thr residue (Thr-43 in hAIG1) that was completely conserved (**Figure 3.1b** and **Figure 3.5**). We next mutated several Ser/Thr residues within the hAIG1 sequence to alanine (Ala, or A), including Thr-43 (T43), expressed these AIG1 variants in HEK293T cells, and evaluated their reactivity with FP-Rh by gel-based ABPP. Among the 15 individual Ser/Thr-to-Ala mutant proteins evaluated, only the T43A mutant showed a complete loss of FP-labeling (**Figure 3.6a** and **Figure 3.7**). We also mutated the corresponding Thr residue in ADTRP (T47; **Figure 3.1b**) and the resulting T47A mutant showed a similar loss of FP-labeling (**Figure 3.6b**).

Despite extensive efforts using established LC-MS methods for mapping small-molecule probe-labeling sites in proteins[18], we were unsuccessful in directly identifying Thr-43 as the site of FP-reactivity in AIG1. Thr-43 is predicted to reside within a long and hydrophobic tryptic peptide (aa 41-67), which may have complicated its detection by MS. We do note, however, that our ABPP-SILAC experiments with FP probes, in aggregate, provided 74% overall coverage of the AIG1 sequence and, in none of these experiments, was an unmodified form of the tryptic peptide bearing Thr-43 detected (**Figure 3.8**).

Ser/Thr hydrolases also possess conserved basic residues that activate the Ser/Thr nucleophile for catalysis. In most (but not all) Ser hydrolases, this basic residue is a histidine (His), while catalytic proteasomal subunits and other N-terminal Thr (or Ser or Cys) nucleophile-dependent enzymes use the N-terminal α-amine group as a base[19,20]. Review of the sequence alignment of AIG1 with homologous proteins identified a single conserved His residue His134 (**Figure 3.1b**). Mutation of His134 to Ala in AIG1 (H134A) eliminated FP-labeling (**Figure 3.6c**), while mutation of two other non-conserved His residues (H32A and H150A mutants) had no effect (**Figure 3.7**). Mutation of the corresponding conserved His residue in ADTRP to alanine (H131A) also blocked FP labeling of this protein (**Figure 3.6d**).

We next analyzed the protein sequences for both AIG1 and ADTRP using six different transmembrane topology prediction programs (CCTOP, Phobius, PSORT II, TMHMM, TMpred,

and Uniprot) and found that these programs consistently predicted that both the conserved Thr and His residues of AIG1 and ADTRP were located within transmembrane domains of these proteins (**Figure 3.9**).

AIG1 and ADTRP hydrolyze FAHFA lipids

The strong reactivity displayed by AIG1 and ADTRP with FP probes and the dependency of these interactions on conserved Thr and His residues suggested that these poorly characterized proteins could represent a novel class of Thr hydrolases. The predicted multipass transmembrane structure of AIG1 and ADTRP also led us to hypothesize that one or more lipids may serve as substrates for these enzymes. We directly tested this premise by screening AIG1 and ADTRP against a panel of lipid substrates. The membrane lysates of hAIG1- and hADTRP-transfected HEK293T cells showed negligible hydrolytic activity above a mock-transfected control proteome with the majority of tested lipid substrates, including common classes of (lyso)-phospholipids and neutral lipids (e.g., tri-, di- and mono-glycerides) (**Figure 3.10a**). In contrast, both AIG1 and ADTRP-transfected cell membrane lysates robustly hydrolyzed several fatty-acid esters of hydroxy-fatty acids (FAHFAs) (**Figure 3.10a** and **Figure 3.11a**). FAHFAs are a recently identified class of bioactive lipids isolated from murine adipose tissue and their levels correlate with insulin sensitivity in both rodents and humans[21]. AIG1 and ADTRP displayed a preference for FAHFAs with branching distal from the carboxylate head group of the lipids (**Figure 3.10a**).

The FAHFA hydrolase activities of AIG1 and ADTRP were abolished by mutating their putative catalytic nucleophilic residues Thr-43 and Thr-47, respectively (**Figure 3.10b** and **Figure 3.11b**). Of note, mutation of Thr-43 to Ser in AIG1 impaired, but did not totally eliminate FAHFA hydrolytic activity or FP labeling of the mutant protein (**Figure 3.10b,c**). We also tested the H134A mutant of AIG1 and H131A mutant of ADTRP and found that these proteins showed

no detectable FAHFA hydrolase activity above a mock-transfected control (**Figure 3.10d** and **Figure 3.11c**).

Discovery and characterization of AIG1 inhibitors

Beyond their reactivity with FPs, many Ser/Thr hydrolases are sensitive to inhibition by other types of small molecules, in particular, compounds bearing electrophilic carbonyl centers[2]. We performed competitive gel-based ABPP experiments with a structurally diverse library of carbamates[22], β-lactones[23], and activated ureas[14] and identified several compounds that blocked FP-Rh labeling of hAIG1 (**Figure 3.12a**). Inhibitors of AIG1 included the β-lactone KC01[23] and the *N*-hydroxyhydantoin (NHH) carbamate JJH260 (**1**) (**Figure 3.13a**), which blocked FP-labeling of AIG1 with IC_{50} values of 0.17 ± 0.03 μM and 0.50 ± 0.14 μM, respectively (**Figure 3.13b** and **Figure 3.12b**) and $k_{obs}/[I]$ values of 2820 ± 780 $M^{-1}s^{-1}$ and 300 ± 25 $M^{-1}s^{-1}$, respectively (**Figure 3.12c**). Both KC01 and JJH260 also inhibited FAHFA hydrolysis by AIG1 with IC_{50} values of 0.21 ± 0.08 μM and 0.57 ± 0.14 μM, respectively (**Figure 3.13c**). We finally identified structurally related inactive control compounds – the β-lactone tetrahydrolipstatin (THL) and the NHH carbamate ABC34[22] (**Figure 3.13a**) – that did not inhibit the FP reactivity (**Figure 3.13b** and **Figure 3.12b**) or FAHFA hydrolysis activity (**Figure 3.13c**) of AIG1. KC01 and JJH260 also inhibited ADTRP as assessed by competitive gel-based ABPP, albeit with much lower potency (IC_{50} values of 1.3 and 8.5 μM, respectively; **Figure 3.14**).

The activity of KC01 suggested that a fluorescent analogue WHP01[23] might also serve as a tailored activity-based probe for AIG1. Consistent with this premise and with a covalent mode of inhibition of AIG1 by β-lactones, we found that wild-type hAIG1, but not the T43A mutant, was robustly labeled by WHP01 in transfected HEK293T cell membrane proteomes (**Figure 3.15**).

KC01[23], THL[24], and ABC34[22] have been previously characterized for their selectivity across the Ser hydrolase class by competitive ABPP experiments. We complemented these past studies by also evaluating the selectivity profile of JJH260 by ABPP-SILAC in human cancer cell proteomes, which confirmed inhibition of endogenously expressed AIG1 and established ABHD6, LYPLA1, and LYPLA2 as additional off-targets of JJH260 (**Figure 3.16a**). PPT1, a common target of NHH carbamates[22], was also found to be inhibited at low micromolar concentrations of JJH260 by gel-based ABPP (**Figure 3.16b**). Comparing the inhibitor selectivity profiles revealed complementary sets of off-targets, as neither LYPLA1 nor LYPLA2 were inhibited by KC01[23], while the AIG1-inactive control compound ABC34 blocked both ABHD6 and PPT1[22] (**Figure 3.13d**). Thus, we concluded that the function of AIG1 could be pharmacologically characterized in biological systems by evaluating the effects of both active compounds (KC01 and JJH260) compared to their inactive controls (THL and ABC34).

AIG1 is a principal FAHFA hydrolase in human cells

Little is known about how FAHFAs are inactivated in human cells, so we next asked whether AIG1 was a principal regulator of the metabolism of this lipid class *in situ*. RNA expression profiling indicated strong AIG1 expression in the human prostate cancer cell line (LNCaP)[25], which we confirmed by ABPP-MudPIT (12 spectral counts/1 mg proteome). We were also able to detect a 15 kDa WHP01-reactive band in LNCaP cells by gel-based ABPP, and the WHP01 labeling of this protein was blocked by pre-treatment with KC01 and JJH260, but not THL and ABC34 (**Figure 3.17a**), consistent with its designation as endogenous AIG1. Both KC01 and JJH260, but not THL or ABC34 also inhibited the FAHFA hydrolase activity of LNCaP cell lysates, which was mostly found in the membrane fraction (**Figure 3.18a,b**). We next established an *in situ* FAHFA hydrolysis assay by treating human cells with a doubly isotopically labeled substrate [$^{13}C_{16}$]-palmitic acid (PA) ester of [$^{2}H_{19}$]-9-hydroxy-stearic acid (HSA) (^{13}C,^{2}H-PAHSA; **Figure 3.17b**). Cells were treated with inhibitor or control compound (5

μM) for 4 h followed by the addition of $^{13}C,^{2}H$-PAHSA (2 μM, 5 mL of media) for 2 h, and then harvested and PAHSA and its hydrolytic products – $^{13}C_{16}$-PA and $^{2}H_{19}$-9-HSA ($^{2}H_{19}$-HSA) – extracted and analyzed by LC/MS. After first validating this experimental approach with multiple concentrations of $^{13}C,^{2}H$-PAHSA and HEK293T cells that heterologously express AIG1 (**Figure 3.18c,d**), we measured $^{13}C,^{2}H$-PAHSA hydrolysis in LNCaP cells treated with various inhibitors. KC01 and JJH260-treated cells exhibited a substantial (~70-80%) reduction in $^{13}C_{16}$-PA and $^{2}H_{19}$-HSA products, while cells treated with the control compounds THL and ABC34 showed negligible alterations in $^{13}C,^{2}H$-PAHSA hydrolysis compared to DMSO-treated cells (**Figure 3.17c**). A similar profile of inhibitor activity on $^{13}C,^{2}H$-PAHSA hydrolysis was observed in AIG1-transfected HEK293T cells (**Figure 3.18e**).

We complemented these pharmacological studies by knocking down AIG1 expression in LNCaP cells using RNA-interference (RNAi) technology. We generated two stable shRNA-knockdown lines targeting AIG1 (shAIG1-1 and -2 lines) and a control line expressing an shRNA targeting an unrelated protein (GFP; shControl line). Substantial and selective reductions in AIG1 expression were observed in both shAIG1 lines compared to the shControl line by gel-based ABPP using the tailored and broad-spectrum probes WHP01 and FP-Rh, respectively (**Figure 3.17d** and **Figure 3.19a**). Proteomic lysates from shAIG1 lines also showed significant reductions in 9-PAHSA hydrolysis compared to lysates from the shControl line (**Figure 3.19b**). We next treated shAIG1 and shControl cells with $^{13}C,^{2}H$-PAHSA and observed a ~70% reduction in hydrolysis products in the shAIG1 cells compared to shControl or uninfected cell lines (**Figure 3.17e**). Finally, we analyzed FAHFA hydrolysis in human T-cells, where we detected AIG1 by gel-based ABPP (**Figure 3.20a**). The FAHFA hydrolase activity of human T-cell membrane lysates was substantially reduced following treatment with KC01 or JJH260, but not THL or ABC34 (**Figure 3.20b**). Similar results were obtained for *in situ* experiments, where pre-treatment of human T-cells with KC01 or JJH260, but not THL or ABC34 blocked the

cellular hydrolysis of $^{13}C,^{2}H$-PAHSA (**Figure 3.17f**). These results, taken together, indicate that AIG1 functions as a major FAHFA hydrolase in human cells.

3.3 Discussion

We have discovered herein using ABPP that the poorly characterized multipass transmembrane proteins AIG1 and ADTRP represent a new family of hydrolytic enzymes that degrade the FAHFA class of signaling lipids. Several lines of biochemical evidence support that AIG1 and ADTRP use conserved Thr and His residues as a catalytic nucleophile and base, respectively. That these residues are generally predicted to be embedded within transmembrane domains of AIG1 and ADTRP indicates these enzymes could have evolved to perform hydrolytic chemistry within the cell membrane environment, reminiscent of the regulated intramembrane proteolysis (RIP) class of transmembrane proteases[26-29], which have also been studied by ABPP[30-32]. This feature, if experimentally validated, may endow AIG1 and ADTRP with a special capacity to hydrolyze FAHFAs, which, unlike most neutral- and phospho-lipids, possess ester bonds along the length of their otherwise hydrophobic acyl chains, and these bonds are presumably also buried within the lipid bilayer. It is not yet clear why AIG1 and ADTRP migrate as much lower MW proteins than that predicted from their sequence, but it is possible that these proteins are proteolytically processed in cells or migrate aberrantly by SDS-PAGE due to their high transmembrane content[33]. We also do not yet understand the functional differences between AIG1 and ADTRP, although we note that the cell/tissue distributions of these enzymes are quite distinct, with AIG1 being broadly expressed with highest signals in brain and macrophages, and ADTRP showing a more restricted profile of expression principally in metabolic organs, such as liver, kidney, intestine, and brown fat (biogps.org).

We have identified an initial set of pharmacological tools to study AIG1, including multiple classes of lead inhibitors (KC01, JJH260) and structurally related inactive control compounds (THL, ABC34), as well as tailored ABPP probes (WHP01) for enhanced detection of

endogenous AIG1 activity in native proteomes. While further research will be required to optimize the potency and specificity of AIG1 (and ADTRP) inhibitors, we should note that NHH carbamates have been developed into selective and *in vivo*-active inhibitors for other Ser hydrolases[22]. If optimized inhibitors verify that AIG1 and/or ADTRP regulate FAHFA metabolism *in vivo*, these enzymes could represent new targets for treating metabolic disorders, such as type 2 diabetes[21].

Finally, we offer some speculation on the existence of additional outlier members of the Ser/Thr hydrolase class. Our studies to date of FP-reactive proteins in mammalian cells have not uncovered clear examples of other proteins beyond AIG1 and ADTRP that lack designation as Ser/Thr hydrolases (e.g., see **Figure 3.1a**), suggesting that the annotation of enzymes from this class may be near-completion in humans. The HHpred search results, however, uncovered a distinct set of uncharacterized AIG1/ADTRP-like proteins that possess the conserved Thr and His residues and are found in non-mammalian eukaryotic organisms (Panther family PTHR12242; members in insects, plants, protozoa, and other non-vertebrates). Microbial proteomes also remain much less extensively characterized, and, considering their massive evolutionary and metabolic diversity[34], we would not be surprised if bacteria contain many additional classes of unassigned Ser/Thr hydrolases. Our findings underscore the power of chemical proteomic methods like ABPP for the discovery and functional characterization of such enzymes.

3.4 Figures and Tables

a

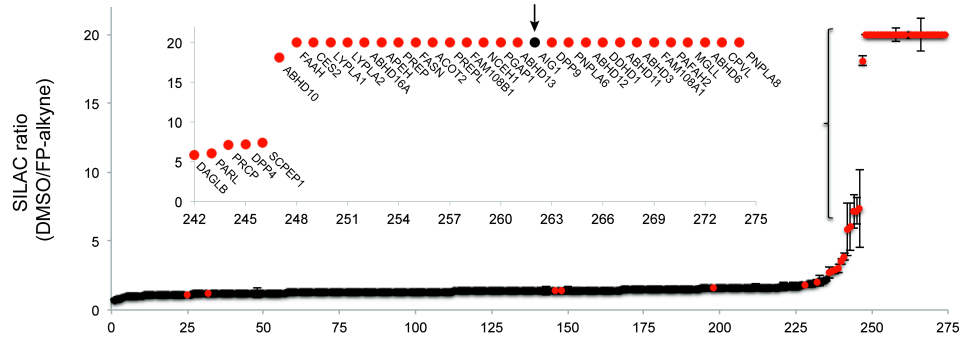

b

Figure 3.1. Discovery and characterization of AIG1 and ADTRP as FP-reactive proteins in the human proteome. (**a**) Competitive ABPP-SILAC analysis to identify FP-alkyne-inhibited proteins, where protein enrichment and inhibition were measured in proteomic lysates from SKOV3 cells treated with FP-alkyne (20 μM, 1 h) or DMSO using the FP-biotin probe following established protocols[14]. Annotated Ser hydrolases are indicated by red markers; AIG1 is marked in black and with an arrow. Data represent the median SILAC ratios ± s. d. for peptides quantified for each protein from one experiment representative of two biological replicates. (**b**) Sequence alignment of AIG1 orthologues from multiple species, as well as homologous ADTRP proteins (http://www.st-va.ncbi.nlm.nih.gov/tools/cobalt/cobalt.cgi). Residues conserved between all sequences are marked with asterisks. The conserved Thr (Thr43 in human AIG1) and His (His134 in human AIG1) residues are boxed in red.

Figure 3.2. Additional analysis of AIG1 signals in MS-based ABPP experiments. (**a**) Upper graph, mean spectral count values for AIG1 in previous ABPP-MudPIT experiments performed on human cancer cell lines using the FP-biotin probe. These data were extracted from reference [35] and show enrichment of AIG1 from FP-biotin, but not no-probe control experiments performed with cancer cell membrane proteomes. Lower graph, ABPP-SILAC analysis of a control experiment comparing proteins from heavy amino acid-labeled SKOV3 cell proteome treated with FP-biotin (5 μM) with proteins from an untreated light amino acid-labeled SKOV3 cell proteome, confirming enrichment of the Ser hydrolases identified in **Figure 3.1a** (including AIG1). Data represent the median SILAC ratios ± s. d. for peptides quantified for each protein from two biological replicates. (**b**) ABPP-SILAC analysis of a control experiment comparing FP-biotin-enriched proteins from heavy and light amino acid-labeled SKOV3 cell proteomes each treated with the same concentration of FP-biotin (5 μM), confirming a SILAC ratio of ~1.0 for the Ser hydrolases identified in **Figure 3.1a** (including AIG1). Data represent the median SILAC ratios ± s. d. for peptides quantified for each protein from two biological replicates.

a

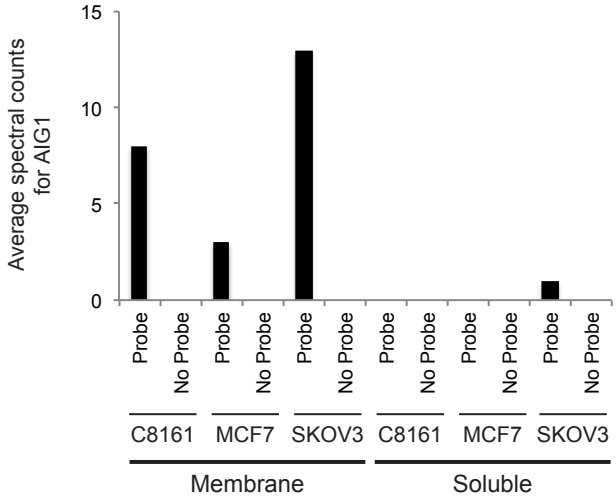
Average spectral counts for AIG1
15
10
5
0
Probe
No Probe
C8161
MCF7
SKOV3
Membrane
Soluble

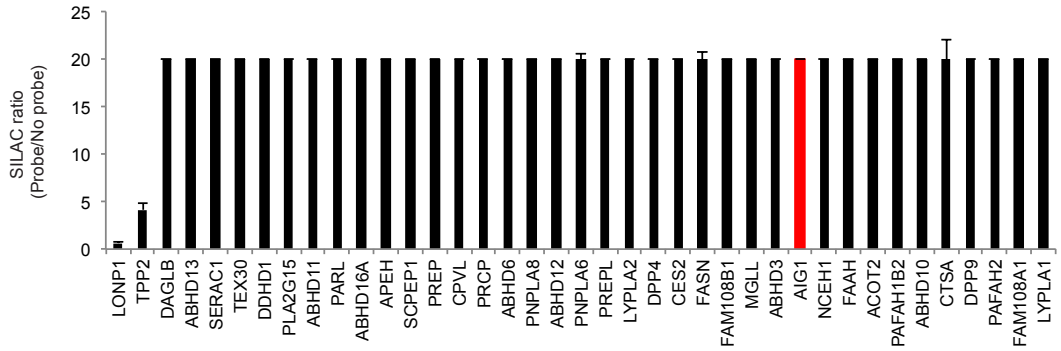
SILAC ratio (Probe/No probe)
25
20
15
10
5
0
LONP1
TPP2
DAGLB
ABHD13
SERAC1
TEX30
DDHD1
PLA2G15
ABHD11
PARL
ABHD16A
APEH
SCPEP1
PREP
CPVL
PRCP
ABHD6
PNPLA8
ABHD12
PNPLA6
PREPL
LYPLA2
DPP4
CES2
FASN
FAM108B1
MGLL
ABHD3
AIG1
NCEH1
FAAH
ACOT2
PAFAH1B2
ABHD10
CTSA
DPP9
PAFAH2
FAM108A1
LYPLA1

b

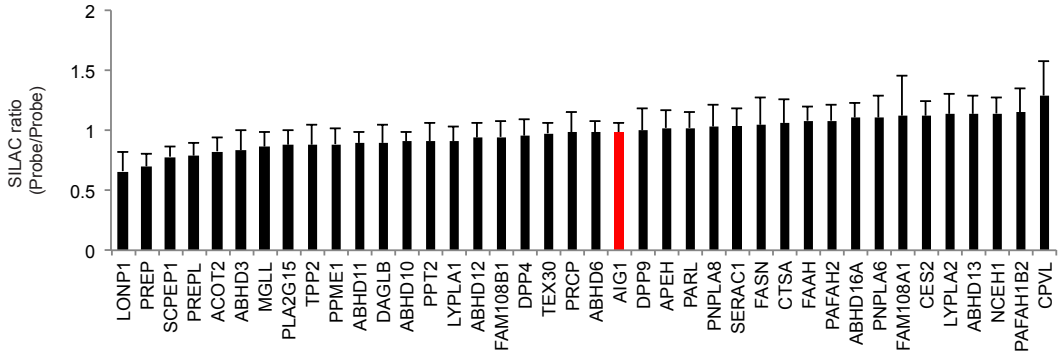
SILAC ratio (Probe/Probe)
2
1.5
1
0.5
0
LONP1
PREP
SCPEP1
PREPL
ACOT2
ABHD3
MGLL
PLA2G15
TPP2
PPME1
ABHD11
DAGLB
ABHD10
PPT2
LYPLA1
ABHD12
FAM108B1
DPP4
TEX30
PRCP
ABHD6
AIG1
DPP9
APEH
PARL
PNPLA8
SERAC1
FASN
CTSA
FAAH
PAFAH2
ABHD16A
PNPLA6
FAM108A1
CES2
LYPLA2
ABHD13
NCEH1
PAFAH1B2
CPVL

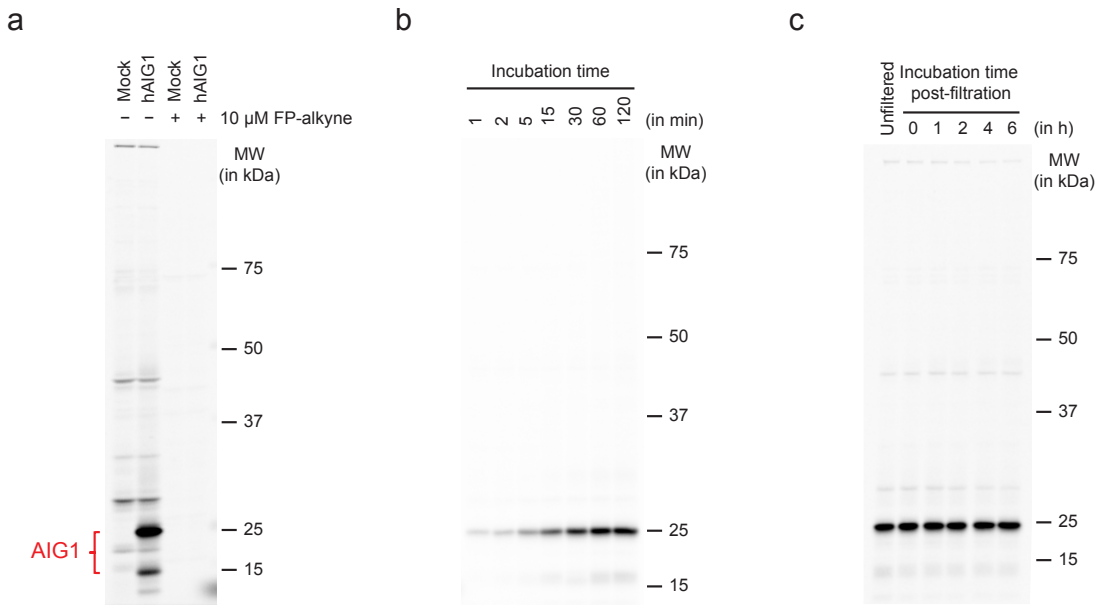

Figure 3.3. Characterization of FP-reactivity of recombinant hAIG1. (**a**) ABPP gel of the membrane proteomes (1.0 mg proteome mL^{-1}) of mock- and hAIG1-transfected HEK293T cells showing FP-labeling of AIG1. Proteomes were treated with either DMSO or FP-alkyne for 30 min at 37 °C, followed by FP-rhodamine (1 µM, 30 min, 37 °C). (**b**) ABPP gel of the membrane proteome (0.5 mg proteome mL^{-1}) of hAIG1-transfected HEK293T cells showing time course of FP labeling. Proteomes were treated with 1 µM FP-Rh at 37 °C for the indicated time. (**c**) ABPP gel of the membrane proteome (0.5 mg proteome mL^{-1}) of hAIG1-transfected HEK293T cells showing irreversibility of FP labeling. Proteome was treated with FP-rhodamine (1 µM, 30 min, 37 °C) and, following gel filtration to remove excess probe, samples were incubated at 37 °C for the indicated time before SDS-PAGE and in-gel fluorescence scanning.

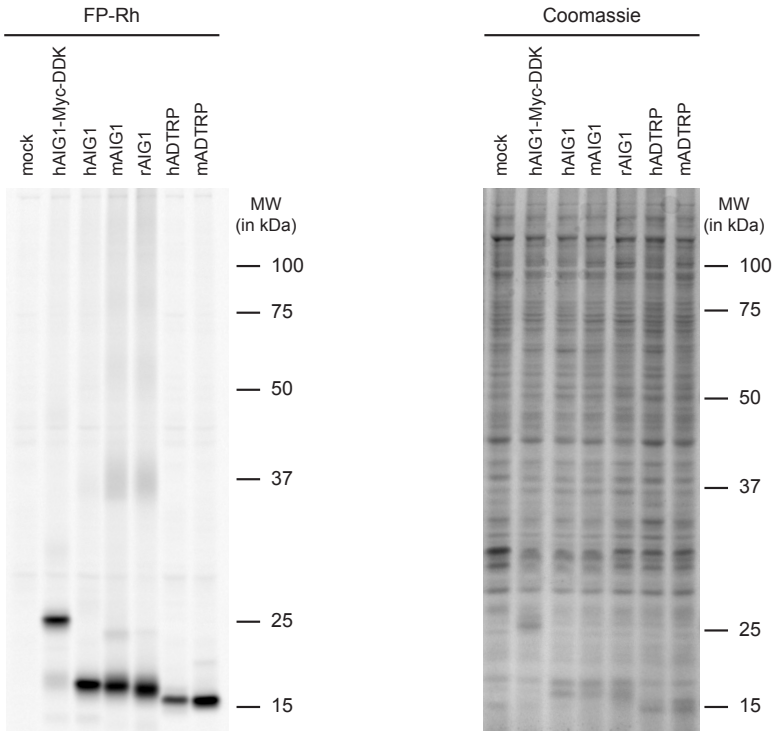

Figure 3.4. AIG1 and ADTRP orthologues also react with FP probes. *Left image*, ABPP gel of the membrane proteomes (0.5 mg proteome mL^{-1}) of mock-, C-terminal-tagged hAIG1-, and untagged hAIG1-, mouse (m)AIG1-, rat (r)AIG1-, hADTRP-, and mADTRP-transfected HEK293T cells demonstrating labeling of all variants by FP-Rh. Proteomes were treated with 1 μM FP-Rh for 30 min at 37 °C and analyzed by SDS-PAGE and in-gel fluorescence scanning. *Right image*, Coomassie blue-stained gel to assess relative protein expression (right gel).

a

```
H. sapiens                  MALVPCQVLRMAILLSYCSILCNYKAIEMPSHQTYGGSWKFLTFIDLVIQAVFFGICVLT
M. mulatta                  MALVPCQVLRVAILLSYCSILCNYKAIEMPSHQTYGGSWKFLTFIDLVIQAVFFGICVLT
C. lupus                    MALVPCQVLRVAILLSYCSILCNYKAIEMPSHQTYGGSWKFLTFIDLVIQAVFFGICVLT
B. taurus                   MALVPCQVLRVAILLSYCSILCNYKAIEKPSHQTYGGSWKFLTFIDLVIQAVFFGICVLT
M. musculus                 MALVPCQVLRVAILLSYCSILCNYKAIEMPSHQTYGGSWKFLTFIDLVIQAVFFGICVLT
R. norvegicus               MALVPCQVLRVAILLSYCSILCNYKAIEMPSHQTYGGSWKFLTFIDLVIQAVFFGICVLT
G. gallus                   MALVPCQVLRAAILLSYCSILCNYKAIDMPAHQTYGGSWKFLTFIDLVIQAVFFGICVLT
X. tropicalis               MALIPCQVLRAAILLSYLSVLCHYKAIEMPAHQTYGGSWKFLTFIDLVIQAVFFGICVLS
                            *** ****** ****** * ** ****  * ***********************

H. sapiens                  DLSSLLTRGSGNQEQERQLKKLISLRDWMLAVLAFPVGVFVVAVFWIIYAYDREMIYPKL
M. mulatta                  DLSSLLTRGSGNQEQERQLKKLISLRDWMLAVLAFPVGVFVVAVFWIIYAYDREMIYPKL
C. lupus                    DLSSLLTRGSGNQEQERQLKKLISLRDWMLAVLAFPVGVFVVAVFWIIYAYDREMIYPKL
B. taurus                   DLSSLLTRGSGNQEQERQLKKLISLRDWMLAVLAFPVGVFVVAVFWIIYAYDREMIYPKL
M. musculus                 DLSSLLTRGSGNQEQERQLRKLISLRDWTLAVLAFPVGVFVVAVFWTIYAYDREMIYPRL
R. norvegicus               DLSSLLTRGSGNQEQERQLRKLISLRDWTLAVLAFPVGVFVVAVFWTIYAYDREMIYPRL
G. gallus                   DLSSLLTKGNDSQEQERQLKKLISLRDWMMAVLAFPIGVFVVTMFWSIYIYDRELVYPKL
X. tropicalis               DLSSLLTKGSDNQEQERQLKKLISLRDWVMAVLAFPVGVFVVTMFWILYIYDRELVYPKL
                            ******* *   ******* ********  ****** *****  **  * ****  ** *

H. sapiens                  LDNFIPGWLNHGMHTTVLPFILIEMRTSHHQYPSRSSGLTAICTFSVGYILWVCWVHHVT
M. mulatta                  LDNFIPGWLNHGMHTTVLPFILIEMRTSHHQYPSRSSGLTAICTFSVGYILWVCWVHHVT
C. lupus                    LDNFIPGWLNHGMHTTVLPFILIEMRTSHHAYPSRSSGLAAICTFSVGYILWVCWIHHVT
B. taurus                   LDNFIPGWLNHGMHTTVLPFILIEMRTSHHAYPSRSSGLAAICTFSVGYILWVCWVHHVT
M. musculus                 LDNFIPGWLNHGMHTTVLPFILIEMRTSHHQYPSRSSGLAAICTFSVGYILWVCWIHHVT
R. norvegicus               LDNFIPGWLNHGMHTTVLPFILIEMRTSHHQYPSRSSGLAAICTFSVGYILWVCWIHHVT
G. gallus                   LDNFIPAWLNHGMHTTVLPFILIEMRTTHHQYPSRSCGLAAVCTFAVGYILWVCWIHHVT
X. tropicalis               LDNFIPPWLNHGMHTTVLPFILIEMRTTHHQYPSRTCGIVTVCLFSICYILWVCWVHHMT
                            ****** ******************** ** ****  *    * *   ******* ** *

H. sapiens                  GMWVYPFLEHIGPGARIIFFGSTTILMNFLYLLGEVLNNYIWDTQK---S----------
M. mulatta                  GMWVYPFLEHIGPGARIIFFGSTTILMNFLYLLGEVLNNYIWDTQRKPLS----------
C. lupus                    GMWVYPFLEHIGPGARIVFFGSTTILMNFLYLLGEVLNSYIWDTQR---T----------
B. taurus                   GMWVYPFLEHIGPGARILFFGSTTILMNFLYLLGEVLNSYIWDTQR---S----------
M. musculus                 GMWVYPFLEHIGSGARIIFFGSTTILMNFLYLLGEVLNSYIWDTQR---TKAPSCQDTQS
R. norvegicus               GMWVYPFLEHIGSGARIIFFGSTTLLMNSLYLLGEALNSYIWDAPR---S----------
G. gallus                   GVWVYPLLEHLSPGVKIIFFAAVTVVINIFYVMGEVLNNYIWDTQK---C----------
X. tropicalis               GMWVYPLLEYISPGAKIVFFIIVTVVINMFYILGEKLNNFIWEAEK---C----------
                            * **** **    *  * **   *   *  *  ** **  **

H. sapiens                  ------------------MEEEKEK-----PKLE
M. mulatta                  ------------------WQDMKINFMYLGPSS-
C. lupus                    ------------------AE--PRN-----PM--
B. taurus                   ------------------MEEDKEK-----PKLE
M. musculus                 SLSCAKPVQNLCKDTFMLEGGKAR-----A---
R. norvegicus               ------------------LEEEKEK-----PKLE
G. gallus                   ------------------IEEEKEK-----PKLD
X. tropicalis               ------------------DALRDKR-----PKMD
```

b

```
hADTRP          MTKTSTCIYHFLVLSWYTFLNYYISQEGKDEVKPKILANGARWKYMTLLNLLLQTIFYGV
mADTRP          MTKTTTCVYHFLVLNWYIFLNYHIPQIGRNEEKLREFHDGGRSKYLTLLNLLLQAIFFGV
                **** ** ****** ** **** * * *  * *      * * ** *******  ** **

hADTRP          TCLDDVLKRTKGGKDIKFLTAFRDLLFTTLAFPVSTFVFLAFWILFLYNRDLIYPKVLDT
mADTRP          ACLDDVLKRVIGRKDIKFVTSFRDLLFTTMAFPISTFVFLVFWTLFHYDRSLVYPKGLDD
                 ********  * ***** * ******** *** ****** ** ** * * * *** **

hADTRP          VIPVWLNHAMHTFIFPITLAEVVLRPHSYPSKKTGLTLLAAASIAYISRILWLYFETGTW
mADTRP          FFPAWVNHAMHTSIFPFSLFETILRPHNYPSKKLGLTLLGAFNFAYIIRILWRYVQTGNW
                  * * ******* ***  * *  **** ***** ***** *   *** **** *  ** *

hADTRP          VYPVFAKLSLLGLAAFFSLSYVFIASIYLLGEKLNHWKWGDMRQPRKKRK
mADTRP          VYPVFDSLSPLGIIIFFSAAYILVAGIYLFGEKINHWKWGAIAKPQMKKN
                *****  ** **   ***  *   * *** *** ******    *  *
```

Figure 3.5. Additional sequence alignments of AIG1 and ADTRP proteins from different species. (**a**) Sequence alignment of AIG1 orthologues across multiple species (http://www.st-va.ncbi.nlm.nih.gov/tools/cobalt/cobalt.cgi). Asterisks indicate residues conserved across all of the displayed proteins; the proposed Thr nucleophile and His base are shown in red. (**b**) Sequence alignment of mouse and human ADTRP (http://www.stva.ncbi.nlm.nih.gov/tools/cobalt/cobalt.cgi). Asterisks indicate residues conserved between the two sequences; the proposed Thr nucleophile and His base are shown in red.

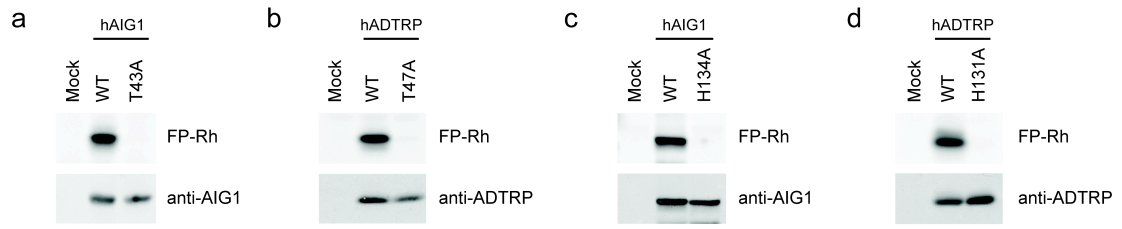

Figure 3.6. Identification of Thr and His residues critical for FP labeling of AIG1 and ADTRP. (**a-d**) ABPP gels and Western blots of membrane proteomes (0.5 mg proteome mL^{-1}) showing selective FP-Rh labeling of WT-, but not the indicated Thr-to-Ala and His-to-Ala mutants of human (h) AIG1 (**a, c**) and ADTRP (**b, d**) in transfected HEK293T cell lysates. Proteomes were treated with 1 μM FP-Rh for 30 min at 37 °C. Full images of gels and Western blots are provided in **Figure 3.21**.

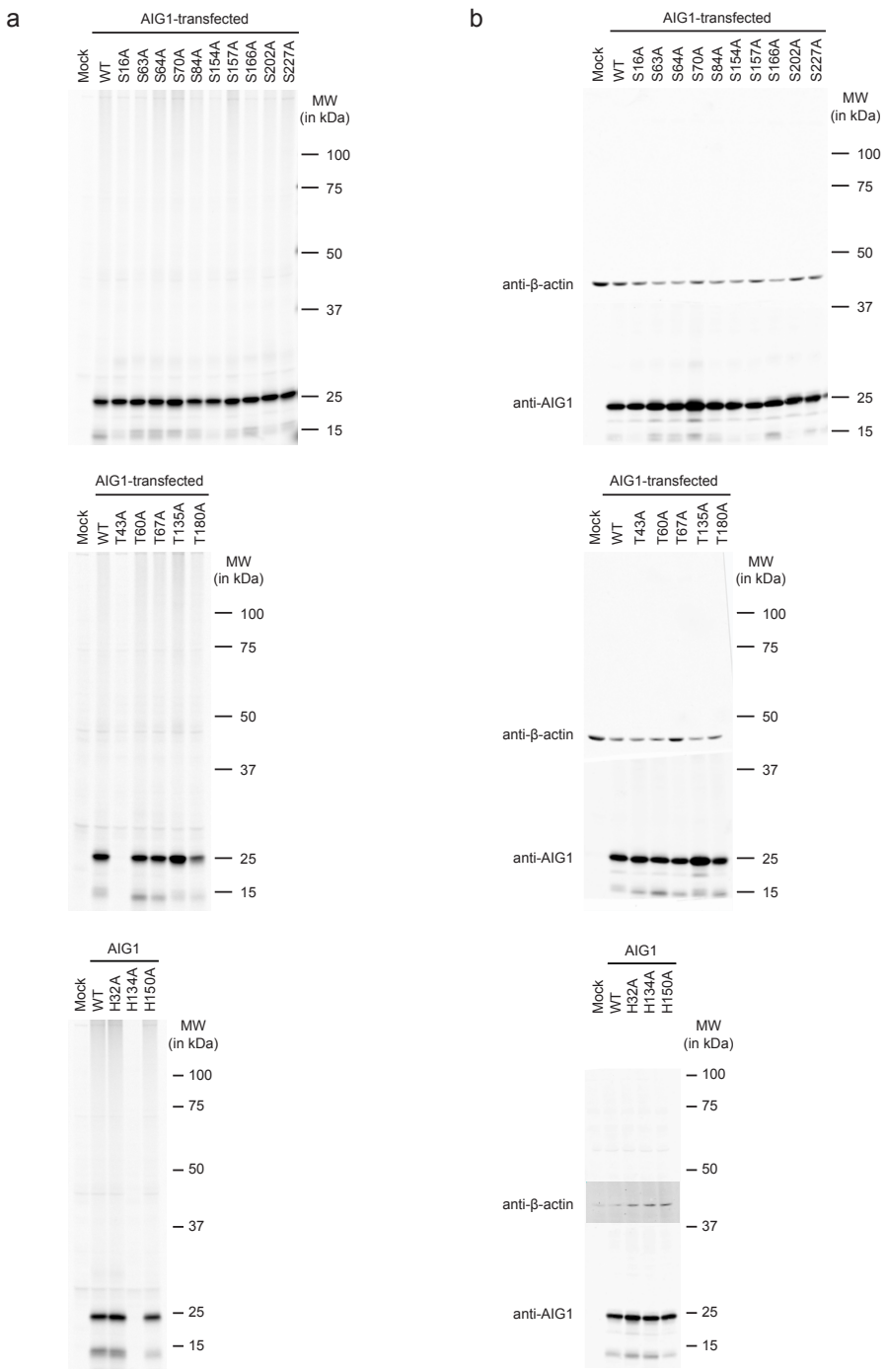

Figure 3.7. Assessment of FP reactivity of hAIG1 Ser, Thr, and His mutants. (**a**) ABPP gels of membrane proteomes (0.5 mg proteome mL^{-1}) of mock-, wild-type hAIG1-, and mutant hAIG1-transfected HEK293T cells. Proteomes were treated with 1 μM FP-Rh for 30 min at 37 °C and analyzed by SDS-PAGE and in-gel fluorescence scanning. (**b**) Western blots of membrane proteomes (0.5 mg proteome mL^{-1}) of mock-, wild-type hAIG1-, and mutant hAIG1-transfected HEK293T cells. β-actin was measured as a loading control.

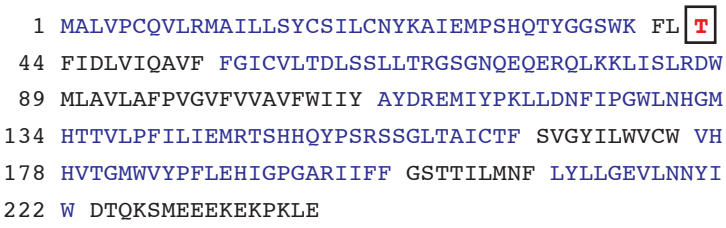

Figure 3.8. Sequence coverage of hAIG1 enriched and characterized from transfected HEK293T cells using ABPP-MudPIT and ABPP-SILAC experiments with the FP-biotin probe. Portions of the hAIG1 sequence observed by LC-MS are colored in blue; Thr43 is boxed and colored red.

Figure 3.9. Predicted transmembrane domains and topology of AIG1 and ADTRP. Predicted transmembrane domains and topology maps for AIG1 (**a**) and ADTRP (**b**) based on six different transmembrane topology prediction programs (CCTOP, Phobius, PSORT II, TMHMM, TMpred, and Uniprot). Each table entry represents the span of residues in the protein sequence predicted to be transmembrane-embedded by the indicated program. Five of the six programs predict six transmembrane domains (TM1 through TM6) for AIG1 and ADTRP. In the topology maps, residues are color-coded based on the percentage of programs that predict localization in the membrane. Thr-43 and His-134 of AIG1 and Thr-47 and His-131 of ADTRP are indicated in red.

a

Program	TM1	TM2	TM3	TM4	TM5	TM6
Uniprot	1-21	39-59	88-108	124-144	167-187	197-217
Tmpred	3-27	41-59	88-112	124-143	161-184	194-213
PSORT II	6-22	42-58	92-108	——	158-174	197-213
TMHMM	13-30	45-67	88-110	125-144	157-179	194-216
Phobius	7-27	47-67	88-108	128-147	159-185	197-217
CCTOP	8-27	44-66	88-110	127-145	158-177	194-214

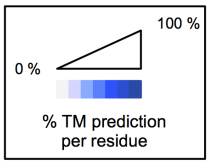

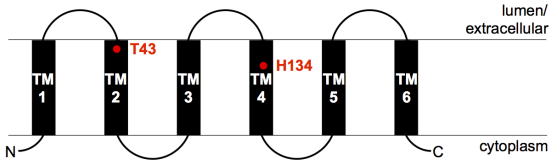

b

Program	TM1	TM2	TM3	TM4	TM5	TM6
Uniprot	4-24	47-67	86-106	120-140	155-175	190-210
Tmpred	6-25	45-63	91-109	121-144	156-175	190-211
PSORT II	——	47-63	90-106	——	155-171	188-204
TMHMM	7-25	45-64	85-107	122-144	156-173	188-210
Phobius	7-25	45-64	85-105	125-144	156-175	190-210
CCTOP	7-27	45-64	85-107	125-144	154-173	192-211

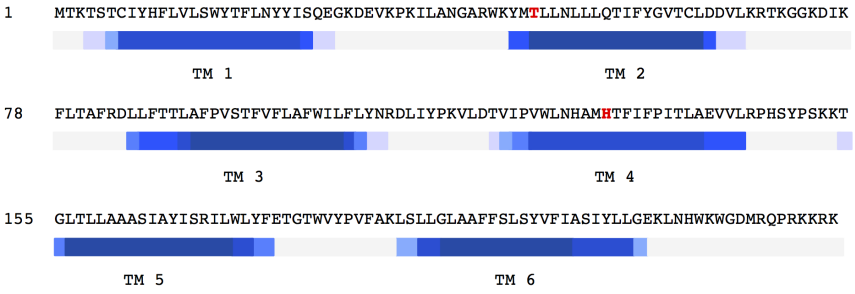

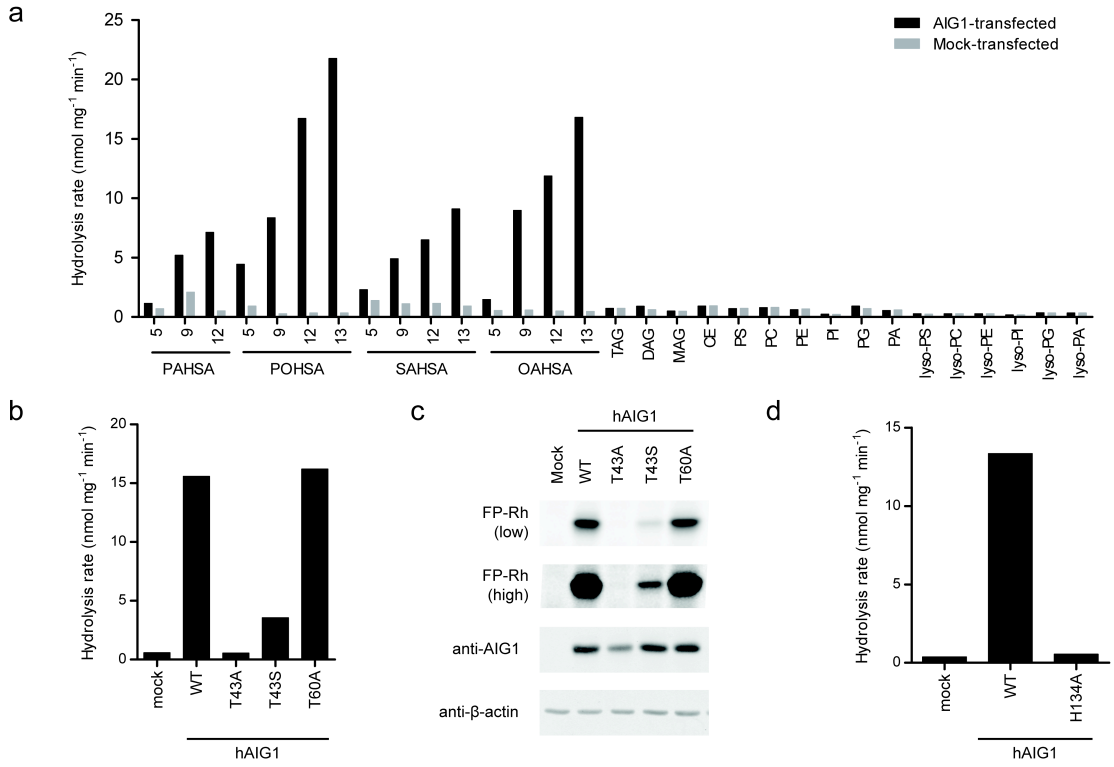

Figure 3.10. AIG1 and ADTRP are FAHFA hydrolases. (**a**) *In vitro* lipid substrate hydrolysis assays for membrane proteomes of mock and hAIG1-transfected HEK293T cells. PAHSA, palmitic acid ester of hydroxy-stearic acid; POHSA, palmitoleic acid ester of hydroxy-stearic acid; SAHSA, stearic acid ester of hydroxy-stearic acid; OAHSA, oleic acid ester of hydroxy-stearic acid; TAG, triacylglycerol (tri-C18:1); DAG, diacylglycerol (C16:0/C18:1); MAG, monoacylglycerol (C18:1); CE, cholesterol ester (C18:1); PS, phosphatidylserine (18:0, 18:2); PC, phosphatidylcholine (C17:0, C20:4); PE, phosphatidylethanolamine (C17:0, C20:4); PI, phosphatidylinositol (C16:0, C18:1); PG, phosphatidylglycerol (C16:0, C18:1); PA, phosphatidic acid (C17:0, C20:4); lyso-phospholipids (all C18:1). For each assay, 20 µg of mock or AIG1-transfected proteome was incubated with 100 µM substrate for 30 min at 37 °C. Data represent mean values for two biological replicates. (**b-d**) 12-OAHSA hydrolysis (**b, d**) and gel-based ABPP (**c**) assays for membrane proteomes from mock, wild-type hAIG1, and mutant hAIG1-transfected HEK293T cells. For (**b, d**), 20 µg of each proteome was incubated with 100 µM 12-OAHSA for 30 min at 37 °C. Data represent mean values for two biological replicates. For (**c**), proteomes were treated with 1 µM FP-Rh for 30 min at 37 °C, and β-actin was used as a loading control for gel experiments. Low and high exposures of the FP-Rh-labeled samples are shown to demonstrate the residual FP-labeling observed with the T43S, but not T43A mutant of hAIG1. Full images of the gel and Western blot are provided in **Figure 3.22**.

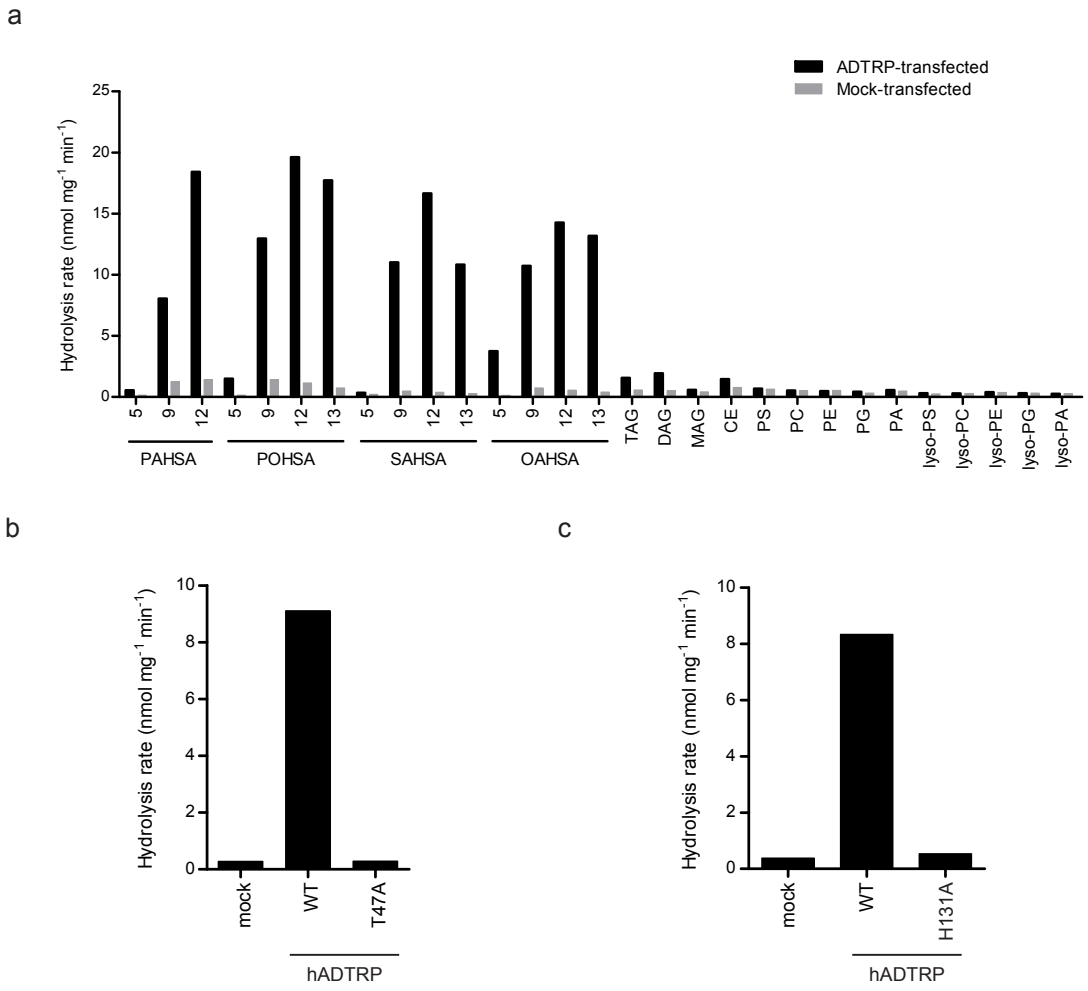

Figure 3.11. ADTRP shows FAHFA hydrolase activity. (**a**) *In vitro* lipid substrate hydrolysis assays for membrane proteomes of mock- and hADTRP-transfected HEK293T cells. See legend for **Figure 3** for definitions of lipid substrates. For each assay, 20 µg of mock or ADTRP-transfected proteome was incubated with 100 µM substrate for 30 min at 37 °C. Data represent mean values for two biological replicates. (**b** & **c**) *In vitro* 12-OAHSA hydrolysis assays for the membrane proteomes of mock, wild-type hADTRP, and mutant hADTRP-transfected HEK293T cells. 20 µg of each proteome was incubated with 100 µM 12-OAHSA for 30 min at 37 °C. Data represent mean values for two biological replicates.

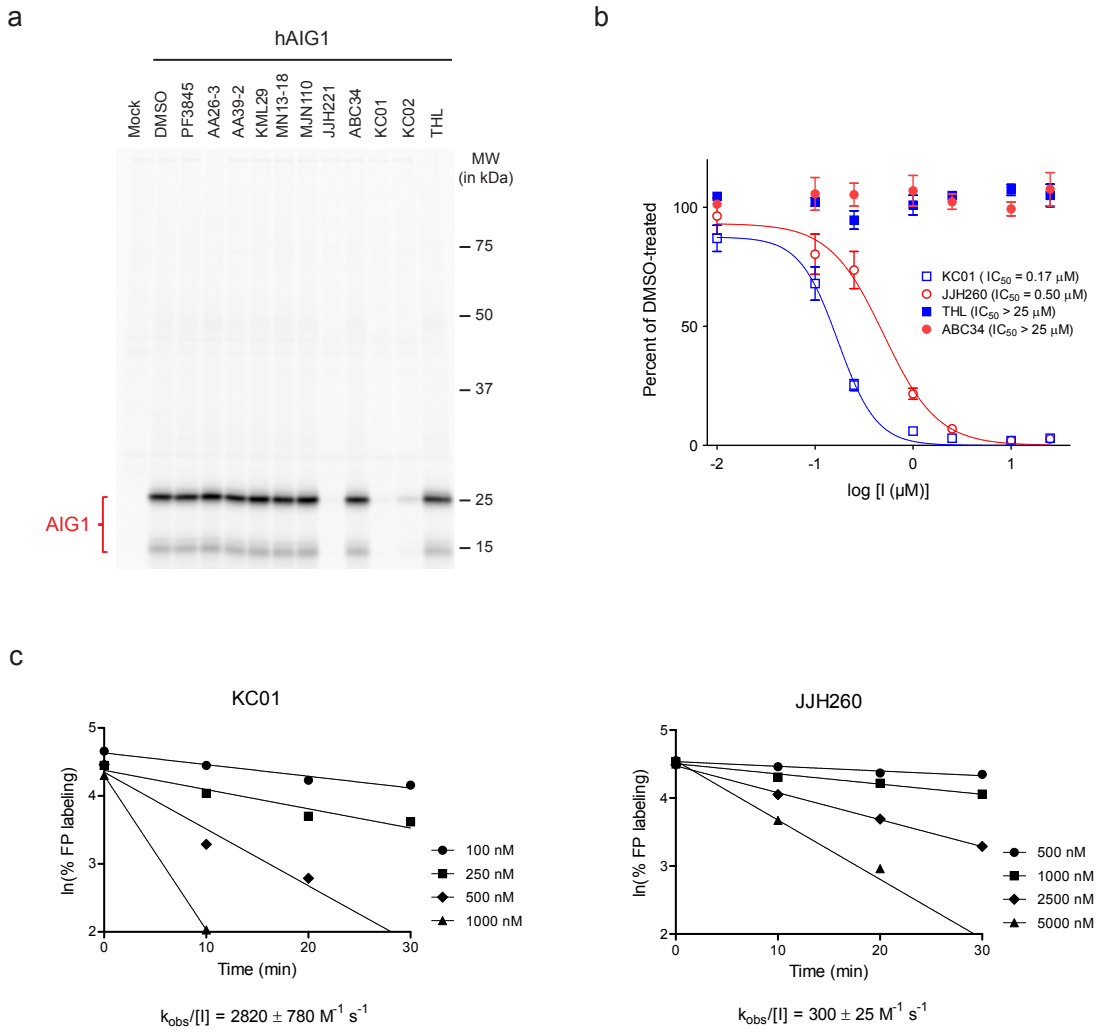

Figure 3.12. Evaluation of inhibitor sensitivity of AIG1 by competitive ABPP. (**a**) ABPP gel of the membrane proteome of hAIG1-transfected HEK293T cells (0.5 mg proteome mL^{-1}), treated with a collection of previously described Ser hydrolase inhibitors[22,23,36-38]. Proteomes were incubated with 20 μM inhibitor for 30 min at 37 °C and then treated with 1 μM FP-Rh for 30 min at 37 °C. (**b**) IC_{50} curves quantifying the inhibition of hAIG1 by KC01 (IC_{50} = 0.17 ± 0.03 μM) and JJH260 (IC_{50} = 0.50 ± 0.15 μM) as measured by gel-based competitive ABPP with the FP-Rh probe. Band intensities were quantified relative to the DMSO-treated control lane using ImageJ software (http://imagej.nih.gov/ij/). Data represent mean values ± s. e. m. for three biological replicates. (**c**) Time-dependent inhibition of AIG1 by KC01 and JJH260 with calculated $k_{obs}/[I]$ values as measured by competitive ABPP with the FP-Rh probe (1 μM, 2 min) following the indicated pre-treatment times with inhibitors. Data represent average values for three biological replicates; calculated $k_{obs}/[I]$ values are expressed ± s. d

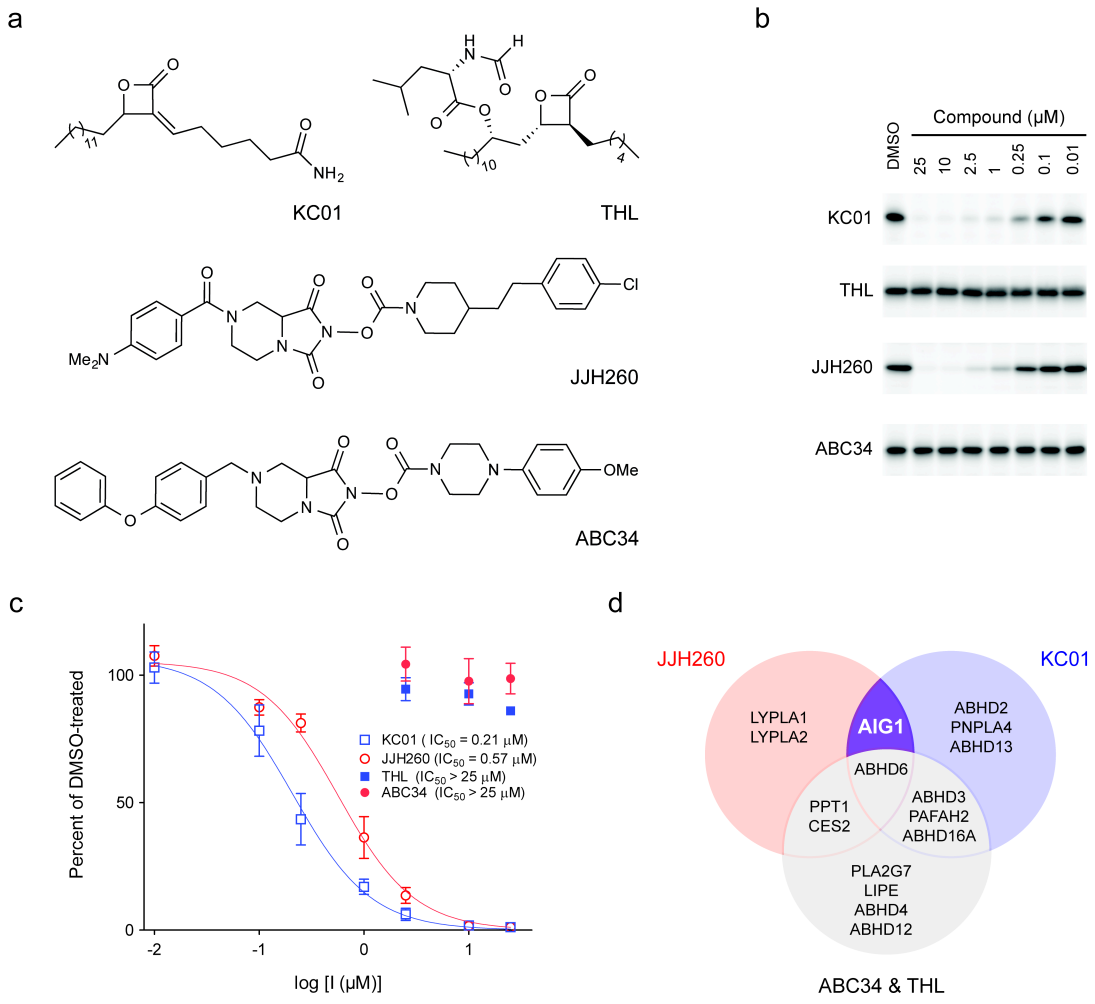

Figure 3.13. Discovery of inhibitors and structurally related inactive control compounds for AIG1. (**a**) Chemical structures of two hAIG1 inhibitors, KC01 and JJH260, and the respective control compounds, THL and ABC34. (**b**) ABPP gels demonstrating inhibition of FP-Rh labeling of hAIG1 by KC01 and JJH260, but not THL and ABC34. Proteomes were treated with each inhibitor at the indicated concentrations for 30 min at 37 °C, followed by FP-Rh (1 μM, 30 min, 37 °C). Full images of the gels are provided in **Figure 3.23**. (**c**) Concentration-dependent inhibition of the 9-PAHSA hydrolysis activity of hAIG1-transfected HEK293T membrane proteome by KC01 (IC_{50} = 0.21 ± 0.08 μM) and JJH260 (0.57 ± 0.14 μM), but not THL and ABC34. For these experiments, proteomes were incubated with each inhibitor at the indicated concentration for 30 min at 37 °C. 20 μg of each proteome was then incubated with 100 μM 9-PAHSA for 30 min at 37 °C. Data represent mean values ± s. e. m. for three biological replicates. (**d**) Venn diagram showing overlapping and distinct target profiles for AIG1 inhibitors KC01 and JJH260 and control compounds THL and ABC34.

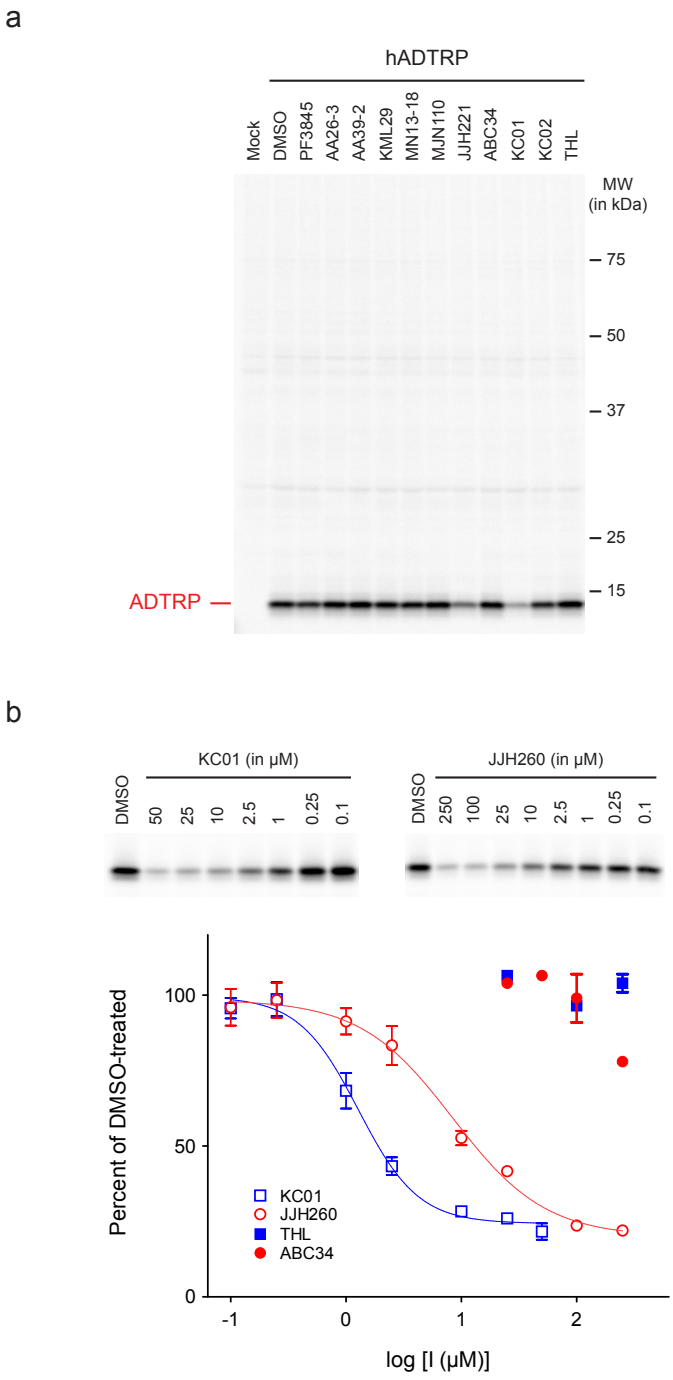

Figure 3.14. Evaluation of inhibitor sensitivity of ADTRP by competitive ABPP. (**a**) ABPP gel of the membrane proteome of hADTRP-transfected HEK293T cells (0.5 mg proteome mL^{-1}), treated with a collection of previously described Ser hydrolase inhibitors[22,23,36-38]. Proteomes were incubated with 20 μM inhibitor for 30 min at 37 °C and then treated with 1 μM FP-Rh for 30 min at 37 °C. (**b**) IC_{50} curves quantifying the inhibition of hADTRP by KC01 (IC_{50} = 1.3 ± 0.4 μM) and JJH260 (IC_{50} = 8.5 ± 3.0 μM) as measured by gel-based competitive ABPP with the FP-Rh probe. Data represent average values ± s. e. m. for three biological replicates.

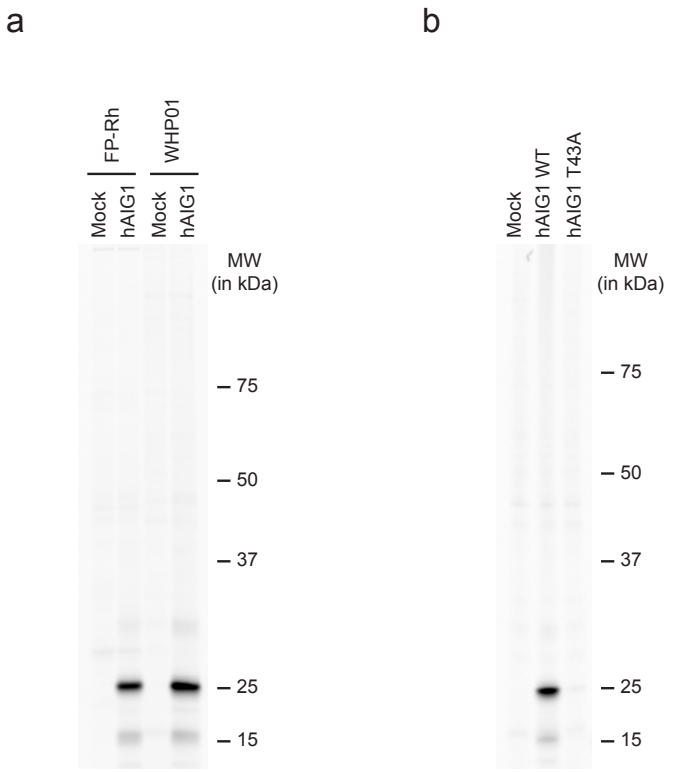

Figure 3.15. WHP01 labeling of AIG1. (**a**) ABPP gel of the membrane proteomes (0.5 mg proteome mL^{-1}) of mock- and hAIG1-transfected HEK293T cells, showing labeling of AIG1 by WHP01. Proteomes were treated with either 1 μM FP-Rh or 2 μM WHP01 for 30 min at 37 °C.. (**b**) ABPP gel of the membrane proteomes of mock-, wild-type hAIG1-, and mutant hAIG1-transfected HEK293T cells. Proteomes were treated with 2 μM WHP01 for 30 min at 37 °C.

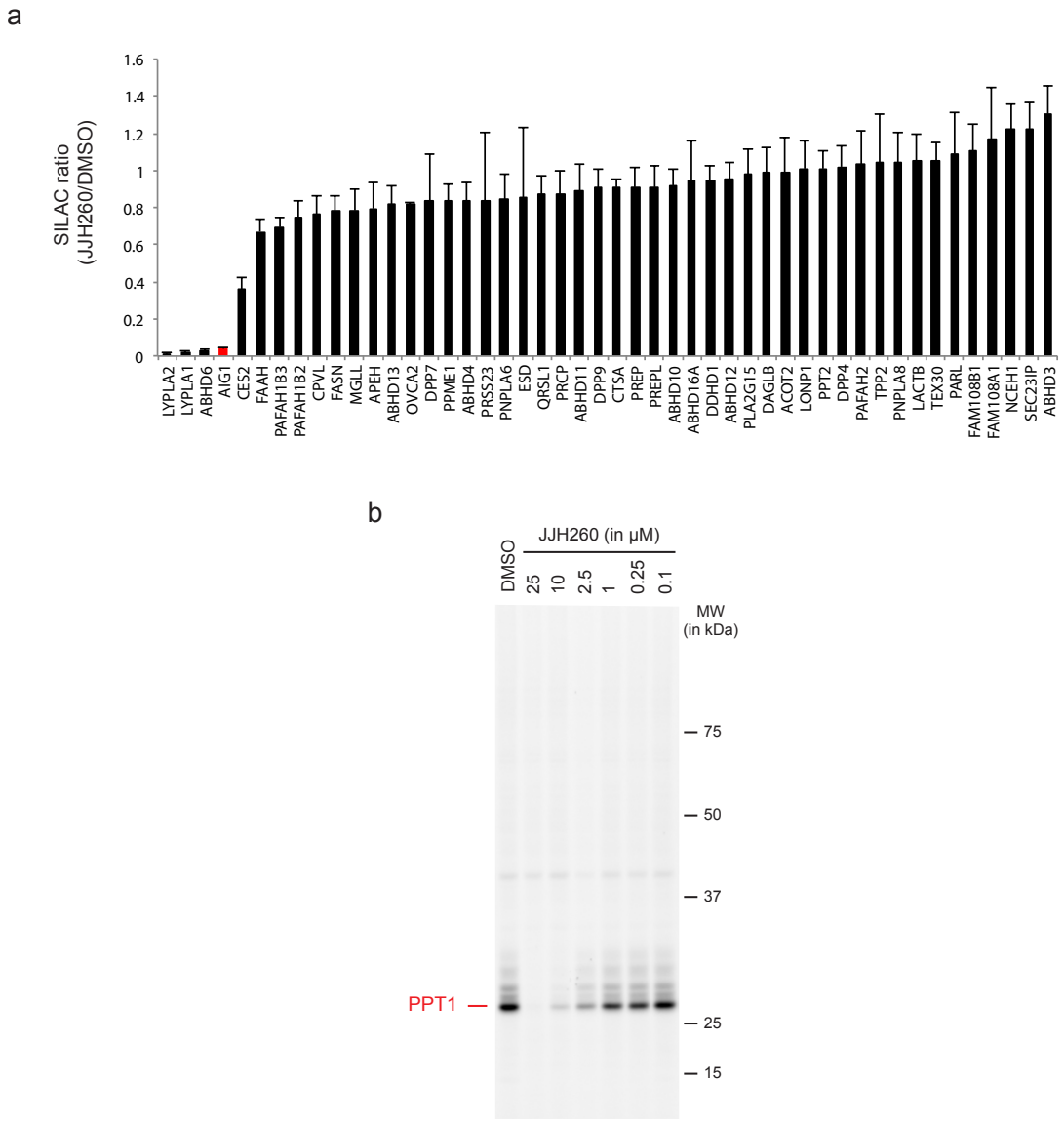

Figure 3.16. Competitive ABPP experiments to assess the selectivity of JJH260 against human Ser hydrolases. (**a**) Competitive ABPP-SILAC analysis to identify JJH260-inhibited proteins, where protein enrichment and inhibition were measured in SKOV3 cell proteomic lysates treated with DMSO or JJH260 (5 μM, 1 h) followed by FP-biotin (5 μM, 1 h) using established protocols[14]. Data represent the median SILAC ratios ± s. d. for peptides quantified for each protein from two biological replicates. (**b**) ABPP gel of the soluble fraction (1.0 mg proteome mL^{-1}) of PPT1-transfected HEK293T cells showing concentration-dependent inhibition with JJH260. Proteome was incubated with the indicated concentration of JJH260 for 30 min at 23 °C, chased with 1 μM ABC45 for 30 min at 23 °C, treated with PNGase F, and then reacted with Rh-N_3 under standard click conditions and analyzed by SDS-PAGE and in-gel fluorescence scanning.

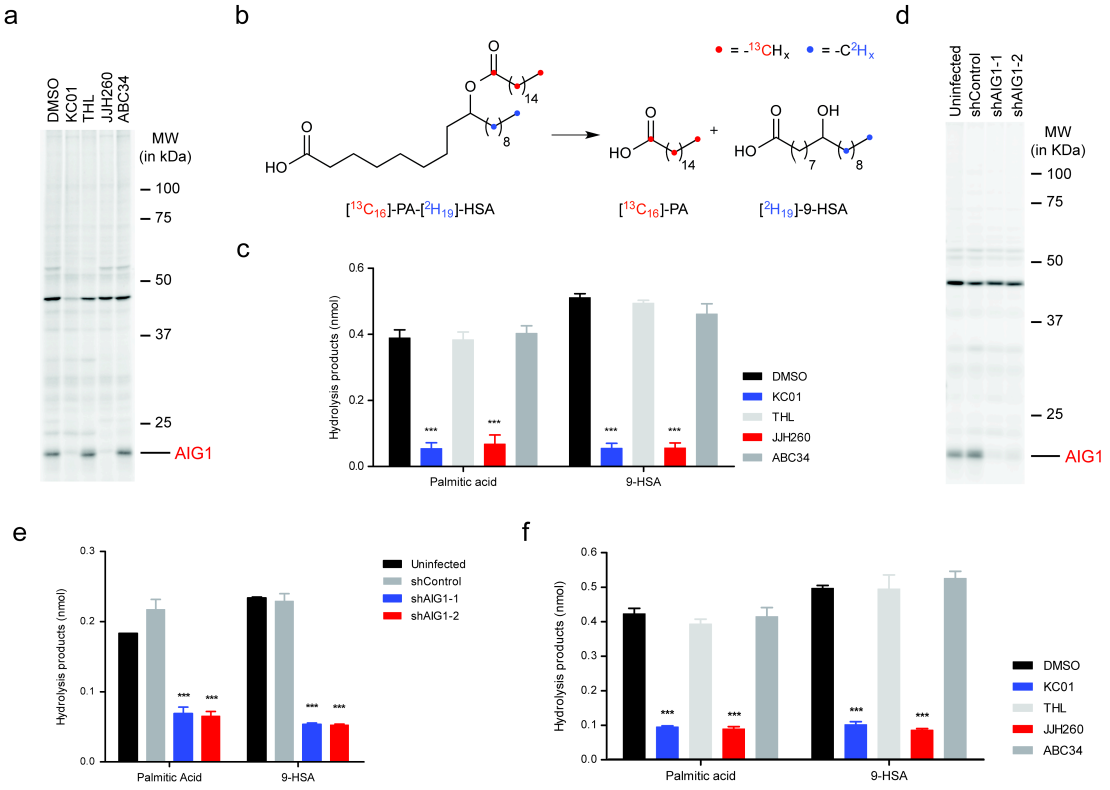

Figure 3.17. AIG1 inhibitors block FAHFA hydrolysis in mammalian cells. (**a**) ABPP gel of the membrane proteome of LNCaP cells demonstrating inhibition of endogenous AIG1 by KC01 and JJH260. Cells were treated with 5 μM of each compound for 4 h at 37 °C. lysed, and membrane proteomes labeled with WHP01 (2 μM, 30 min, 37 °C) before gel-based ABPP. (**b**) Structure of double-labeled 9-PAHSA ([$^{13}C_{16}$]-PA-[D_{19}]-HSA, or ^{13}C,^{2}H-PAHSA) and its hydrolytic products $^{13}C_{16}$-palmitic acid ($^{13}C_{16}$-PA) and $^{2}H_{19}$-hydroxystearic acid ($^{2}H_{19}$-HSA). (**c**) ^{13}C,^{2}H-PAHSA hydrolysis activity of LNCaP cells treated *in situ* with DMSO or inhibitors (5 μM) for 4 h at 37 °C and then fed 2 μM [$^{13}C_{16}$]-PA-[D_{19}]-HSA for 2 h. Data represent mean ± s. e. m. for four biological replicates. (**d**) ABPP gel of the membrane proteomes of shAIG1 and control LNCaP cell lines. Proteomes were treated with 2 μM WHP01 for 30 min at 37 °C. (**e**) ^{13}C,^{2}H-PAHSA hydrolysis activity of shAIG1 and control LNCaP cell lines. Cells were fed 2 μM ^{13}C,^{2}H-PAHSA for 2 h prior to analysis. Data represent mean ± s. e. m. for five biological replicates. (**f**) ^{13}C,^{2}H-PAHSA hydrolysis activity of human T-cells treated *in situ* with DMSO or inhibitors. Cells were treated with 5 μM of each inhibitor for 4 h at 37 °C and then fed 2 μM [$^{13}C_{16}$]-PA-[D_{19}]-HSA for 2 h. Data represent mean ± s. e. m. for three biological replicates. ***$p < 0.001$ by two-sided Student's *t*-test for inhibitors-treated or shAIG1 versus control cell lines.

Figure 3.18. Further assessment of AIG1-dependent FAHFA hydrolysis in human cells. (**a**) *In vitro* 9-PAHSA hydrolysis assays for the membrane and soluble proteomes of LNCaP cells, showing that the majority of the hydrolytic activity resides in the membrane proteome. 20 μg of each proteome was incubated with 100 μM 9-PAHSA for 30 min at 37 °C. Data represent mean values for two biological replicates. (**b**) *In vitro* 9-PAHSA hydrolysis assays for the membrane proteome of LNCaP cells treated with DMSO or the indicated inhibitors (each at 5 μM, 30 min pre-treatment). 20 μg of each proteome was then incubated with 100 μM 9-PAHSA for 30 min at 37 °C. Data represent mean values ± s. e. m. for three biological replicates. $^{**}p < 0.01$ by Student's *t*-test for inhibitor-treated versus DMSO-treated controls. (**c**) $^{13}C,^{2}H$-PAHSA hydrolysis activity of HEK293T cells transfected with wild-type AIG1, the T43A-AIG1 mutant, or a mock control. Transfected cells were fed 2 μM $^{13}C,^{2}H$-PAHSA for 1 h. Data represent mean values ± s. e. m. for three biological replicates. (**d**) $^{13}C,^{2}H$-PAHSA hydrolysis activity of HEK293T cells transfected with wild-type AIG1, wild-type ADTRP, or a mock control. Transfected cells were fed a lower concentration of $^{13}C,^{2}H$-PAHSA (500 nM) for 1 h. Data represent mean values ± s. e. m. for three biological replicates. (e) $^{13}C,^{2}H$-PAHSA hydrolysis activity of hAIG1-transfected HEK293T cells treated *in situ* with DMSO or the indicated inhibitors (each at 5 μM, 4 h pre-treatment). Cells were fed 2 μM $^{13}C,^{2}H$-PAHSA for 1 h. Data represent mean values ± s. e. m. for four biological replicates. $^{***}p < 0.001$ by two-sided Student's *t*-test for inhibitor-treated versus DMSO-treated controls.

a

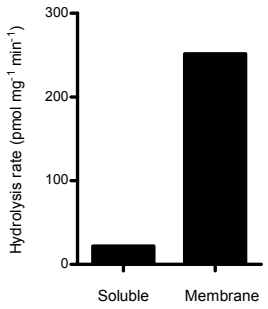
Hydrolysis rate (pmol mg-1 min-1)
300
200
100
0
Soluble
Membrane

b

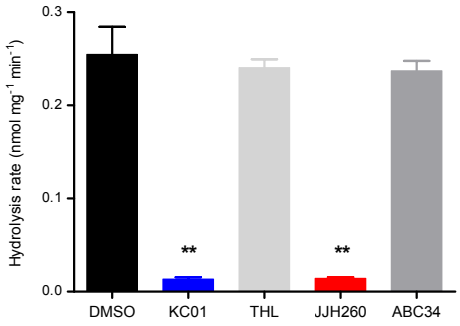
Hydrolysis rate (nmol mg-1 min-1)
0.3
0.2
0.1
0.0
**
**
DMSO
KC01
THL
JJH260
ABC34

c

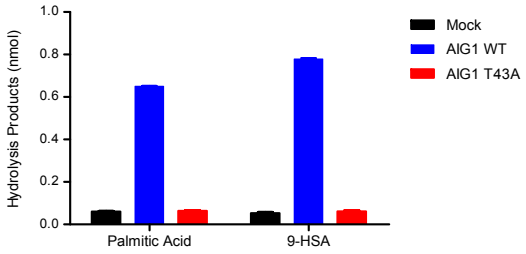
Hydrolysis Products (nmol)
1.0
0.8
0.6
0.4
0.2
0.0
Palmitic Acid
9-HSA
Mock
AIG1 WT
AIG1 T43A

d

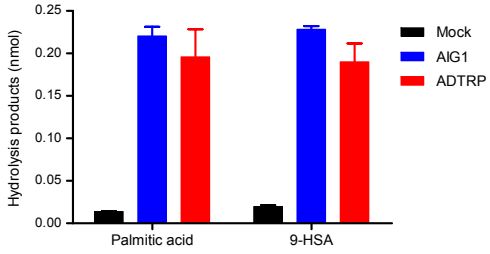
Hydrolysis products (nmol)
0.25
0.20
0.15
0.10
0.05
0.00
Palmitic acid
9-HSA
Mock
AIG1
ADTRP

e

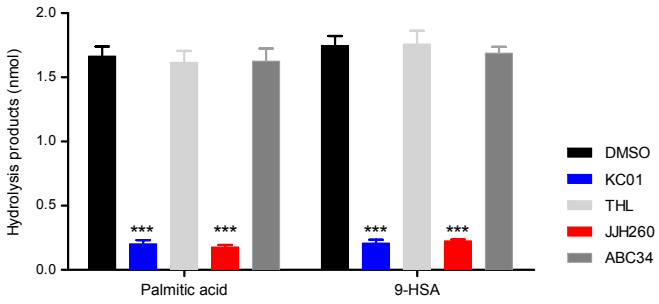
Hydrolysis products (nmol)
2.0
1.5
1.0
0.5
0.0
***
***
***
***
Palmitic acid
9-HSA
DMSO
KC01
THL
JJH260
ABC34

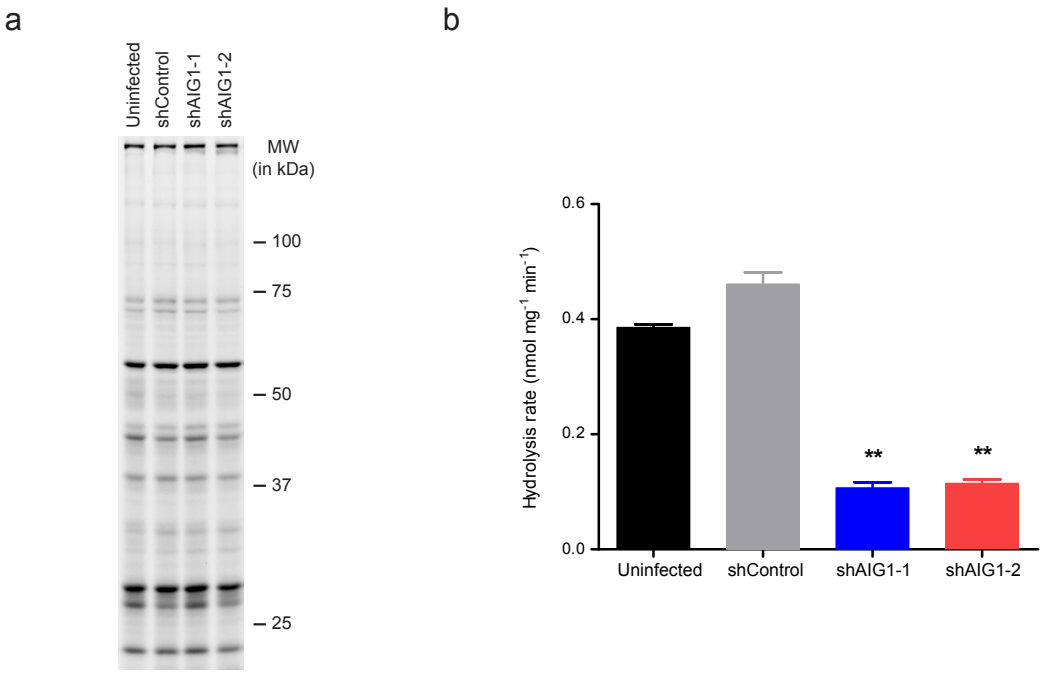

Figure 3.19. Further assessment of AIG1-knockdown human LNCaP cell lines. (**a**) ABPP gel of the membrane proteomes (1.0 mg proteome mL^{-1}) of the indicated shRNA cell lines. Proteomes were treated with 1 μM FP-Rh for 30 min at 37 °C and then analyzed by SDS-PAGE and in-gel fluorescence scanning. Note that global serine hydrolase signals are similar between shAIG1 and shControl cells (AIG1 is not detected with the FP-Rh probe in these cells due to overlapping serine hydrolase signals, but is shown in **Figure 5d** using the WHP01 probe). (**b**) *In vitro* 9-PAHSA hydrolysis assays for the membrane proteomes of the indicated shRNA cell lines (shControl, shAIG1-1, and shAIG1-2) and an uninfected control LNCaP cell line. 20 μg of each proteome was incubated with 100 μM 9-PAHSA for 30 min at 37 °C. Data represent mean values ± s. e. m. for three biological replicates. $^{**}p < 0.01$ by two-sided Student's *t*-test for shAIG1 versus control cell lines.

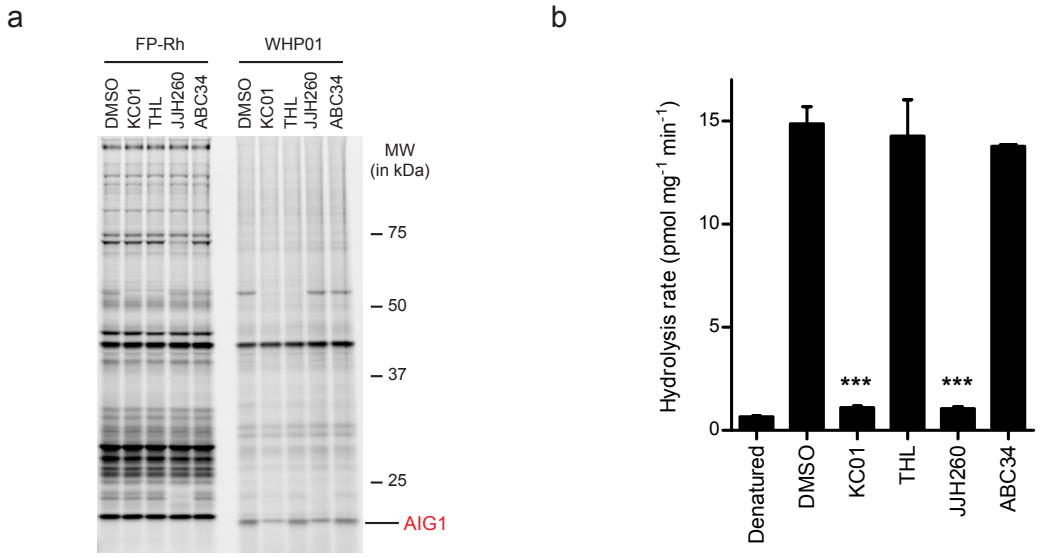

Figure 3.20. Further assessment of AIG1 and FAHFA hydrolysis in primary human T-cells. (**a**) ABPP gel of the membrane proteome (1.0 mg proteome mL^{-1}) of primary human T-cells treated with DMSO or inhibitors (each at 5 μM, 30 min, 37 °C). Proteomes were subsequently treated with either 1 μM FP-Rh or 2 μM WHP01 for 30 min at 37 °C and analyzed by SDS-PAGE and in-gel fluorescence scanning. The proposed band for AIG1 (partially obscured by an overlapping band) is indicated by a red label. (**b**) *In vitro* 9-PAHSA hydrolysis assays for the membrane proteomes of human T-cells treated with DMSO or inhibitors (each at 5 μM, 30 min pre-treatment). 20 μg of each proteome was incubated with 100 μM 9-PAHSA for 30 min at 37 °C. Data represent mean values ± s. e. m. for three biological replicates. ***$p < 0.001$ by two-sided Student's *t*-test for inhibitor-treated versus DMSO-treated controls.

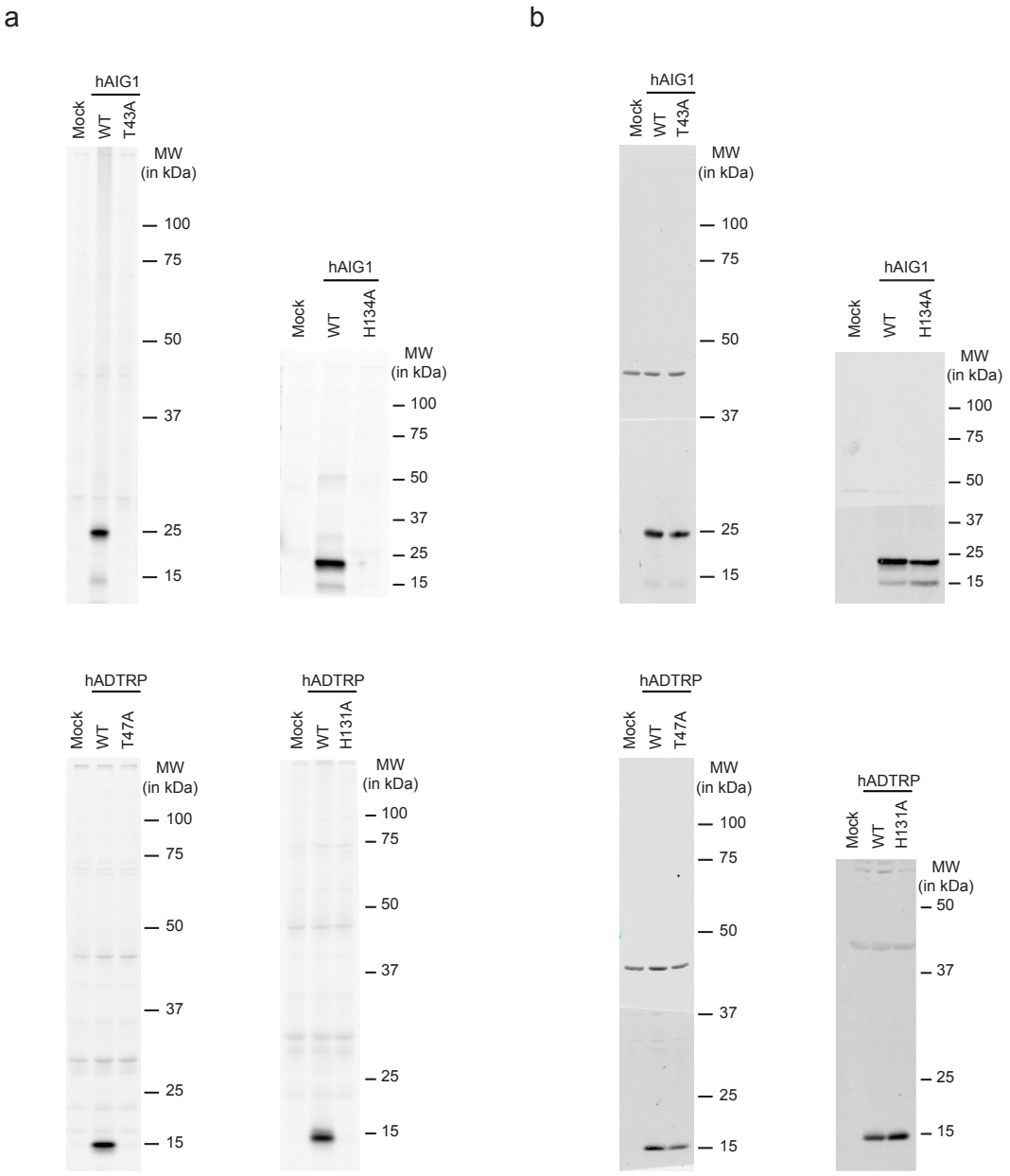

Figure 3.21. (**a**) Full gel images and (**b**) full Western blots for **Figures 3.6a-d**.

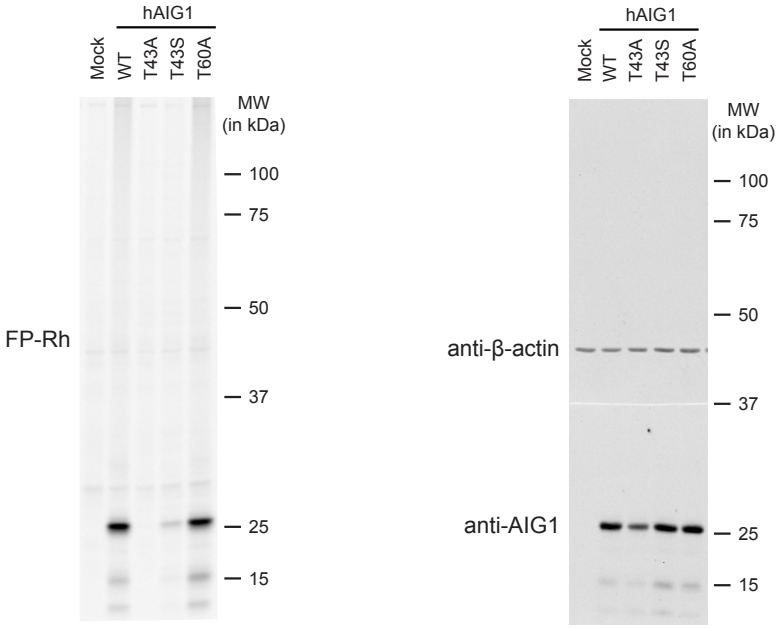

Figure 3.22. Full gel image and Western blot for **Figure 3.10c**.

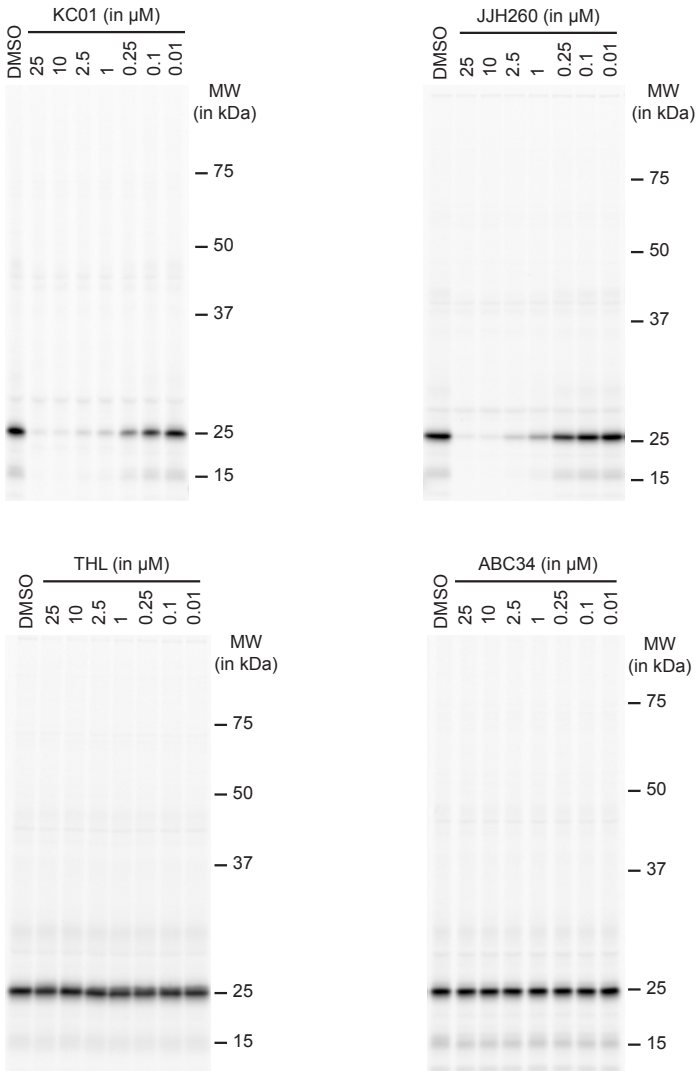

Figure 3.23. Full gel images for **Figure 3.13b**.

Table 3.1 Primers used for site-directed mutagenesis of hAIG1 and hADTRP.

Mutation	Forward primer sequence
hAIG1	
S16A	5'-GATGGCAATCCTGCTGGCTTACTGCTCTATCCTGTG-3'
H32A	5'-CCATCGAAATGCCCTCAGCCCAGACCTACGGAGG-3’
T43A	5'-GGAGGGAGCTGGAAATTCCTGGCGTTCATTGATCTGG-3'
T43S	5'-GGAGGGAGCTGGAAATTCCTGTCGTTCATTGATCTGG-3'
T60A	5'-GGCATCTGTGTGCTGGCTGATCTTTCCAGTCTTCTGAC-3'
S63A	5'-GCTGACTGATCTTGCCAGTCTTCTGACTCGAGGAAGTGG-3'
S64A	5'-GCTGACTGATCTTTCCGCTCTTCTGACTCGAGGAAGTGG-3'
T67A	5'-CCAGTCTTCTGGCTCGAGGAAGTGGGAACCAGG-3'
S70A	5'-CTTCTGACTCGAGGAGCTGGGAACCAGGAGCAAGAGAGGC-3'
S84A	5'-GCTCAAGAAGCTCATCGCTCTCCGGGACTGG-3'
H134A	5'-GCTGAATCACGGAATGGCCACGACGGTTCTGCC-3’
T135A	5'-GCTGAATCACGGAATGCACGCGACGGTTCTGCC-3'
H150A	5’-GGACATCGCACGCTCAGTATCCCAGCAGGAGCAGC-3’
S154A	5'-CCATCAGTATCCCGCCAGGAGCAGCGGACTTACC-3'
S157A	5'-GTATCCCAGCAGGAGCGCCGGACTTACCGCC-3'
S166A	5'-CATATGTACCTTCGCTGTTGGCTATATATTATGGGTGTGCTGGG-3'
T180A	5'-GGTGCATCATGTAGCTGGCATGTGGGTGTACC-3'
S202A	5'-CAGGAGCCAGAATCATCTTCTTTGGGGCTACAACCATCTTAATG-3'
S227A	5'-CTGGGATACACAGAAAGCTATGGAAGAAGAGAAAGAAAAGCC-3'
hADTRP	

T47A	5'-GCAAGGTGGAAATATATGGCGCTGCTTAATCTGCTC-3'
H131A	5’-GGCTGAATCATGCAATGGCCACTTTCATATTCCCCATCAC-3’

Table 3.2. Detailed MRM transitions used for the targeted LC-MS analysis.

Species detected	Precursor ion	Product ion	Collision energy	Dwell time	Polarity
[$^{13}C_{16}$]-PA-[D_{19}]-HSA	572.7	271.3	30	100	Negative
[$^{13}C_{16}$]-PAHSA	553.5	271.3	30	100	Negative
[D_{19}]-HSA	318.4	318.4	0	25	Negative
9-HHDA	285.2	285.2	0	25	Negative
[$^{13}C_{16}$]-PA	271.3	271.3	0	25	Negative
C17:1 FFA	267.2	267.2	0	25	Negative

3.5 Experimental Section

ABPP-MudPIT and competitive ABPP-MudPIT sample preparation. For ABPP-MudPIT samples, proteomes (1 mg/mL in 1 mL of PBS) were labeled with FP-biotin (5 μM) for 1 h at 23 °C while rotating. After labeling, the proteomes were denatured and precipitated using 4:1 MeOH/$CHCl_3$, resuspended in 0.5 ml of 6 M urea in PBS, reduced using tris(2-carboxyethyl)phosphine (TCEP, 10 mM) for 30 min at 37 °C, and then alkylated using iodoacetamide (40 mM) for 30 min at 23 °C in the dark. The biotinylated proteins were enriched with PBS-washed avidin-agarose beads (100 μL; Sigma-Aldrich) by rotating at 23 °C for 1.5 h in PBS with 0.2% SDS to a final volume of 6 mL. The beads were then washed sequentially with 10 mL PBS with 0.2% SDS, 10 mL PBS (3x) and 10 mL DI H_2O (3x). On-bead digestion was performed using sequencing-grade trypsin (2 μg; Promega) in 2 M urea in PBS with 2 mM $CaCl_2$ for 12–14 h at 37 °C (200 μL). Peptides obtained from this procedure were acidified with formic acid (5%) and stored at –20 °C prior to analysis. SILAC experiments were performed using the human SKOV3 breast cancer cell line (ATC HTB-77). The isotopically labeled cell lines were generated by ≥ 5 passages in either light (100 μg/mL each of L-arginine and L-lysine) or heavy (100 μg/mL each of [$^{13}C_6{}^{15}N_4$]L-arginine and [$^{13}C_6{}^{15}N_4$]L-lysine) SILAC RPMI medium (ThermoScientific) supplemented with 10% dialyzed FBS (Omega Scientific) and penicillin-streptomycin (GE Life Sciences). Light and heavy cells were treated with the test compound or DMSO, respectively, at 37 °C. Cells were then washed with sterile PBS (3x), harvested, and lysed by sonication in PBS. The membrane and soluble fractions were separated by ultra-centrifugation at 100,000 g for 45 min at 4 °C. 2 mg/mL light proteome (0.5 mL) and 2 mg/mL heavy proteome (0.5 mL) were subsequently treated with FP-biotin (5 μM) for 1 h at 23 °C, combined, and processed as above for the ABPP-MudPIT protocol. For competitive ABPP experiments with FP-alkyne, the concentration of probe (20 μM) was chosen based on prior gel-based experiments demonstrating saturation of labeling for many serine hydrolases at

comparable concentrations of FP probe.[13] In addition, previous studies have shown effective competition of most FP-Rh labeled bands in mouse brain with 10 μM FP-alkyne.[39]

HHpred searches. Remote homology detection was performed using the HHpred algorithm[40]. Briefly, a seed alignment was generated using the CLUSTALW algorithm on the seven protein sequences shown in **Figure 3.1** (UniProt IDs: AIG1_HUMAN, AIG1_MOUSE, ADTRP_HUMAN, F1QYR4_DANRE, Q7Q8H9_ANOGA, YHU0_YEAST, E7FAT8_DANRE). The CLUSTALW alignment was used as input for the HHpred server (http://toolkit.tuebingen.mpg.de/hhpred) and it was run using the default parameters to search all available HMM databases.

Cell culture methods. HEK293T cells (ATCC CRL-3216) were cultured in DMEM (Gibco), supplemented with L-glutamine (2 mM), 10% FCS (Omega Scientific), and penicillin-streptomycin (GE Life Sciences) at 37 °C and 5% CO_2. LNCaP cells (ATCC CRL-1740) were cultured in RPMI 1640 (Gibco), supplemented with L-glutamine (2 mM), 10% FCS, and penicillin-streptomycin at 37 °C and 5% CO_2. T-cells were purified from peripheral blood mononuclear cells (PBMCs) obtained from human subjects using STEMCELL Technologies kits as per manufacturers instructions. Typically 100-150 million T-cells were obtained from 500 mL human subject derived PBMCs at > 95% purity as confirmed by flow cytometry analysis. T-cells were cultured in dye-free RPMI supplemented with 10% FCS at 37 °C and 5% CO_2.

Cloning and recombinant expression of AIG1 and ADTRP. Full-length cDNA encoding human AIG1 (GE Healthcare, in pOTB7 vector) was cloned into the pCMV6-Entry vector with C-terminal Myc and DDK tags. (Sense primer: 5'-GGG CGG CCG GGA ATT CGC GAA CAT GG-3'; Antisense primer: 3'-AAG CCT AAA TTG GAA ACG CGG CCG CTT TA-5'). Full-length cDNA encoding for human ADTRP in the pCMV6-XL5 vector was purchased from Origene. Full-length cDNA constructs encoding for mouse AIG1 in the pCMV-Sport6 vector, rat AIG1 in pExpress-1 vector, and mouse ADTRP in the pCMV-Sport6 vector were purchased from GE Life Sciences. To recombinantly express AIG1 or ADTRP, HEK293T cells were grown

to 40% confluence in a 10 cm tissue culture plate and transiently transfected with 4 μg of the desired construct using polyethyleneimine 'MAX' (MW 40,000, PEI; Polysciences, Inc.) as the transfection reagent per the manufacturer's protocol. 'Mock' transfected cells were transfected with 4 μg of empty vector. 48 h after transfection, cells were washed with PBS (3x), harvested by scraping, and lysed by sonication in PBS. The membrane and soluble fractions were separated by ultra-centrifugation at 100,000 g for 45 min at 4 °C. Protein concentrations were measured using the DC Protein Assay kit (Bio-Rad). Aliquots were flash-frozen and stored at – 80 °C for further use.

Site-directed mutagenesis. Point mutations in both human AIG1 and ADTRP were generated by the QuikChange site-directed mutagenesis protocol (Strategene) as per the manufacturer's instructions. For primers used for each mutation, see **Table 1**. Primers were obtained from Integrated DNA Technologies. All DNA sequencing was performed by Eton Biosciences Inc.

Gel-based ABPP analysis. Tissue and cell proteomes (50 μL) were treated with either FP-rhodamine (1 μM) or WHP01 (2 μM) for 30 min at 37 °C. The reactions were then quenched by addition of 4x SDS-PAGE loading buffer (20 μL). Competitive gel-based ABPP experiments were performed as previously described.[7] Samples were visualized in-gel using a ChemiDoc MP imaging system (Bio-Rad). The fluorescence from rhodamine is presented in gray scale. 2-5 s exposure times and 20-60 s exposure times were used for AIG1/ADTRP-transfected and native proteomes, respectively. Relative band intensities were quantified using ImageJ software (http://imagej.nih.gov/ij/).

Western blotting. Cell proteomes were separated by SDS-PAGE, transferred to nitrocellulose membrane (60 V for 90 min), and blocked by 5% milk in TBS-Tween. The primary antibodies used and dilutions are as follows: anti-AIG1 (Rabbit, Sigma-Aldrich, SAB1304597, 1:250), anti-ADTRP (Rabbit, Atlas, HPA048113, 1:500), and anti-β-actin (Mouse, Cell Signaling,

3700S, 1:1000). IRDye 800CW anti-rabbit and anti-mouse secondary antibodies (LI-COR, 1:10000) were used as secondary antibodies for visualization.

AIG1 and ADTRP LC/MS substrate hydrolysis assays. FAHFA substrates were purchased from Cayman Chemical Co. All non-FAHFA lipid substrates were purchased from Avanti Polar Lipids Inc. unless mentioned otherwise. 20 µg of proteome was incubated with 100 µM lipid substrate in a reaction volume of 250 µL in PBS at 37 °C with constant shaking. After 30 minutes the reaction was quenched with 400 µL of 2:1 (vol/vol) $CHCl_3$: MeOH, doped with internal standard (0.5 nmol C17:1 heptadecenoic acid (C17:1 FFA) and 0.05 nmol 9-hydroxy-heptadecanoic acid (9-HHDA)). The mixture was vortexed and centrifuged at 2800 g for 5 min to separate the aqueous (top) and organic (bottom) phase. The organic phase was collected and dried under a stream of N_2, re-solubilized in 100 µL of 2:1 (vol/vol) $CHCl_3$: MeOH, and subjected to LC-MS analysis. A fraction of the organic extract (~ 15 µL) was injected onto an Agilent 6520 quadrupole-time-of-flight (QTOF) LC-MS and analyzed as described previously.[23] All data presented for substrate hydrolysis assays is the average of 2-5 independent biological replicates, error bars represent S.D. (n = 2), and S.E.M. (n = 3-5).

Synthesis of AIG1 inhibitors and probes. FP-biotin, FP-rhodamine, and FP-alkyne were synthesized in-house as previously described.[4,41,42] KC01 and WHP01 were synthesized in-house as previously described.[23] ABC34 was synthesized in-house as previously described.[22] Tetrahydrolipstatin (THL) was purchased from Sigma-Aldrich. [$^{13}C_{16}$]-PA-[D_{19}]-HSA was synthesized according to the previously described method, using isotopically labeled starting materials.[21]

9-PAHSA feeding assay. For the pharmacology studies, cells were treated *in situ* with 5 µM KC01, THL, JJH260, or ABC34 for 4 h at 37 ^oC in a volume of 5 mL in dye-free RPMI (LNCaP cells, T-cells) or dye-free DMEM (HEK293T cells) supplemented with 10% FCS. 2 µM [$^{13}C_{16}$]-PA-[D_{19}]-HSA was then added to the media for 1 h (HEK293T cells) or 2 h (LNCaP cells, T-cells) at 37 ^oC. Thereafter the media was collected (5 mL) and the cells were washed with

sterile PBS (3x) and harvested by scraping. The cells were re-suspended in 1 mL sterile PBS and mixed by vortexing with 3 mL of 2:1 $CHCl_3$: MeOH with the internal standard mix (50 pmol each of C17:1 FFA, 9-HHDA, and [$^{13}C_{16}$]-PAHSA). The two phases were separated by centrifugation at 2800 g for 10 min, and the organic phase (bottom) was collected and dried under stream of N_2. The lipid extracts were re-solubilized using 100 µL of 2:1 $CHCl_3$: MeOH, and 10 µL was used for the targeted LC-MS analysis. The MRM transitions for the targeted LC-MS analysis are presented in **Table 2**.

shRNA knockdown studies. AIG1 MISSION shRNA bacterial glycerol stocks were purchased, and the lentiviral-based shRNA gene knockdown was performed in LNCaP cells using the manufacturer's protocol (Sigma-Aldrich). Briefly, 1 µg shRNA transfer vector, 0.1 µg of the VSVG envelope vector and 0.9 µg packaging vector dVPR were transfected using 6 µL of X-tremeGENE 9 (GE Life Sciences) into 1.8 ×10^6 HEK293T cells cultured in 5 mL DMEM with L-glutamine (2 mM) and 10% FCS and 5% CO_2 to generate the lentiviral transduction particles (LTP). 0.25 × 10^6 LNCaP cells were infected with the LTP generated from the transfections along with 5 µg/mL polybrene (to enhance infection) cultured in 5 mL RPMI 1640 with 10% FCS and 5% CO_2, and thereafter the lentiviral-infected LNCaP cells were selected on puromycin (1 µg/ml). After six rounds of puromycin selection, LNCaP cells infected with the LTP generated using the constructs TRCN0000142987 (shAIG1-1; Sigma-Aldrich) and TRCN0000422331 (shAIG1-2; Sigma-Aldrich) showed >75% knockdown of AIG1 by gel-based ABPP and substrate hydrolysis assays and were selected for further studies. As a negative control (shControl), shRNA transfer vector targeting GFP was used.

MS and data analysis. MS was performed using a LTQ (for spectral counting studies), or LTQ-Orbitrap or Orbitrap Velos (for SILAC studies), following previously described protocols (ThermoFinnigan).[7,43] Peptides were eluted using a five-step multidimensional LC-MS protocol in which increasing concentrations of ammonium acetate are injected followed by a gradient of increasing acetonitrile, as previously described.[44] For all samples, data were collected in data-

dependent acquisition mode over a range from 400–1,800 *m*/*z*. Each full scan was followed by up to 7 or 30 fragmentation events for experiments using the LTQ and Orbitrap or Orbitrap Velos instruments, respectively. Dynamic exclusion was enabled (repeat count of 1, exclusion duration of 20 s) for all experiments. The data were searched using the ProLuCID algorithm against a human reverse-concatenated nonredundant (gene-centric) FASTA database that was assembled from the Uniprot database. ProLuCID searches specified static modification of cysteine residues (+57.0215 *m*/*z*; iodoacetamide alkylation) and required peptides to contain at least one tryptic terminus. For SILAC samples, data sets were searched independently with the following parameter files; for the light search, all amino acids were left at default masses; for the heavy search, static modifications on lysine (+8.0142 *m*/*z*) and arginine (+10.0082 *m*/*z*) were specified. For data collected on the Orbitrap mass spectrometers, precursor-ion mass tolerance was set to 50 ppm. The resulting peptide spectral matches were filtered using DTASelect (version 2.0.47), and only half-tryptic or fully tryptic peptides were accepted for identification. Peptides were restricted to a specified false positive rate of <1%. SILAC ratios were quantified using in-house CIMAGE software.[18] Briefly, a 10-min retention time window was used for peak identification using 10 ppm mass accuracy and requiring a coelution R2 value greater than 0.8. Peptides detected as singletons, where only the heavy or light isotopically labeled peptide was detected and sequenced but which passed all other filtering parameters, were given a ratio of 20, which is the maximum SILAC ratio reported here.

Statistical analysis. Statistical analyses were performed using the GraphPad Prism 6 (for Mac OS X) software. Data derived from three or more replicates are shown as mean values ± s. e. m. Student's t-test (two-tailed) was used to study statistically significant differences between study groups. A P value of <0.05 was considered statistically significant for this study.

3.6 Acknowledgments

Chapter 3, in full, is a reprint with slight modifications as it appears in AIG1 and ADTRP are atypical integral membrane hydrolases that degrade bioactive FAHFAs, *Nature Chemical Biology* 12, 367-372 (2016). The dissertation author was the co-primary investigator and author of this paper along with William H. Parsons. Other authors include Siddhesh S. Kamat, Armand B. Cognetta III, Jonathan J. Hulce, Enrique Saez, Barbara B. Kahn, Alan Saghatelian, and Benjamin F. Cravatt.

3.7 References

1 Willems, L. I., Overkleeft, H. S. & van Kasteren, S. I. Current developments in activity-based protein profiling. *Bioconjug Chem* 25, 1181-1191 (2014).

2 Niphakis, M. J. & Cravatt, B. F. Enzyme inhibitor discovery by activity-based protein profiling. *Annu Rev Biochem* 83, 341-377 (2014).

3 Berger, A. B., Vitorino, P. M. & Bogyo, M. Activity-based protein profiling: applications to biomarker discovery, in vivo imaging and drug discovery. *Am J Pharmacogenomics* 4, 371-381 (2004).

4 Liu, Y., Patricelli, M. P. & Cravatt, B. F. Activity-based protein profiling: The serine hydrolases. *Proc Natl Acad Sci U S A* 96, 14694-14699 (1999).

5 Simon, G. M. & Cravatt, B. F. Activity-based proteomics of enzyme superfamilies: serine hydrolases as a case study. *J Biol Chem* 285, 11051-11055 (2010).

6 Bachovchin, D. A., Ji, T., Li, W., Simon, G. M., Blankman, J. L., Adibekian, A., Hoover, H., Niessen, S. & Cravatt, B. F. Superfamily-wide portrait of serine hydrolase inhibition achieved by library-versus-library screening. *Proc Natl Acad Sci U S A* 107, 20941-20946 (2010).

7 Jessani, N., Niessen, S., Wei, B. Q., Nicolau, M., Humphrey, M., Ji, Y., Han, W., Noh, D. Y., Yates, J. R., 3rd, Jeffrey, S. S. & Cravatt, B. F. A streamlined platform for high-content functional proteomics of primary human specimens. *Nat Methods* 2, 691-697 (2005).

8 Higa, H. H., Diaz, S. & Varki, A. Biochemical and genetic evidence for distinct membrane-bound and cytosolic sialic acid O-acetyl-esterases: serine-active-site enzymes. *Biochemical and biophysical research communications* 144, 1099-1108 (1987).

9 Jessani, N., Young, J. A., Diaz, S. L., Patricelli, M. P., Varki, A. & Cravatt, B. F. Class assignment of sequence-unrelated members of enzyme superfamilies by activity-based protein profiling. *Angew Chem Int Ed Engl* 44, 2400-2403 (2005).

10 Long, J. Z. & Cravatt, B. F. The metabolic serine hydrolases and their functions in mammalian physiology and disease. *Chem Rev* 111, 6022-6063 (2011).

11 Elias, M. & Tawfik, D. S. Divergence and convergence in enzyme evolution: parallel evolution of paraoxonases from quorum-quenching lactonases. *J Biol Chem* 287, 11-20 (2012).

12 Lone, A. M., Bachovchin, D. A., Westwood, D. B., Speers, A. E., Spicer, T. P., Fernandez-Vega, V., Chase, P., Hodder, P. S., Rosen, H., Cravatt, B. F. & Saghatelian, A. A Substrate-Free Activity-Based Protein Profiling Screen for the Discovery of Selective PREPL Inhibitors. *J Am Chem Soc* (2011).

13 Kidd, D., Liu, Y. & Cravatt, B. F. Profiling serine hydrolase activities in complex proteomes. *Biochemistry* 40, 4005-4015 (2001).

14 Adibekian, A., Martin, B. R., Wang, C., Hsu, K.-L., Bachovchin, D. A., Niessen, S., Hoover, H. & Cravatt, B. F. Click-generated triazole ureas as ultrapotent *in vivo*-active serine hydrolase inhibitors. *Nat Chem Biol* 7, 469-478 (2011).

15 Seo, J., Kim, J. & Kim, M. Cloning of androgen-inducible gene 1(AIG1) from human dermal papilla cells. *Mol. Cells* 11, 35-40 (2001).

16 Wu, G., Sun, M., Zhang, W. & Huo, K. AIG1 is a novel Pirh2-interacting protein that activates the NFAT signaling pathway. *Frontiers in Bioscience E3*, 834-842 (2011).

17 Lupu, C., Zhu, H., Popescu, N. I., Wren, J. D. & Lupu, F. Novel protein ADTRP regulates TFPI expression and function in human endothelial cells in normal conditions and in response to androgen. *Blood* 118, 4463-4471 (2011).

18 Weerapana, E., Wang, C., Simon, G. M., Richter, F., Khare, S., Dillon, M. B., Bachovchin, D. A., Mowen, K., Baker, D. & Cravatt, B. F. Quantitative reactivity profiling predicts functional cysteines in proteomes. *Nature* 468, 790-795 (2010).

19 Dodson, G. & Wlodawer, A. Catalytic triads and their relatives. *Trends in Biochemical Sciences* 23, 347-352 (1998).

20 Ekici, O. D., Paetzel, M. & Dalbey, R. E. Unconventional serine proteases: variations on the catalytic Ser/His/Asp triad configuration. *Protein Sci* 17, 2023-2037 (2008).

21 Yore, M. M., Syed, I., Moraes-Vieira, P. M., Zhang, T., Herman, M. A., Homan, E. A., Patel, R. T., Lee, J., Chen, S., Peroni, O. D., Dhaneshwar, A. S., Hammarstedt, A., Smith, U., McGraw, T. E., Saghatelian, A. & Kahn, B. B. Discovery of a class of endogenous mammalian lipids with anti-diabetic and anti-inflammatory effects. *Cell* 159, 318-332 (2014).

22 Cognetta, A. B., 3rd, Niphakis, M. J., Lee, H. C., Martini, M. L., Hulce, J. J. & Cravatt, B. F. Selective N-Hydroxyhydantoin Carbamate Inhibitors of Mammalian Serine Hydrolases. *Chemistry & biology* 22, 928-937 (2015).

23 Kamat, S. S., Camara, K., Parsons, W. H., Chen, D. H., Dix, M. M., Bird, T. D., Howell, A. R. & Cravatt, B. F. Immunomodulatory lysophosphatidylserines are regulated by ABHD16A and ABHD12 interplay. *Nat Chem Biol* 11, 164-171 (2015).

24 Hoover, H. S., Blankman, J. L., Niessen, S. & Cravatt, B. F. Selectivity of inhibitors of endocannabinoid biosynthesis evaluated by activity-based protein profiling. *Bioorg Med Chem Lett* 18, 5838-5841 (2008).

25 Nomura, D. K., Lombardi, D. P., Chang, J. W., Niessen, S., Ward, A. M., Long, J. Z., Hoover, H. H. & Cravatt, B. F. Monoacylglycerol lipase exerts dual control over endocannabinoid and fatty acid pathways to support prostate cancer. *Chemistry & biology* 18, 846-856 (2011).

26 Brown, M. S., Ye, J., Rawson, R. B. & Goldstein, J. L. Regulated intramembrane proteolysis: a control mechanism conserved from bacteria to humans. *Cell* 100, 391-398 (2000).

27 Wolfe, M. S. Intramembrane-cleaving proteases. *J Biol Chem* 284, 13969-13973 (2009).

28 Urban, S., Lee, J. R. & Freeman, M. *Drosophila* rhomboid-1 defines a family of putative intramembrane serine proteases. *Cell* 107, 173-182 (2001).

29 Strisovsky, K. Why cells need intramembrane proteases - a mechanistic perspective. *FEBS J* (2015).

30 Sherratt, A. R., Blais, D. R., Ghasriani, H., Pezacki, J. P. & Goto, N. K. Activity-based protein profiling of the Escherichia coli GlpG rhomboid protein delineates the catalytic core. *Biochemistry* 51, 7794-7803 (2012).

31 Vosyka, O., Vinothkumar, K. R., Wolf, E. V., Brouwer, A. J., Liskamp, R. M. J. & Verhelst, S. H. L. Activity-based probes for rhomboid proteases discovered in a mass spectrometry-based assay. *Proc Natl Acad Sci U S A* 110, 2472-2477 (2013).

32 Nguyen, M. T., Kersavond, T. V. & Verhelst, S. H. Chemical Tools for the Study of Intramembrane Proteases. *ACS Chem Biol* 10, 2423-2434 (2015).

33 Rath, A., Glibowicka, M., Nadeau, V. G., Chen, G. & Deber, C. M. Detergent binding explains anomalous SDS-PAGE migration of membrane proteins. *Proc Natl Acad Sci U S A* 106, 1760-1765 (2009).

34 Gerlt, J. A., Allen, K. N., Almo, S. C., Armstrong, R. N., Babbitt, P. C., Cronan, J. E., Dunaway-Mariano, D., Imker, H. J., Jacobson, M. P., Minor, W., Poulter, C. D., Raushel, F. M., Sali, A., Shoichet, B. K. & Sweedler, J. V. The Enzyme Function Initiative. *Biochemistry* 50, 9950-9962 (2011).

35 Nomura, D. K., Long, J. Z., Niessen, S., Hoover, H. S., Ng, S. W. & Cravatt, B. F. Monoacylglycerol lipase regulates a fatty acid network that promotes cancer pathogenesis. *Cell* 140, 49-61 (2010).

36 Adibekian, A., Martin, B. R., Wang, C., Hsu, K. L., Bachovchin, D. A., Niessen, S., Hoover, H. & Cravatt, B. F. Click-generated triazole ureas as ultrapotent in vivo-active serine hydrolase inhibitors. *Nat Chem Biol* 7, 469-478 (2011).

37 Ahn, K., Johnson, D. S., Mileni, M., Beidler, D., Long, J. Z., McKinney, M. K., Weerapana, E., Sadagopan, N., Liimatta, M., Smith, S. E., Lazerwith, S., Stiff, C., Kamtekar, S., Bhattacharya, K., Zhang, Y., Swaney, S., Van Becelaere, K., Stevens, R. C. & Cravatt, B. F. Discovery and characterization of a highly selective FAAH inhibitor that reduces inflammatory pain. *Chemistry & biology* 16, 411-420 (2009).

38 Chang, J. W., Cognetta, A. B., 3rd, Niphakis, M. J. & Cravatt, B. F. Proteome-Wide Reactivity Profiling Identifies Diverse Carbamate Chemotypes Tuned for Serine Hydrolase Inhibition. *ACS Chem Biol* 8, 1590-1599 (2013).

39 Adibekian, A., Martin, B. R., Chang, J. W., Hsu, K. L., Tsuboi, K., Bachovchin, D. A., Speers, A. E., Brown, S. J., Spicer, T., Fernandez-Vega, V., Ferguson, J., Hodder, P. S., Rosen, H. & Cravatt, B. F. Confirming target engagement for reversible inhibitors in vivo by kinetically tuned activity-based probes. *J Am Chem Soc* 134, 10345-10348 (2012).

40 Soding, J., Biegert, A. & Lupas, A. N. The HHpred interactive server for protein homology detection and structure prediction. *Nucleic Acids Res* 33, W244-248 (2005).

41 Patricelli, M. P., Giang, D. K., Stamp, L. M. & Burbaum, J. J. Direct visualization of serine hydrolase activities in complex proteomes using fluorescent active site-directed probes. *Proteomics* 1, 1067-1071 (2001).

42 Tully, S. E. & Cravatt, B. F. Activity-based probes that target functional subclasses of phospholipases in proteomes. *Journal of the American Chemical Society* 132, 3264-3265 (2010).

43 Hsu, K. L., Tsuboi, K., Adibekian, A., Pugh, H., Masuda, K. & Cravatt, B. F. DAGLbeta inhibition perturbs a lipid network involved in macrophage inflammatory responses. *Nat Chem Biol* 8, 999-1007 (2012).

44 Washburn, M. P., Wolters, D. & Yates, J. R., 3rd. Large-scale analysis of the yeast proteome by multidimensional protein identification technology. *Nat Biotechnol* 19, 242-247 (2001).

Chapter 4:

Stereochemistry of Endogenous Palmitic Acid Ester of 9-Hydroxystearic Acid and Relevance of Absolute Configuration to Regulation

Abstract

Lipids have fundamental roles in the structure, energetics, and signaling of cells and organisms. The recent discovery of fatty acid esters of hydroxy fatty acids (FAHFAs), lipids with potent anti-diabetic and anti-inflammatory activities, indicates that our understanding of the composition of lipidome and the function of lipids is incomplete. The ability to synthesize and test FAHFAs was critical in elucidating the roles of these lipids, but these studies were performed with racemic mixtures, and the role of stereochemistry remains unexplored. Here, we synthesized the *R*- and *S*- palmitic acid ester of 9-hydroxystearic acid (*R*-9-PAHSA, *S*-9-PAHSA). Access to highly enantioenriched PAHSAs enabled the development of a liquid chromatography-mass spectrometry (LC-MS) method to separate and quantify *R*- and *S*-9-PAHSA, and this approach identified *R*-9-PAHSA as the predominant stereoisomer that accumulates in adipose tissues from transgenic mice where FAHFAs were first discovered. Furthermore, biochemical analysis of 9-PAHSA biosynthesis and degradation indicate that the enzymes and pathways for PAHSA production are stereospecific, with cell lines favoring the production of *R*-9-PAHSA and carboxyl ester lipase (CEL), a PAHSA degradative enzyme, selectively hydrolyzing *S*-9-PAHSA. These studies highlight the role of stereochemistry in the production and degradation of PAHSAs and define the endogenous stereochemistry of 9-PAHSA in adipose tissue. This information will be useful in the identification and characterization of the pathway responsible for PAHSA biosynthesis, and access to enantiopure PAHSAs will elucidate the role of stereochemistry in PAHSA activity and metabolism *in vivo*.

4.1 Introduction

Mice engineered to overexpress the glucose transporter, GLUT4, selectively in their adipose tissue (AG4OX mice)[1-3] have provided insights into the link between obesity and Type 2 diabetes because they are obese but have lower fasting glycemia and enhanced glucose tolerance. Analysis of adipose tissues from AG4OX mice demonstrated marked increases in *de novo* lipogenesis,[2,3] and this activity is necessary for the enhanced glucose tolerance in these animals. Lipidomics analysis of adipose tissue from AG4OX mice to identify specific lipids that might contribute to the insulin sensitive phenotype led to the discovery of a novel class of lipids[4] that are highly elevated in AG4OX adipose tissues.[4] These lipids were named Fatty Acid esters of Hydroxy Fatty Acids (FAHFAs) to describe their structures (**Figure 4.1**).

FAHFAs contain two acyl chains connected through a single ester bond (**Figure 4.1**), and further targeted liquid chromatography-mass spectrometry (LC-MS) determined that at least 16 different FAHFA families exist,[4] which differ in their acyl chain constituents (**Figure 4.1**), and additional FAHFA families have been found since.[5,6] For instance, palmitic acid esters of hydroxy stearic acids (PAHSAs) and oleic acid esters of hydroxy stearic acid (OAHSAs) are two of the most abundant families that were identified.[4] In addition, for each FAHFA family that has been looked at in detail, different ester regioisomers exist (**Figure 4.1**). In adipose tissue of wild-type and AG4OX mice, eight distinct PAHSA regioisomers (5, 7, 8, 9, 10, 11, 12, and 13) were identified.[4] Regioisomers demonstrate differential regulation and biological activity. For example, all the PAHSA regioisomers were markedly elevated in adipose tissue and serum of AG4OX mice while the isomers in liver were decreased. Furthermore, when wild type mice were placed on a high-fat diet, only two PAHSA isomers were changed in serum, while all isomers were reduced in subcutaneous adipose tissue but some were elevated in perigonadal adipose tissue[4]. This suggests that PAHSAs can be regulated as a family or individually under different conditions and in different tissues. Furthermore, 5- and 9-PAHSA have potent anti-diabetic

effects *in* vivo and enhance glucose transport and insulin secretion in vitro, but only 9-PAHSA has anti-inflammatory effects in dendritic cells, highlighting regiospecific biological activity.[4]

Interest in the PAHSAs was piqued further by the analysis of human sera that revealed that PAHSA levels are lower in insulin-resistant humans relative to their insulin-sensitive counterparts, suggesting that PAHSAs may play an important role in maintaining normal blood sugar and insulin sensitivity in people.[4] Indeed, oral administration of 9-PAHSA or 5-PAHSA to mice on a high-fat diet improved glucose tolerance through multiple pathways that include increases in glucagon-like peptide 1 (GLP-1) and insulin secretion.[4]

The anti-inflammatory properties of FAHFAs can also extend to the treatment of inflammatory diseases as was demonstrated by recent work showing that oral 9-PAHSA treatment reduces the severity and impedes inflammation and damage associated with colitis in a mouse model.[7] And other novel FAHFA families with anti-inflammatory activities have recently been discovered. Omega-3 fatty acid FAHFAs, produced after the addition of omega-3-fatty acids to cells, have potent anti-inflammatory activity.[5]

Thus, FAHFAs, and in particular PAHSAs, are an exciting class of novel lipids with a range of biological activities. One important structural question that remains unanswered is the natural configuration of the chiral center in PAHSAs. We studied 9-PAHSA, the most abundant and a biologically active PAHSA. Herein we report the first asymmetric synthesis of *R*- and *S*-9-PAHSA (**Figure 4.2**) and *R*- and *S*-9-HSA, and utilize these compounds to define the stereochemistry of endogenous 9-PAHSA from AG4OX mouse adipose tissue. This work represents a critical step in understanding PAHSA biology by defining endogenous FAHFA structure.

4.2 Results and Discussion

Synthesis of enantiopure R- and S-9-PAHSA and 9-HSA

We developed multi-gram scale syntheses of enantiopure *R*- and *S*-9-PAHSA and HSA to further understand the influence of FAHFA structure on their pronounced biological effects. Building upon previous work synthesizing related compounds such as palmitic acid esters of hydroxy palmitic acid (PAHPAs)[8] and methods for accessing enantioenriched 9-HSA (54% ee)[9] we have developed a route that provides material on large scale (> 5 gram batches), high enantiomeric excess (>98% ee), and free from heavy metal impurities - all enabling extensive biological testing.

Using epichlorohydrin as both a readily available chiral starting material and lynchpin that connects the three regions of PAHSAs, the synthesis of both enantiomers was achieved. The synthesis of *R*-9-PAHSA (**1-*R***) began with the addition of 7-octenylmagnesium bromide into *S*-(+)-epichlorohydrin **4** using catalytic copper (I) iodide to generate chlorohydrin **5** (**Scheme 4.1**). Epoxide formation from chlorohydrin **5**, yielding epoxide **6**, was followed by a second epoxide opening reaction at the less substituted position using octylmagnesium chloride in the presence of cuprous iodide to afford secondary alcohol **7** as a solid. The relay of enantiopurity, and retention of configuration at the chiral center, was assessed by derivatization of **7** as the *S*-O-acetylmandelate ester[9,10] with the diastereomeric ratio found to be greater than 99:1 (supporting info). Palmitoylation of alcohol **7** with palmitoyl chloride and pyridine provided ester **8**. Reaction of **8** with ozone in the presence of *N*-methylmorpholine *N*-oxide (NMO)[11] followed by Pinnick oxidation[12] of the crude intermediate provided *R*-9-PAHSA (**1-*R***) in 55% yield. Degradation of *R*-9-PAHSA (**1-*R***) by saponification yielded *R*-9-HSA (Supporting Information). *S*-9-PAHSA (**1-*S***) and *S*-9-HSA were synthesized in an analogous manner, substituting *R*-(+)-epichlorohydrin **9** at the start of the synthesis (in place of *S*-(+)-epichlorohydrin **4**) through the same 5 step sequence in 61% overall yield (**Scheme 4.1**).

Determination of endogenous 9-PAHSA stereochemistry

Fatty acid oxidation is a common event in the production of bioactive lipids. Prostaglandins and leukotrienes, for example, are generated from the oxidation of arachidonic acids.[13] The enzymatic introduction of oxygen occurs in a stereospecific manner and the stereochemistry in these lipids define their activity.[14] The PAHSAs also contain an oxidized fatty acid, the HSA, which places a stereocenter in this lipid. Since stereochemistry has an important role in bioactive lipid function, and can provide information about the enzymes and biochemical pathways for lipid metabolism, we sought to define the endogenous stereochemistry of 9-PAHSA.

We have an established method to separate and analyze these different families and isomers using reversed-phase chromatography,[15] however, this method is unable to resolve stereoisomers. The first step in determining the stereochemistry of natural FAHFAs required us to develop a method capable of separating the different isomers. We attempted several approaches to separate PAHSAs (**Scheme 4.2**). First, we used chiral GC, where **1-*R*** and **1-*S*** were converted to the corresponding methyl ester using TM*S*-diazomethane, but we were unable to separate these stereoisomers. Next, we converted ***rac*-1** to the corresponding amide with *S*-1-phenylethan-1-amine to generate diastereomers that we hoped to separate. These attempts were also unsuccessful, likely owing to the large distance between to two chiral centers.

Unable to separate the 9-PAHSA stereoisomers with our resources, we decided to use Phenomenex's (Torrance, CA) chiral screening service. We provided enantiopure *R*-9-PAHSA and *rac*-9-PAHSA. These compounds were tested on 6 of their chiral columns (Cellulose-1, Cellulose-2, Cellulose-3, Cellulose-4, Amyolse-2, and Amylose-1) using 3 different mobile phases (water/acetonitrile, hexane/ethanol, and methanol/isopropanol). The column and mobile phase that provided the best resolution was the Lux 5 μm Cellulose-3 column with methanol/isopropanol/trifluoroacetic acid (TFA) (90:10:0.1) (**Figure 4.3**). Using these conditions

and column as a starting point, we continued to refine the method for our purposes. Specifically, we needed to modify the method since TFA is not compatible with LC-MS,[16] and we needed the sensitivity of mass spectrometry to be able to detect 9-PAHSA from endogenous sources.

These efforts led to an optimized method that uses a Lux 3 μm Cellulose-3 column in combination with an isocratic MeOH/H_2O/formic acid (96:4:0.1) mobile phase (**Figure 3A**). Under these conditions, *R*-9-PAHSA elutes from the column at 20.2 min, while *S*-9-PAHSA elutes at 17.4 min, affording 2.8 min of peak separation to resolve these stereoisomers. One caveat with this method is that liquid chromatography conditions required to separate the stereoisomers use formic acid, a mobile phase modifier typically reserved for positive mode ionization, but 9-PAHSA detection by mass spectrometry requires negative mode ionization. In our initial tests we used a mobile phase that was similar to our established FAHFA measurement method, which includes 0.01% ammonium hydroxide,[15] however, this could not achieve baseline resolution of the stereoisomers (**Figure 4.4**). It is important to note that with the presence of 0.1% formic acid, we observed a 25-fold reduction in the sensitivity of our detection due to the impaired ionization of the 9-PAHSA (**Figure 4.4**). As a result, any possibility of detecting endogenous 9-PAHSA requires a sample with high concentrations of this lipid.

We have previously shown that FAHFA levels are dramatically upregulated in AG4OX mice.[3] Specifically, 9-PAHSA levels were elevated ~16-18 fold in the white adipose tissue (WAT) of AG4OX and the final concentration of 9-PAHSA is ~1000pmol/g in perigonadal white adipose tissue (PGWAT). The high 9-PAHSA concentrations make the PGWAT from AG4OX mice the best tissue to measure endogenous 9-PAHSA under conditions of reduced sensitivity. Additionally, by comparing WT and AG4OX samples by chiral LC-MS we can readily identify the 9-PAHSA peak as the one with the largest fold change between the two samples to provide an unambiguous identification of this lipid in the resulting chromatograms. LC-MS analysis of the samples revealed that *R*-9-PAHSA was elevated in AG4OX samples compared to WT PGWAT, with the *R*-9-PAHSA peak clearly elevated in the LC-MS chromatogram (**Figure 4.5A**). There is

also a much smaller peak that overlaps with the *S*-9-PAHSA standard. We cannot determine if this is *S*-9-PAHSA or a 10-PAHSA stereoisomers because *S*-9-PAHSA or a 10-PAHSA have similar retention times (**Figure 4.6**). We analyzed these same samples using our standard (i.e. non-chiral reverse phase) method (**Figure 4.7**) and found an equivalent fold change for *R*-9-PAHSA (chiral column) and total 9-PAHSA (reversed-phase column) (**Figure 4.5B**) highlighting that *R*-9-PAHSA is the main source of the elevated 9-PAHSA levels we observe in AG4OX PGWAT.

Stereospecificity of 9-PAHSA degradation and biosynthesis

Having identified the predominant stereoisomer in AG4OX PGWAT, we wanted to test whether the biochemical pathways or enzymes that control 9-PAHSA biosynthesis and degradation are stereospecific. We have recently identified the enzyme carboxyl ester lipase (CEL) to be a FAHFA hydrolase.[17] CEL is an enzyme of the exocrine pancreas and is secreted into the gut to assist with the digestion of lipids from the diet.[18] Though originally identified as a triglyceride and cholesterol ester hydrolase, our recent work clearly shows that this enzyme prefers FAHFAs, including 9-PAHSA.

The pancreas has the highest 9-PAHSA hydrolytic activity compared to other tissues, and we showed that this FAHFA degrading activity is due to CEL. To determine if CEL prefers *R*- or *S*-9-PAHSA, we carried out a previously reported LC-MS assay to measure hydrolytic activity.[17,19] We expressed CEL in HEK293T cells and isolated membrane lysates from these cells to measure CEL-mediated 9-PAHSA hydrolysis. The data clearly demonstrate that CEL prefers *S*-9-PAHSA to *R*-9-PAHSA as a substrate (**Figure 4.8A**), indicating that the enzyme is stereoselective. In support of this finding, this same trend was also observed when testing the hydrolytic activity of these enantiomers in mouse pancreatic membrane lysate (**Figure 4.8B**). This data supports the idea that PAHSA metabolism *in vivo* is stereoselective, and at least in the pancreas, this activity favors the degradation of *S*-9-PAHSA.

Although the biosynthetic enzymes responsible for FAHFA synthesis are unknown, it has been previously shown that the addition of palmitoyl-CoA and 9-HSA to liver and WAT lysate results in the production of 9-PAHSA.[4] Here, we present a cell-based assay where the addition of HSAs results in the production of FAHFAs, such as 9-PAHSA. In this assay, we treat HEK293T cells with either *R*- or *S*-9-HSA, incubate the cells for two hours, and then harvest the cells and extract the 9-PAHSA for subsequent analysis by LC-MS. The *R*- or *S*-9-HSA is acylated by endogenous free fatty acids such as palmitate and oleate, as these were not added as acyl-donors. *R*-9-HSA-treated cells exhibited a substantial increase of 9-PAHSA and 9-OAHSA (~80%) compared to *S*-9-HSA-treated cells (**Figure 4.9**). The stereospecificity of 9-PAHSA biosynthesis supports the idea of that PAHSA biosynthesis is mediated by an unidentified acyl transferase and is not the result of a non-enzymatic acylation. Furthermore, these preliminary data indicate a preference for the biosynthesis of *R*-9-PAHSA, which, if similar in adipose tissue could explain the observation of *R*-9-PAHSA as the preferred stereoisomer *in vivo*.

4.3 Conclusion

The importance of absolute structure in the biochemistry and biological activity of lipids prompted us to develop the first stereoselective synthesis of PAHSAs, which enabled us to identify the natural isomer in adipose tissue as *R*-9-PAHSA. Starting from this important finding, this chemistry will enable access to numerous enantiopure FAHFAs, necessary to better understand their chemistry and biology. As the synthetic approach is modular, it is readily adaptable to the synthesis of related compounds. With the improved sensitivity of our chiral LC-MS method the measurement of additional FAHFA stereoisomers in other tissues is possible.
An important insight from the current work is that FAHFAs are products of enzymatic, not chemical production of the hydroxylated acids. Chemical oxidation of lipids with reactive oxygen species, such as peroxides, results in the production of racemic fatty acids.[20] By contrast,

enzyme-mediated hydroxy fatty acid production proceeds stereospecifically to produce enantiopure hydroxy lipids.[20,21] The discovery that *R*-9-PAHSA, but not *S*-9-PAHSA, is increasing in the AG4OX WAT supports the idea that this is an enzyme-mediated pathway and chemical oxidation of lipids does not have a role in PAHSA production in these mice. Additional work will endeavor to identify the enzymes and pathways that mediate PAHSA production *in vivo*, and small molecule activators or inhibitors of these PAHSA biosynthetic enzymes might someday allow control over endogenous PAHSAs levels. The continued interplay between chemical synthesis, biology, and biochemistry will reveal the biological potential of FAHFAs and identify new ways to regulate these molecules for therapeutic benefit.

4.4 Figures and Schemes

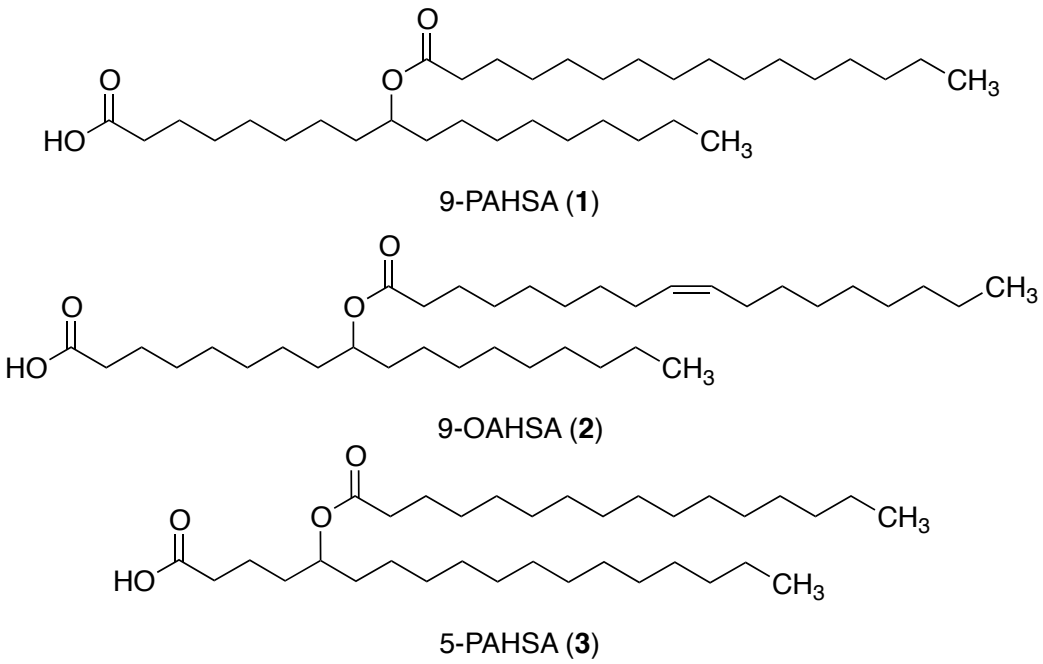

Figure 4.1. Endogenous FAHFA structures. Analysis of AG4OX mice revealed the existence of FAHFAs. Sixteen different FAHFA families, which differ in the composition of their acyl chains (e.g. PAHSA and OAHSA) were observed. And within each family there exist multiple regioisomers such as 9- and 5-PAHSA.

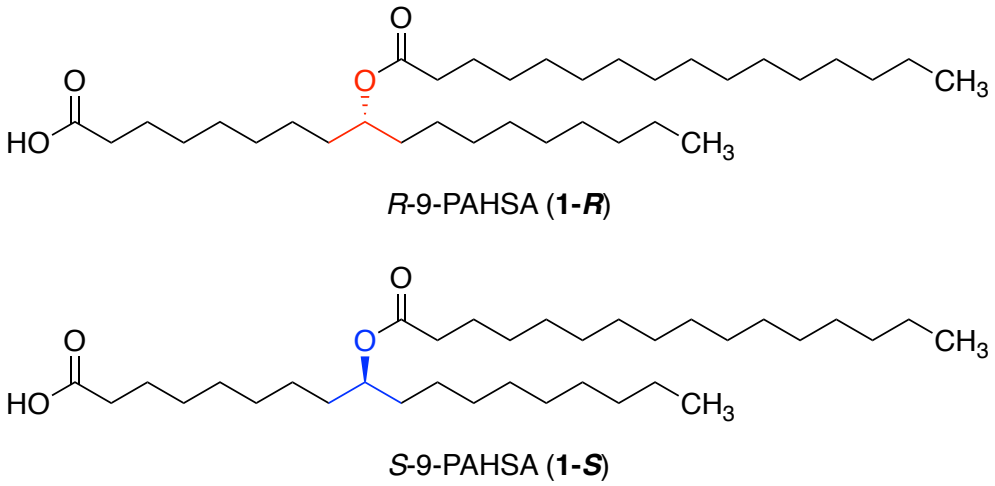

Figure 4.2. Structures of *S*-9-PAHSA (**1-*S***) and *R*-9-PAHSA (**1-*R***).

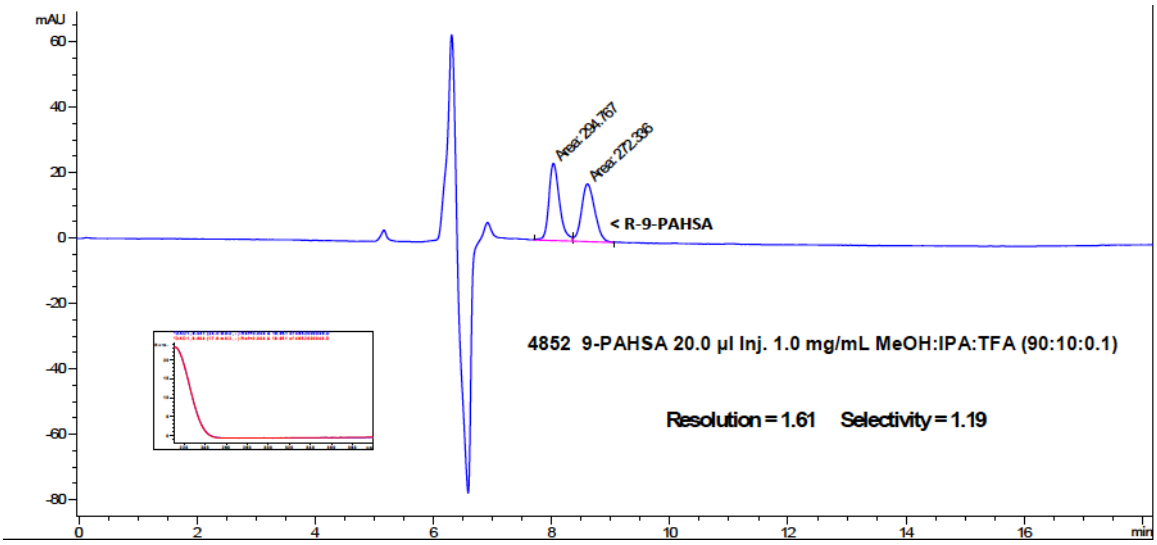

Figure 4.3. Result of screening service by Phenomenex. UV trace (abs=210 nm) showing resolution of rac-9-PAHSA. Resolution was acquired using a Lux 5 µm Cellulose-3 column and an isocratic gradient consisting of 90:10:0.1 (methanol/isopropanol/trifluoroacetic acid).

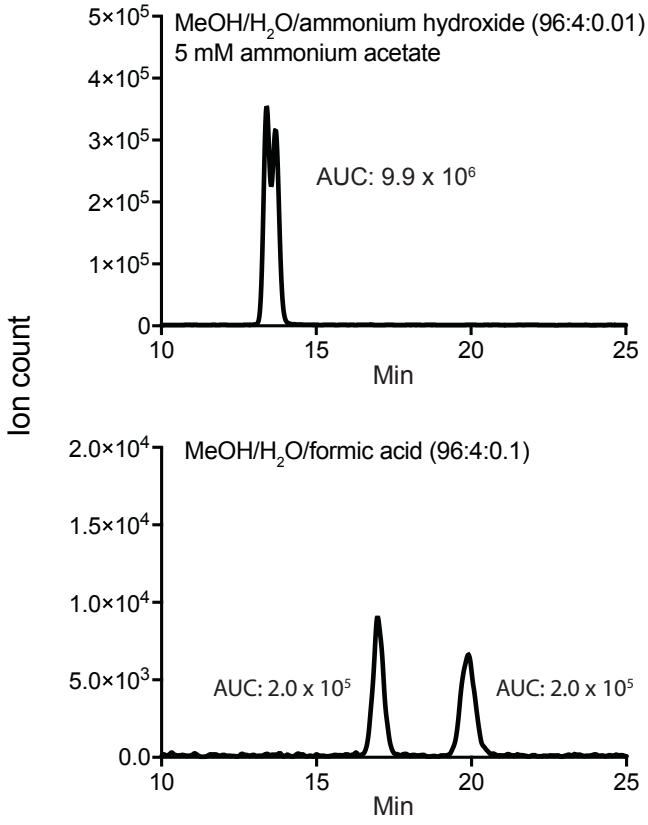

Figure 4.4. Effects of mobile phase additives on separation and intensity with chiral column. LC-MS traces of *rac*-9-PAHSA (2 pmol) with different modifiers in the mobile phase ran on a Lux 3 µm Cellulose-3 column. AUC, area under the curve. With the presence of the basic modifier, ammonium hydroxide *R*- and *S*-9-PAHSA stereoisomers were not well resolved (top trace). With the acidic modifier, formic acid, the stereoisomers were resolved, but with lower ionization efficiency (bottom trace).

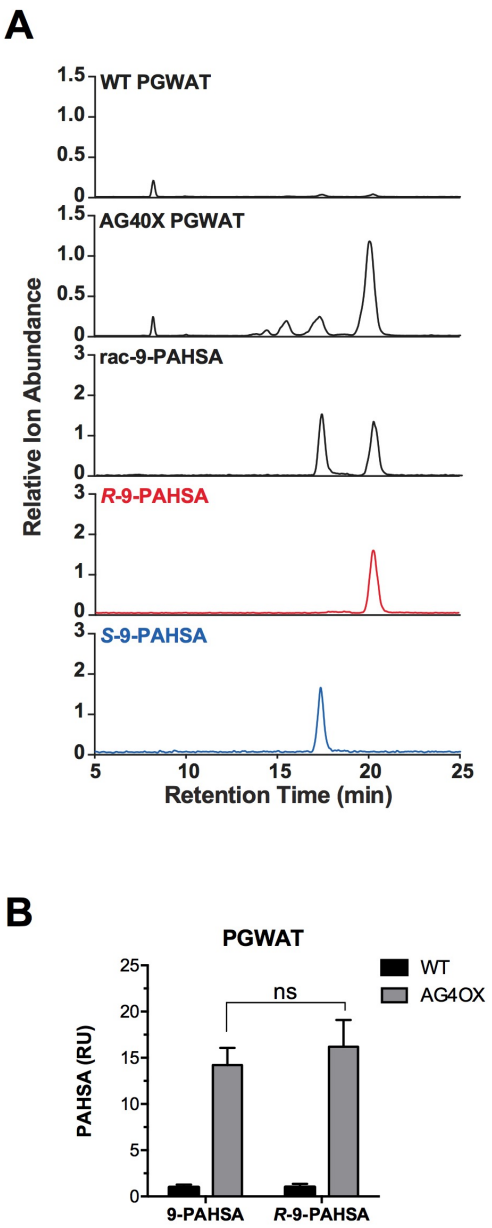

Figure 4.5. *R*-9-PAHSA is the prominent enantiomer in mouse adipose tissue. (**A**) Representative PAHSA MS traces in PGWAT of WT and AG4OX mice with *rac*-, *R*-, and *S*-9-PAHSA standards resolved on a Lux 3 μm Cellulose-3 chiral column. (**B**) 9-PAHSA and *R*-9-PAHSA fold change in AG4OX PGWAT vs WT PGWAT analyzed on a reversed-phase column and chiral column, respectively. PAHSA levels were normalized to the endogenous lipid d18:1/16:0 ceramide. Data represents means ± the standard error of the mean for three biological replicates. ns, not significant.

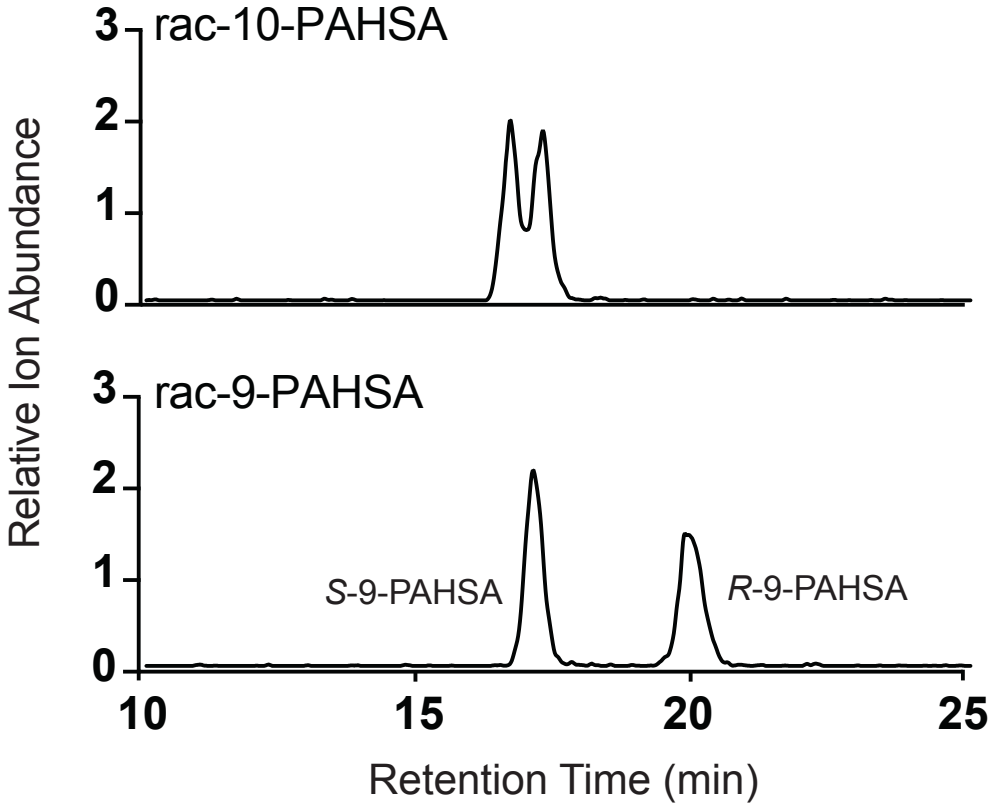

Figure 4.6. LC-MS analysis of *rac*-10- and *rac*-9-PAHSA on a chiral column. PAHSAs were run on a Lux 3 μm Cellulose-3 column with an isocratic flow of 0.4 mL/min of a 96:4 MeOH:H_2O + 0.1% formic acid solution.

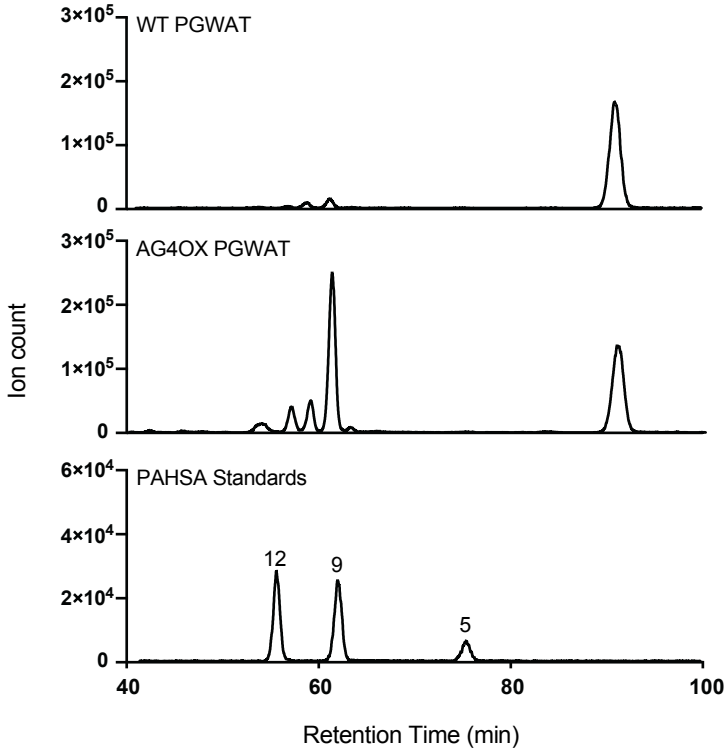

Figure 4.7. Analysis of WT and AG4OX WAT samples using our original method. Isocratic flow at 0.2 mL/min using 93:7 MeOH: H_20 with 5 mM ammonium acetate and 0.01% ammonium hydroxide on a Luna C18(2) reversed-phase column. The increase in 9-PAHSA in the AG4OX PGWAT versus the WT PGWAT is evident and the fold change is similar to the increase of R-9-PAHSA levels (**Figure 4.5**).

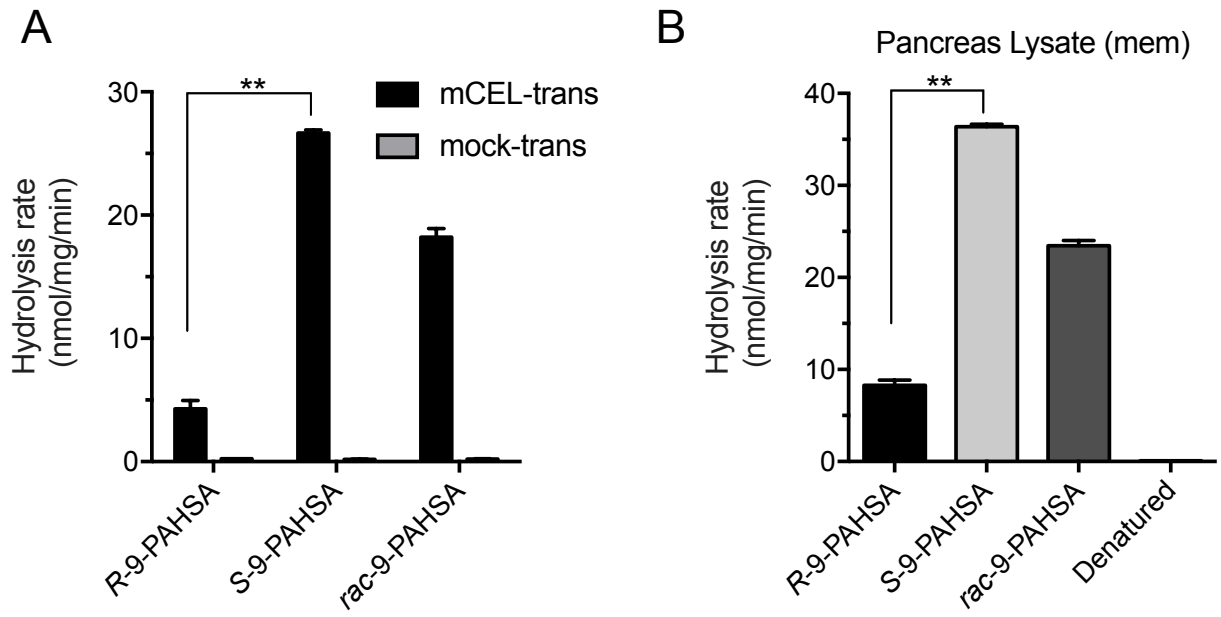

Figure 4.8. CEL prefers *S*-9-PAHSA as a substrate. (**A**) *R*-, *S*-, and *rac*-9-PAHSA hydrolysis activity for membrane lysates from CEL-transfected and mock-transfected HEK293T cells. Data represent means and the standard deviation for two biological replicates. (**B**) *R*-, *S*-, and *rac*-9-PAHSA hydrolysis activity for mouse pancreatic membrane lysates. Data represents mean and the standard error of the mean for three biological replicates. **p < 0.01 by Student's *t* test.

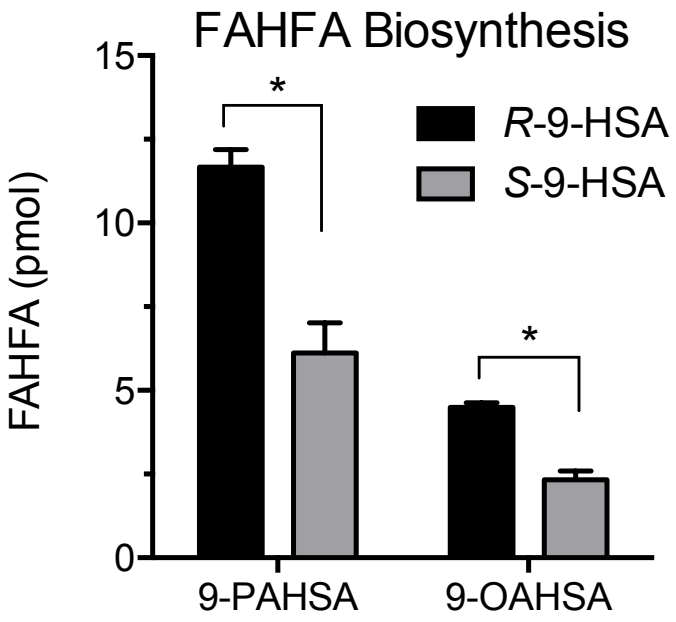

Figure 4.9. *R*-9-HSA is the preferred 9-HSA enantiomer for FAHFA biosynthesis. Biosynthesis of 9-PAHSA and 9-OAHSA in HEK293T cells after incubation with 100 μM of *R*- or *S*-HSA for 2 h. *$p < 0.05$ by two-sided Student's *t*-test comparing *R*-9-HSA-treated versus *S*-9-HSA-treated HEK293T cells.

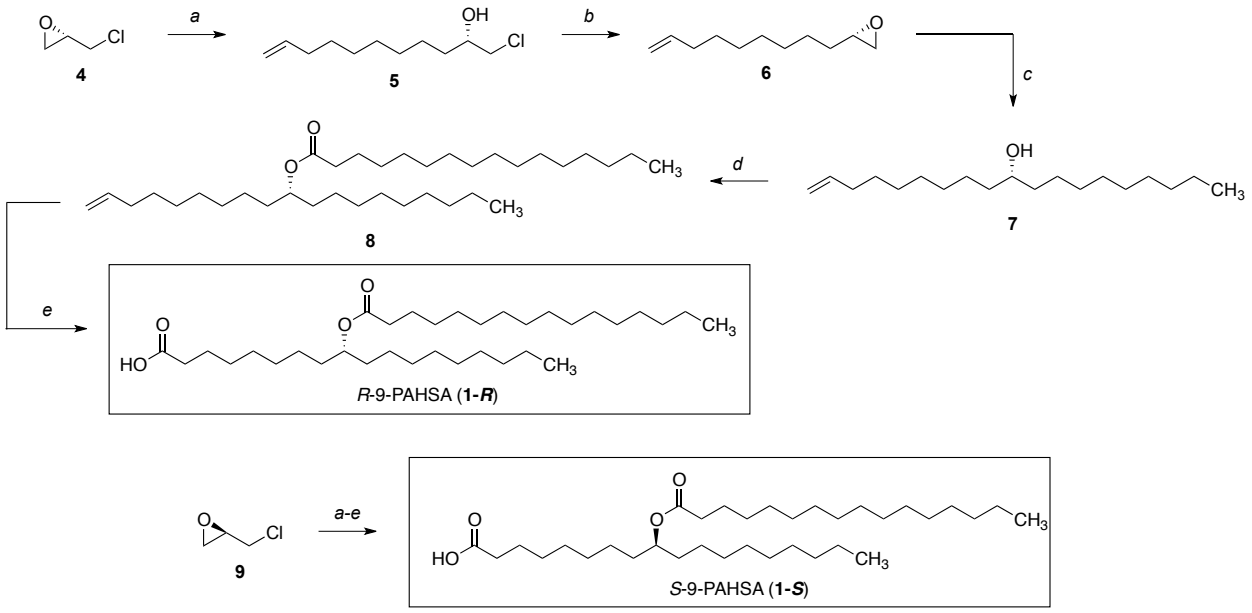

Scheme 4.1. Syntheses of *R*-9-PAHSA from *S*-(+)-epichlorohydrin (**4**) and *S*-9-PAHSA from *R*-(+)-epichlorohydrin (**9**). Conditions: (*a*) 7-octenylmagnesium bromide, CuI, THF, –78 to 23 °C (**1-*R*** sequence 92%, **1-*S*** sequence 91%); (*b*) NaOH, Et_2O, 23 °C; (*c*) octylmagnesium chloride, CuI, Et_2O, –78 to 23 °C (**1-*R*** sequence 70%, **1-*S*** sequence 90%; over two steps); (*d*) palmitoyl chloride, pyr., CH_2Cl_2, 0 to 23 °C(**1-*R*** sequence 91%, **1-*S*** sequence 78%); (*e*) O_3, NMO, CH_2Cl_2, –10 °C then $NaClO_2$, NaH_2PO_4, 2-methyl-2-butene, *t*-BuOH, 23 °C (**1-*R*** sequence 94%, **1-*S*** sequence 96%).

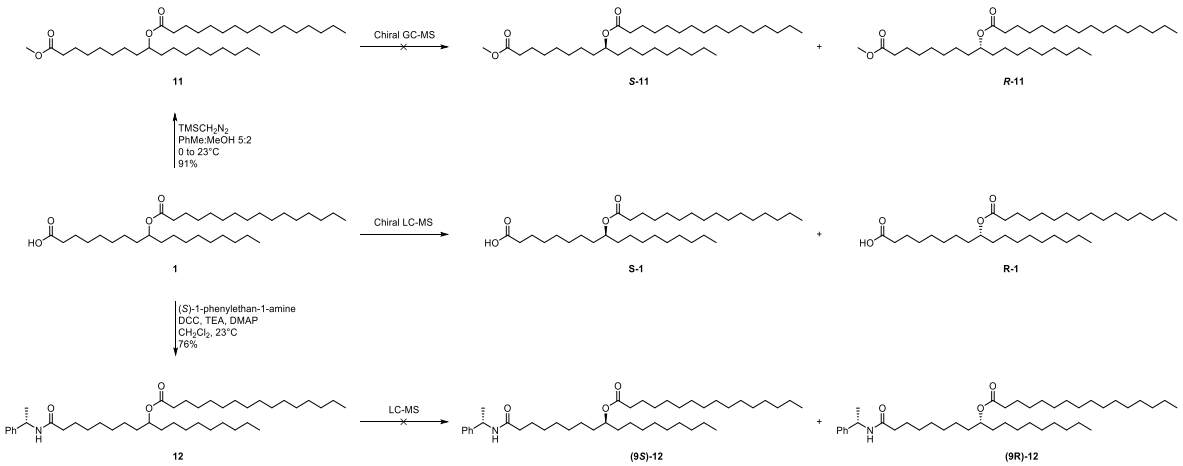

Scheme 4.2. Synthesis of 9-PAHSA derivatives prepared for chiral separation.

4.5 Experimental Section

Materials. All chemical reagents were purchased from Sigma-Aldrich unless otherwise stated. 5-, 9-, 12-PAHSA LC-MS standards were purchased from Cayman Chemical. [^{13}C16]-Palmitic acid was purchased from Cambridge Isotopes and used to synthesize the 13C-9-PAHSA used as an internal standard. Organic solvents for chemical synthesis were purchased from EMD Millipore (Billerica, MA). Solvents for HPLC were purchased from EMD Millipore and solvents for LC-MS were from Honeywell Burdick & Jackson.

Biological sample preparation. Lipid extraction was performed based on known protocol.[22,23] Murine tissues (60–150 mg), human fat biopsy (50–70 mg) were Dounce homogenized on ice for 40 strokes in a mixture of 1.5 ml: 1.5 ml: 3 ml citric acid buffer (100 mM trisodium citrate, 1 M NaCl, pH 3.6): methanol: chloroform. 13C-9-PAHSA standard (0.5–5 pmol per sample depending on tissue type) was added to chloroform prior to extraction. The resulting mixture was centrifuged at 2,200 g, 6 min, 4 °C to separate organic and aqueous phases, and the organic phase containing extracted lipids was removed with a Pasteur pipette, dried under a gentle stream of Nitrogen and stored at -80 °C prior to solid phase extraction (SPE). SPE was performed at room temperature via gravity flow. SPE cartridge (500 mg silica, 6 ml, Thermo Scientific, 60108-411) was conditioned with 15 ml hexane. Extracted lipids (reconstituted in 200 ml chloroform) were loaded onto column. Vial containing lipids was washed with an additional 100 ml chloroform and the wash also loaded onto the column. Neutral lipids were eluted with 16 ml 5% ethyl acetate in hexane, followed by elution of FAHFAs with 16 ml ethyl acetate. FAHFA fraction was dried under nitrogen and stored at -80 °C prior to LC-MS.

9-PAHSA enantiomer hydrolysis assay. *Rac*-, *S*-, and *R*-9-PAHSA hydrolysis was measured and analyzed as described.[7] Briefly, tissue/cell membrane lysates (20 μg) were incubated with *rac*-, *R*-, or *S*-9-PAHSA (100 μM) in PBS (200 μL) at 37 °C while being shaken.

Lipids were then extracted using a 2:1 $CHCl_3$/MeOH mixture (400 μL) spiked with 9-hydroxyheptadecanoic acid (50 pmol) as an internal standard. This mixture was votexed, and spun for 5 min at 2200g. The bottom organic layer was isolated and dried. The extract was then dissolved in 100 μL MeOH and 10 μL was subjected to LCMS using a Thermo TSQ Quantiva MS fitted with an Acquity UPLC BEH C18 column (Waters).

Targeted LC-MS analysis of PAHSAs. PAHSAs were measured on a TSQ Quantiva LC-MS via Multiple Reaction Monitoring (MRM) in negative ionization mode as described.[21] The following MS source parameters were used: spray voltage, 3.5 kV; ion transfer tube temperature, 325 °C; vaporizer temperature, 275 °C; sheath gas, 2.7 L/min; aux gas, 5.0 L/min; and sweep gas, 1.5 L/min. A Luna C18(2) reversed-phase column (3 μm, 250 x 2.0 mm, Phenomenex) was used. PAHSAs were resolved with isocratic flow at 0.2 mL/min using 93:7 MeOH: H_2O with 5 mM ammonium acetate and 0.01% ammonium hydroxide over 100 minutes. MRM [collision energy (CE) of 28 V , RF lens set at 106 V] was used to detect PAHSA (m/z 537.6 → 255.2).

Targeted LC-MS analysis of PAHSA enantiomers. PAHSA enantiomers were analyzed on a TSQ Quantiva LC-MS in negative mode with the same parameters mentioned above. Resolution of 9-PAHSA enantiomers was achieved using a Lux Cellulose-3 chiral column (3 μm, 250 x 4.6 mm, Phenomenex) with an isocratic flow rate of 0.4 mL/min of a 96:4 MeOH:H_2O + 0.1% formic acid solution.

FAHFA biosynthesis assay. Prior to seeding HEK293T cells, 6-well plates were pretreated with 50 mg/mL poly-lysine for 2 hours. Cells were grown in DMEM supplemented with 10% FCS. After cells reached 90-95% confluence, the media (2 mL/well) was replaced with 100 mM *R*- or *S*-12-HSA. After incubation at 37 °C, 5% CO2 for 2 hours, cells were washed with sterile PBS (3x) and harvested by scraping. Cells were re-suspended in 1 mL sterile PBS and mixed with 3 mL of 2:1 $CHCl_3$:MeOH with internal standard (5 pmol $^{13}C_4$-9-PAHSA). The sample

was vortexed and centrifuged at 2200 g. The bottom organic layer was isolated and dried. The extract was then dissolved in 100 mL MeOH and 10 mL was subjected to LCMS.

4.6 Acknowledgements

Chapter 4, in full, is a reprint with minor modification as it appears in Stereochemistry of Endogenous Palmitic Acid Ester of 9-Hydroxystearic Acid and Relevance of Absolute Configuration to Regulation, *Journal of the American Chemical Society* 139, 4943-4947 (2017). The dissertation author was the co-primary investigator and author of this paper along with Andrew T. Nelson. Other authors include Qian Chu, Ismail Syed, Barbara B. Kahn, Alan Saghatelian, and Dionicio Siegel.

4.7 References

1 Shepherd, P. R., Gnudi, L., Tozzo, E., Yang, H., Leach, F. & Kahn, B. B. Adipose cell hyperplasia and enhanced glucose disposal in transgenic mice overexpressing GLUT4 selectively in adipose tissue. *J Biol Chem* 268, 22243-22246 (1993).

2 Tozzo, E., Shepherd, P. R., Gnudi, L. & Kahn, B. B. Transgenic GLUT-4 overexpression in fat enhances glucose metabolism: preferential effect on fatty acid synthesis. *Am J Physiol* 268, E956-964 (1995).

3 Herman, M. A., Peroni, O. D., Villoria, J., Schon, M. R., Abumrad, N. A., Bluher, M., Klein, S. & Kahn, B. B. A novel ChREBP isoform in adipose tissue regulates systemic glucose metabolism. *Nature* 484, 333-338 (2012).

4 Yore, M. M., Syed, I., Moraes-Vieira, P. M., Zhang, T., Herman, M. A., Homan, E. A., Patel, R. T., Lee, J., Chen, S., Peroni, O. D., Dhaneshwar, A. S., Hammarstedt, A., Smith, U., McGraw, T. E., Saghatelian, A. & Kahn, B. B. Discovery of a class of endogenous mammalian lipids with anti-diabetic and anti-inflammatory effects. *Cell* 159, 318-332 (2014).

5 Kuda, O., Brezinova, M., Rombaldova, M., Slavikova, B., Posta, M., Beier, P., Janovska, P., Veleba, J., Kopecky, J., Jr., Kudova, E., Pelikanova, T. & Kopecky, J. Docosahexaenoic Acid-Derived Fatty Acid Esters of Hydroxy Fatty Acids (FAHFAs) With Anti-inflammatory Properties. *Diabetes* 65, 2580-2590 (2016).

6 Ma, Y., Kind, T., Vaniya, A., Gennity, I., Fahrmann, J. F. & Fiehn, O. An in silico MS/MS library for automatic annotation of novel FAHFA lipids. *J Cheminform* 7, 53 (2015).

7 Lee, J., Moraes-Vieira, P. M., Castoldi, A., Aryal, P., Yee, E. U., Vickers, C., Parnas, O., Donaldson, C. J., Saghatelian, A. & Kahn, B. B. Branched Fatty Acid Esters of Hydroxy Fatty Acids (FAHFAs) Protect against Colitis by Regulating Gut Innate and Adaptive Immune Responses. *J Biol Chem* 291, 22207-22217 (2016).

8 Balas, L., Bertrand-Michel, J., Viars, F., Faugere, J., Lefort, C., Caspar-Bauguil, S., Langin, D. & Durand, T. Regiocontrolled syntheses of FAHFAs and LC-MS/MS differentiation of regioisomers. *Org Biomol Chem* 14, 9012-9020 (2016).

9 Ebert, C., Felluga, F., Forzato, C., Foscato, M., Gardossi, L., Nitti, P., Pitacco, G., Boga, C., Caruana, P. & Micheletti, G. Enzymatic kinetic resolution of hydroxystearic acids: A combined experimental and molecular modelling investigation. *Journal of Molecular Catalysis B: Enzymatic* 83, 38-45 (2012).

10 Yang, W., Dostal, L. & Rosazza, J. P. Stereospecificity of microbial hydrations of oleic acid to 10-hydroxystearic acid. *Applied and environmental microbiology* 59, 281-284 (1993).

11 Schwartz, C., Raible, J., Mott, K. & Dussault, P. H. Fragmentation of carbonyl oxides by N-oxides: An improved approach to alkene ozonolysis. *Organic letters* 8, 3199-3201 (2006).

12 Bal, B. S., Childers, W. E. & Pinnick, H. W. Oxidation of α, β-un saturated aldehydes. *Tetrahedron* 37, 2091-2096 (1981).

13 Funk, C. D. Prostaglandins and leukotrienes: advances in eicosanoid biology. *Science* 294, 1871-1875 (2001).

14 Corey, E., Marfat, A., Goto, G. & Brion, F. Leukotriene B. Total synthesis and assignment of stereochemistry. *Journal of the American Chemical Society* 102, 7984-7985 (1980).

15 Zhang, T., Chen, S., Syed, I., Ståhlman, M., Kolar, M. J., Homan, E. A., Chu, Q., Smith, U., Borén, J. & Kahn, B. B. A LC-MS-based workflow for measurement of branched fatty acid esters of hydroxy fatty acids. *Nature protocols* 11, 747-763 (2016).

16 García, M., Hogenboom, A., Zappey, H. & Irth, H. Effect of the mobile phase composition on the separation and detection of intact proteins by reversed-phase liquid chromatography–electrospray mass spectrometry. *Journal of Chromatography A* 957, 187-199 (2002).

17 Kolar, M. J., Kamat, S. S., Parsons, W. H., Homan, E. A., Maher, T., Peroni, O. D., Syed, I., Fjeld, K., Molven, A. & Kahn, B. B. Branched Fatty Acid Esters of Hydroxy Fatty Acids Are Preferred Substrates of the MODY8 Protein Carboxyl Ester Lipase. *Biochemistry* 55, 4636-4641 (2016).

18 Chen, Q., Sternby, B. & Nilsson, Å. Hydrolysis of triacylglycerol arachidonic and linoleic acid ester bonds by human pancreatic lipase and carboxyl ester lipase. *Biochimica et Biophysica Acta (BBA)-Lipids and Lipid Metabolism* 1004, 372-385 (1989).

19 Parsons, W. H., Kolar, M. J., Kamat, S. S., Cognetta III, A. B., Hulce, J. J., Saez, E., Kahn, B. B., Saghatelian, A. & Cravatt, B. F. AIG1 and ADTRP are atypical integral membrane hydrolases that degrade bioactive FAHFAs. *Nature chemical biology* (2016).

20 Niki, E., Yoshida, Y., Saito, Y. & Noguchi, N. Lipid peroxidation: mechanisms, inhibition, and biological effects. *Biochemical and biophysical research communications* 338, 668-676 (2005).

21 Schneider, C., Pratt, D. A., Porter, N. A. & Brash, A. R. Control of oxygenation in lipoxygenase and cyclooxygenase catalysis. *Chemistry & biology* 14, 473-488 (2007).

22 Saghatelian, A., Trauger, S. A., Want, E. J., Hawkins, E. G., Siuzdak, G. & Cravatt, B. F. Assignment of endogenous substrates to enzymes by global metabolite profiling. *Biochemistry* 43, 14332-14339 (2004).

23 Bligh, E. G. & Dyer, W. J. A rapid method of total lipid extraction and purification. *Can J Biochem Physiol* 37, 911-917 (1959).

Chapter 5:

A Faster Protocol for Endogenous FAHFA Measurements

Abstract

Fatty acid esters of hydroxy fatty acids (FAHFAs) are a recently discovered class of endogenous lipids with anti-diabetic and anti-inflammatory activities. Interest in these lipids is due to their unique biological activity and the observation that insulin resistant people have lower palmitic acid esters of hydroxystearic acid (PAHSAs) levels, suggesting that a FAHFA deficiency may contribute to metabolic disease. Rigorous testing of this hypothesis will require the measurement of many clinical samples; however, current analytical workflows are too slow to enable enough samples to be analyzed quickly. Here, we describe the development of a significantly faster workflow to measure FAHFAs that optimizes the fractionation and chromatography of these lipids. We can measure FAHFAs in 30 minutes with this new protocol versus 90 minutes using the older protocol with comparable performance in regioisomer detection and quantitation. We also discovered through this optimization that oleic acid esters of hydroxystearic acids (OAHSAs), another family of FAHFAs, have a much lower background signal than PAHSAs, which makes them easier to measure. Our faster workflow was able to quantify changes in PAHSAs and OAHSAs from mouse tissues and human plasma highlighting the potential of this protocol for basic and clinical applications, respectively.

5.1 Introduction

The adipose tissue Glut4 overexpressor (AG4OX) mouse model is a valuable system for understanding the molecular pathways related to insulin sensitivity and metabolic disease[1-5]. Normally, obesity in rodents and humans is linked to the onset of insulin resistance and, eventually, the development of diabetes[6,7]. AG4OX mice are unique because they are obese, yet they remain insulin sensitive and are resistant to diabetes[1-5]. Gene expression studies followed by metabolic tracer studies revealed that AG4OX have increased lipid production (i.e., de novo lipogenesis (DNL)) in their adipose tissue and this increased DNL is necessary for the improved metabolism of these mice[3,5]. Elevated fatty acid levels are typically associated with poorer metabolic outcomes[6] suggesting that AG4OX mice might be producing beneficial lipids in their adipose tissue. Lipidomics of these animals followed by structure elucidation of the lipids with the largest fold change between AG4OX and WT samples revealed the existence of a new class of lipids called Fatty Acid Esters of Hydroxy Fatty Acids (FAHFAs). FAHFA are highly elevated in AG4OX mice[8] and subsequent biological studies demonstrated that FAHFAs have potent anti-diabetic and anti-inflammatory activities[8-10]. Serum and adipose tissue PAHSA levels from insulin resistant people are lower indicating that a FAHFA deficiency might underlie metabolic disease[8].

FAHFA families are defined by the composition of the fatty acid and hydroxy fatty acid. Analysis of AG4OX adipose tissue revealed the existence of 16 different FAHFA families[8]. For example, the two most highly upregulated FAHFA families in adipose tissue of AG4OX mice were palmitic acid esters of hydroxy stearic acids (PAHSAs) and oleic acid esters of hydroxy stearic acids (OAHSAs).

Within each FAHFA family discovered so far there are multiple regioisomers, which differ by the position of the ester. The distribution and amounts of the different regioisomers can vary

substantially between tissues. In mice, for example, there are eight different PAHSA regioisomers in adipose tissue three in liver, and six in serum[8]. The structural similarity of these regioisomers poses a challenge for their detection and quantitation. Obtaining baseline separation of different PAHSA regioisomers required extremely long isocratic gradients 90 minutes in length[8,11].

As interest in FAHFAs grows, faster protocols for analyzing and measuring different families and regioisomers[12] are needed. The current protocol for PAHSA measurements, for instance, are time-consuming because of the difficulty in separating PAHSA isomers from each other and from a contaminating ceramide[8,11]. This protocol also had a background which was negligible for most tissues with higher PAHSA levels but constitutes ~10-15% of the PAHSA signal in serum, which has low PAHSA concentrations.

Here, we optimized the protocol for endogenous FAHFA measurements to afford a method with significantly shorter run times but similar analytical performance. Our optimized protocol provides a rapid, robust method for measuring FAHFAs (PAHSAs and OAHSAs) that should increase the throughput and quality of endogenous FAHFA measurements for basic and clinical studies.

5.2 Results and Discussion

Development of a faster FAHFA LC-MS gradient

In our previous studies, we established a 90-minute liquid chromatography (LC) method to resolve PAHSA isomers using a Luna C18(2) (3 μm, 250 x 2.0 mm, Phenomenex) column[11]. Due to the long run time of each sample, this method is not ideal for analyzing hundreds of samples. To increase throughput of FAHFA analysis, we needed to shorten our run time while maintaining chromatographic resolution of FAHFA regioisomers. Our prior method went through extensive optimization of carrier solvents, additives, temperature, and flow rates and we did not want to alter these in developing a new method[11]. We made a mix of different PAHSA isomers

(5-, 9-, and 12-PAHSA) and OAHSA isomers (5-, 9-, and 12-OAHSA) and analyzed their retention times and resolution using different reversed phase columns. We found that the Acquity UPLC BEH C18 column (1.7 μm, 2.1 mm x 100 mm, Waters) afforded the best resolution in a 30-minute time frame (**Figure 5.1**).

In addition to shortening our run time, we also wanted to reduce the time and material for sample preparation. After the extraction of lipids, we enrich for FAHFAs by using solid-phase extraction (SPE). This step is critical in removing other lipids and contaminants that could impair chromatographic resolution and cause signal suppression of FAHFAs. We previously established a FAHFA enrichment setup using a silica extraction cartridge, however, this step would take nearly 4 hours. The majority of this time was waiting for flow through of solvent by gravity and drying down the eluted FAHFAs. To reduce the sample prep time, we modified the SPE method to utilize smaller volumes of elution solvent in addition to using positive pressure (nitrogen) to flow solvent through the column. Strata SI-1 Silica SPE cartridges (500 mg silica, 3 mL, Phenomenex) were conditioned with 6 mL of hexane, followed by sample addition to the cartridge. Neutral lipids were then eluted using 6 mL of 95:5 hexane:ethyl acetate, followed by the elution of FAHFAs with 4 mL of ethyl acetate. Solvents were added in 2 mL increments to avoid overfilling the SPE column. When applying positive pressure through the column, it is important not to dry out the sorbent bed mass to prevent phase collapse. This method can also be used with a vacuum manifold compatible with the SPE cartridges. Overall, this SPE method for FAHFA enrichment will take 1 hour.

Separation of 5-PAHSA from the ceramide contaminant.

The most referenced FAHFAs with biological activity are 5- and 9-PAHSA, therefore it is essential that we can detect these two PAHSA regioisomers in biological samples with our shorter method. In addition to SPE background issues when measuring PAHSA, another challenge to measuring PAHSAs, specifically 5-PAHSA is the existence of a contaminating

signal from a ceramide. Specifically, C16:0 ceramide shares all the major MRM transitions with PAHSAs[11]. This peak can be differentiated from PAHSAs by its differences in MRM transitions ratio. For example, the two most abundant product ions from the collision-induced dissociation of PAHSAs are palmitate (m/z 255.2) and dehydrated HSA (m/z 281.2), with the m/z 255.2 being greater than the m/z 281.2. For the contaminant ceramide, this ratio reversed, with the m/z 281.2 being greater than the m/z 255.2.

When initially measuring mouse serum PAHSAs with our faster method, we had issues separating the 5-PAHSA and the ceramide peak. In order to separate the 5-PAHSA from the ceramide, we tried altering the column temperature and flow rate (**Figure 5.2a,b**). Although lowering the flow rate from 0.2 ml/min to 0.15 ml/min allowed separation of 5-PAHSA and the ceramide peak, this came at the cost of extending the method from 30 minutes to 40 minutes. In order to keep our method under 30 minutes, we decided to increase the pH of the mobile phase by using 0.03% NH_4OH instead of our usual 0.01% NH_4OH (**Figure 5.3c**). The increase in pH allows PAHSAs to elute faster while the neutral ceramide is unaffected, thus allowing resolution of 5-PAHSA and the ceramide.

With the increase in NH_4OH in the mobile phase, we were concerned that this would break down FAHFAs as esters are base-labile. To test this, we ran a PAHSA ladder consisting of 12-, 10-, and 9-PAHSA with either 0.o1% NH_4OH or 0.03% NH_4OH and compared the area under the curves (AUC) (**Figure 5.3**). The increased pH does not degrade FAHFAs as can be seen by comparing the integrated peak areas of the respective PAHSA standards. In addition, with the increased pH, one can also observe the earlier retention shift of PAHSAs.

Solid-phase extraction contributes to the PAHSA background.

We previously reported that the use of silica SPE columns and some buffers yield background when trying to detect PAHSA[11]. For tissues with high levels of FAHFAs such as WAT and liver, this background is negligible. However, for other tissues or serum where FAHFA

levels are low, a background signal can account for up to 15% of the total PAHSA signal[11]. Indeed, we find that this background is problematic when measuring serum PAHSAs using our faster protocol where we observe extremely high background that can account for up to 50% of the signal in some runs.

Previous literature has shown that the SPE cartridges can be major sources of background contamination[13-15]. The most abundant contaminants from the SPE cartridges are phthalates and other plasticizers which are used in the manufacturing process of these cartridges. This background contamination is not constant and can vary from lot-to-lot and even column-to-column[14]. When we tested our SPE columns from two different lots, we observed variation in PAHSA background (**Figure 5.4**). The two lots had background PAHSAs ranging from 5- to 13/12-PAHSA, but with different PAHSA trace profiles. For example, in the cartridge from lot one, 13/12- and 9-PAHSA have similar peak heights, while in lot two, 9-PAHSA has the greatest peak height (**Figure 5.5**). This high level of background PAHSAs poses serious issues when measuring PAHSA from serum or a tissue with low PAHSA levels. The lot-to-lot variation also poses problems as the blank background levels can be significantly different.

The general workflow for the SPE enrichment of FAHFAs begins by prepping the SPE column for sample loading by equilibration with hexanes, loading of the sample in 200 μL of chloroform, followed by stepwise elution of analytes from the SPE column. To address the background issue, we tested a SPE prewash step with different organic solvents to remove the PAHSA background before equilibrating the column with hexanes.

We used different organic solvents in isolation or in combination to see which afforded minimal PAHSA background (**Figure 5.6**). For example, for the “EA + MeOH Prewash” we added 6 mL of ethyl acetate (EA) followed by 6 mL methanol (MeOH) before starting with our conditioning step of 6 mL hexanes. For these blank runs, we added 200 μL CHCL3 to the column after the conditioning step with hexanes to emulate true sample loading. We still

observed some PAHSA background with these prewashes, however it was significantly reduced (**Figure 5.6**).

The triple wash with EA, MeOH, and DCM did not appear to have any added benefit compared to the MeOH prewash alone. Although the MeOH prewash appeared to lower background more than the EA prewash for this lot of SPE cartridges, when using biological samples, we noticed the EA prewash was more reliable than MeOH prewash in sample reproducibility. We believe this is due to the MeOH not being completely removed before the sample is loaded, thus limiting the sample from binding to the stationary phase. We also tried an NH_2 SPE cartridge to enrich for FAHFAs, but this also had high levels of background PAHSAs that could not be removed with a MeOH prewash (**Figure 5.7**).

OAHSAs have lower background signal

Although PAHSAs have been the most studied FAHFAs to date[8,10], we reasoned that other FAHFA families may also serve as excellent markers of FAHFA levels. Indeed, during our discovery of FAHFAs, we found six FAHFA families that were highly elevated in the AG4OX adipose tissue[8]. As mentioned previously, the SPE columns can cause significant PAHSA background if the columns are not prewashed. In addition, if one alters the pH of the mobile phase for FAHFA analysis, this could lead to overlap of the 5-PAHSA and the C16:0 ceramide. Due to the potential diagnostic potential of serum FAHFA measurements, we wondered whether other FAHFAs might have a lower background to obviate this issue.

PAHSAs and OAHSAs only differ by their acyl chains. PAHSAs have a palmitoyl group (C16:0) while OAHSAs have an oleoyl group (C18:1). This physical difference can be seen chromatographically, as the OAHSA regioisomers elute later than analogous PAHSA isomers. For example, with our shorter method, the retention time of 9-OAHSA is ~19 min while the retention time of 9-PAHSA is ~18 min, showing that OAHSAs are slightly more hydrophobic

than PAHSAs (**Figure 5.1c**). This difference is more pronounced when comparing the same OAHSA and PAHSA regioisomers with the original method (**Figure 5.1b**).

Before measuring OAHSAs in tissues, we needed to determine if OAHSAs have background signal after SPE. Here we analyzed background OAHSA levels from two different SPE cartridge lots (**Figure 5.6**). As shown earlier, SPE cartridges have high and varying amounts of PAHSA background (red lines), yet the background OAHSA levels (blue lines), are not distinguishable compared to noise. The non-existent OAHSA background signal is ideal for studying the regulation of these lipids in tissues where total FAHFA levels are low, which includes blood.

FAHFA regioisomers and quantitation

To validate that our optimized FAHFA detection method affords similar results as our previous method, we analyzed PAHSAs in PGWAT of WT and AG4OX mice using our shorter method and the original method (**Figure 5.8a,b**). Previously, we have shown that PAHSAs are significantly upregulated in the WAT of AG4OX mice, with 9-PAHSA being the most abundant PAHSA isomer[8]. We observe the same profile when analyzing PAHSAs on the original and shorter method from this biological sample (**Figure 5.8a,b**). When comparing the traces of the PGWAT from WT and AG4OX mice with the original method and the shorter method, the shape of the peaks and the separation of the isomers look identical and full resolution of PAHSA regioisomers is achieved. No prior data exists on OAHSA regioisomers and their distribution in tissues. When analyzing OAHSAs in PGWAT in WT and AG4OX mice, we observed increased levels of OAHSAs in the AG4OX, with 9-OAHSA having the highest degree of upregulation (**Figure 5.8c,d**). This overall profile is similar to what is seen for PAHSAs and is also consistent when comparing OAHSAs on the original and shorter methods.

When comparing the peak heights (the Y-axis of the chromatograms) with the same sample on the original versus shorter the method, one will notice they are different. The peak

height is shorter for the original method due to the sample being spread out over a longer period of time compared to the shorter method. Although there is an obvious difference in peak height, the area under the curve is unaffected and is the same between both methods (**Figure 5.9**). When the same sample, either PGWAT WT or AG4OX, is analyzed on the shorter method versus the original method, the absolute quantities are the same.

We then quantified the PAHSA and OAHSA regioisomers in the PGWAT of WT and AG4OX mice using the shorter method and the longer method to determine whether there are any performance differences (**Figure 5.10**). All measured PAHSA regioisomers measured were increased in the AG4OX mice, which is consistent with our previously reported measurements.[8] We did notice that this cohort of AG4OX mice had lower levels of 9-PAHSA than what was previously reported, however, this may be due different age and sex of these mice. In our original report of FAHFAs, we used female mice at 8-14 weeks of age[8], while in this study we used male mice at 40 weeks of age. Overall, the two methods performed equivalently with the same concentrations of PAHSAs measured regardless of the gradient utilized.

In order to accurately quantify and properly assign endogenous OAHSA isomers based on their retention times, we synthesized the internal standard $^{13}C_{18}$-12-OAHSA (**Scheme 5.1**; **Figure 5.11**). In WAT, we detected 9-, 10-, 11-, 12, and 13-OAHSA in PGWAT, with 9-OAHSA being the mostly highly upregulated OAHSA regioisomer in AG4OX mice. As with our longer method, we could not achieve baseline resolution of the 12- and 13-OAHSA regioisomers, therefore these two regioisomers are reported as a single value (i.e. 13/12-OAHSA).

Detection of PAHSAs and OAHSAs in human plasma.

Using the shorter method, we wanted to determine if we could detect PAHSAs and OAHSAs in human plasma. To avoid the issue of dietary sources affecting endogenous plasma FAHFAs, we analyzed PAHSAs and OAHSAs in fasting humans (**Figure 5.12**). 5-6 plasma samples were analyzed in addition to two SPE procedural blanks to show background levels

coming from the SPE cartridge. The background for PAHSAs can be seen from the black and gray lines but are not visible when looking at plasma OAHSAs. For the PAHSA measurements plasma was taken from 3 humans twice at on different days. For example, 1A and 1B represent that same human, but with blood draws a couple weeks apart. For PAHSAs, 5-, 6-, 7-, 8-, 9-, 10-, 11-, and 13/12-PAHSA regioisomers were detected in all five human plasma samples. For the OAHSAs, 8-, 9-, 10-, 11-, and 13/12-OAHSA can be identified with 8-,9-, and 10-OAHSA having the highest levels. There is also a peak at ~24 minutes which is 5-OAHSA (see alignment with 5-OAHSA standard (**Figure 5.13**). PAHSA and OAHSA levels not only vary between different human subjects, but also from the same subject, and further human and animal studies should provide more insight into this observation.

5.3 Conclusion

Here, we optimized the FAHFA chromatography to afford shorter run times without a loss in baseline resolution between FAHFA regioisomers. We discovered that solid-phase extraction (SPE) cartridges are the most significant and variable contributors to the PAHSA background signal and the background can be mitigated by additional wash steps in the SPE protocol. At the same time, other FAHFAs, in particular OAHSAs have no background, which might make OAHSAs the ideal markers for blood FAHFA levels. Lastly, the faster protocol was tested on fasting human plasma to determine the feasibility of this approach for clinical studies, and we detected multiple PAHSA and OAHSA regioisomers with excellent analytical performance.

The emerging importance of FAHFAs in biology and medicine will require better and faster methods for their detection. By optimizing several key steps with a better column, we reduced the analysis time by nearly 70%. Moreover, these studies revealed that other FAHFAs, notably OAHSAs, have several qualities that improve their detection in blood, such as lower backgrounds and lack of any contaminating lipids. However, the physiologic and

pathophysiologic regulation and the biological activities of the OAHSAs have not been reported. With this protocol in hand it should now be possible to determine whether FAHFAs, PAHSAs and OAHSAs, are reliable markers of insulin resistance in people.

5.4 Figures

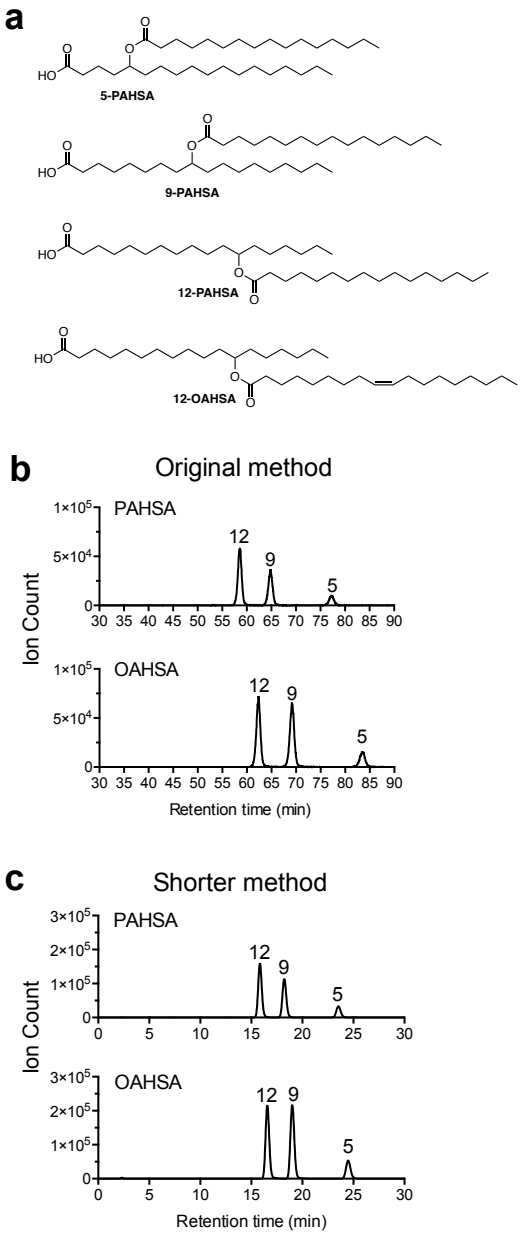

Figure 5.1. Development of a faster FAHFA Analysis Method. (**a**) Structures of 5-, 9-, and 12-PAHSA and 12-OAHSA. Extracted ion chromatograms showing the retention times of 5-, 9-, and 12-PAHSA and 5-, 9-, 12-OAHSA standards on a Luna C18(2) (3 μm, 250 x 2.0 mm, Phenomenex) (**b**) and an Acquity UPLC BEH C18 column (1.7 μm, 2.1 mm x 100 mm, Waters) (**c**).

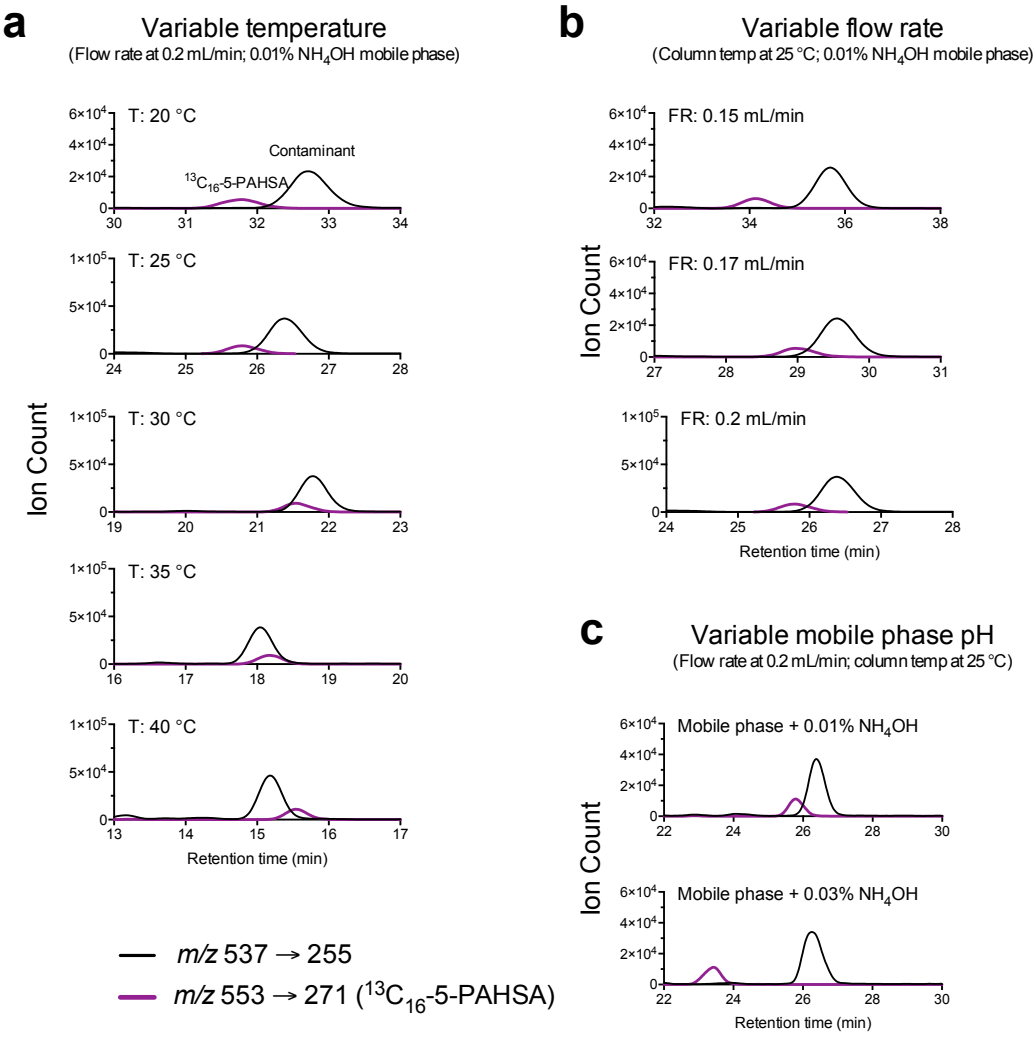

Figure 5.2. Resolution of 5-PAHSA and ceramide. (**a**) Traces showing the effect of altering column temperature ranging from 20 °C to 40 °C on resolution of 5-PAHSA and the ceramide. (**b**) Traces showing the effect of different flow rates on the resolution of 5-PAHSA and ceramide. (**c**) Traces showing the effect of increasing the mobile phase pH. Black lines represent the transition m/z 537 → 255 (which is shared by PAHSAs and the ceramide contaminant). Purple line represents the internal standard $^{13}C_{16}$-5-PAHSA, which is used as a surrogate for analyzing 5-PAHSA retention time. Although 5-PAHSA is present in mouse serum, it is not shown on as the chromatogram has to be magnified in order to be seen.

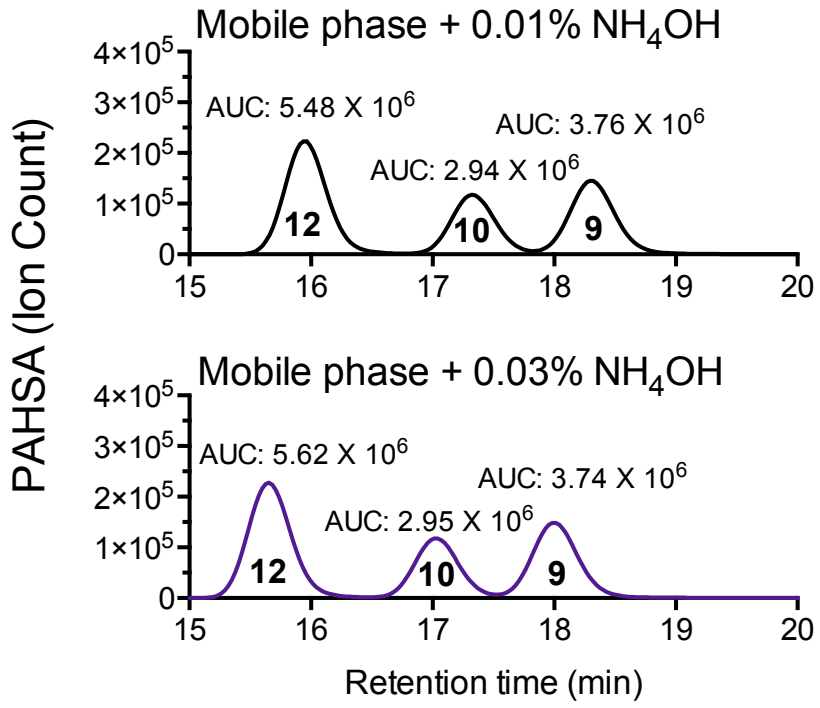

Figure 5.3. Stability of PAHSAs with different NH_4OH percentages in mobile phase. Extracted ion chromatogram of 12-, 10-, and 9-PAHSA with their respective AUC with either 0.01% NH_4OH (top trace) or 0.03% NH_4OH (bottom trace).

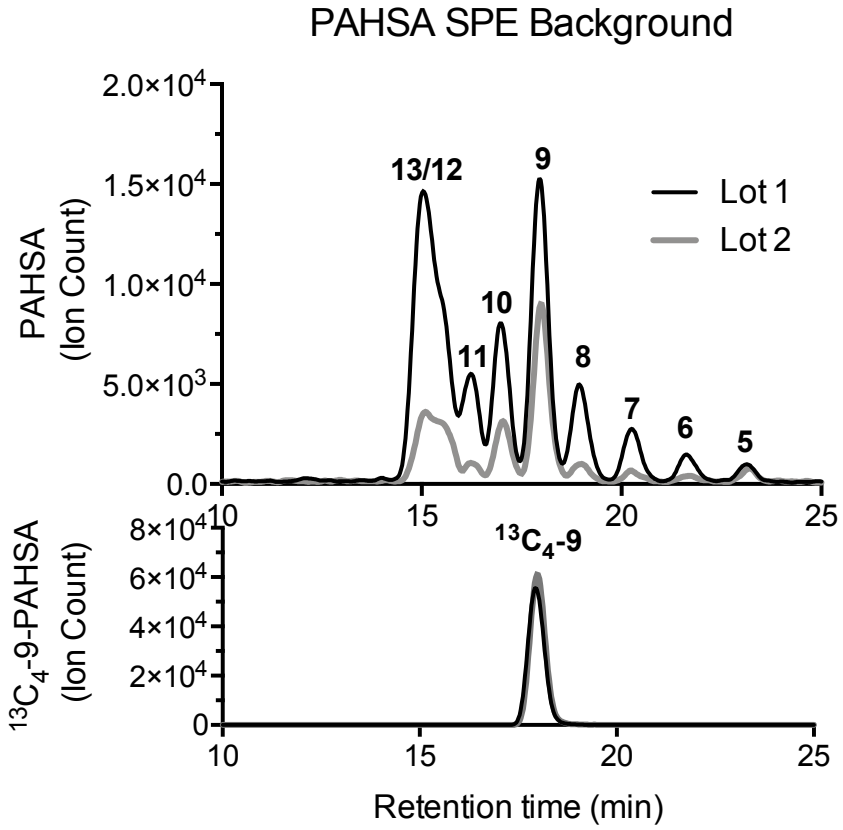

Figure 5.4. SPE cartridges have variable PAHSA background from lot-to-lot. Extracted ion chromatograms for PAHSAs (top) and internal standard $^{13}C_4$-9-PAHSA (bottom). Internal standard was added during the sample loading step to account for variation in the SPE procedure.

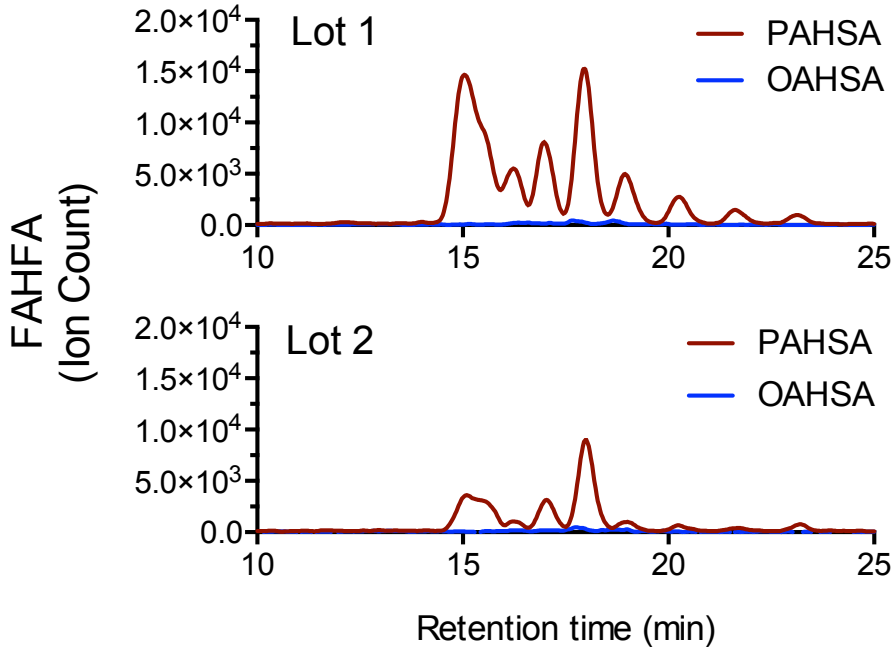

Figure 5.5. Background SPE OAHSAs and PAHSAs. Extracted ion chromatograms for background PAHSAs (red) and OAHSAs (blue) in SPE cartridges from two different lots.

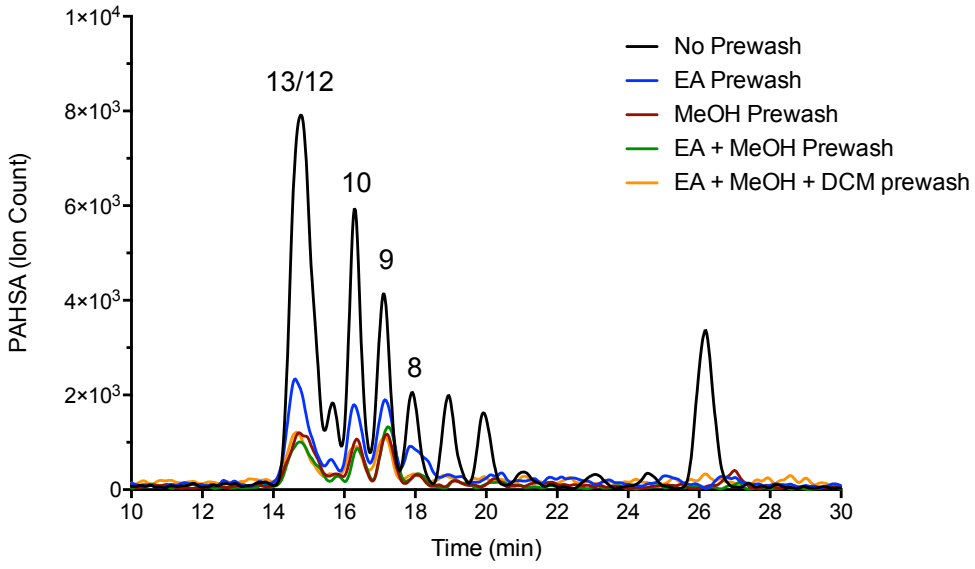

Figure 5.6. Effects of prewashing SPE cartridge on PAHSA background. SPE columns from the same lot number were prewashed with EA alone, MeOH alone, EA + MeOH, or EA + MeOH + DCM and their PAHSA background was compared to PAHSA background from a non-prewashed column (black line).

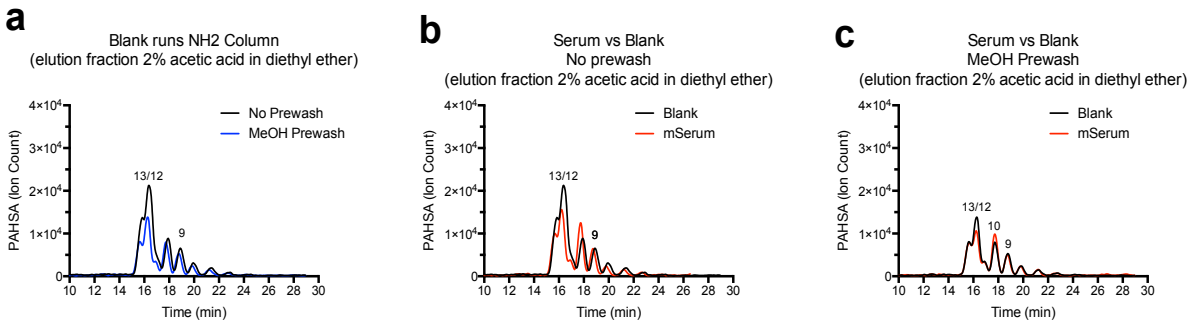

Figure 5.7. SPE background using Strata NH2 (500 mg/ 3 mL) cartridges. Using the NH_2 cartridges, we conditioned the columns with 4 mL of hexane and then followed with sample application. We then eluted neutral lipids with 4 mL of $CHCl_3$:IPA (2:1) and then eluted FAHFAs with 4 mL of 2% acetic acid in diethyl ether. **(a)** Comparison of background PAHSAs with and without a methanol prewash. Mouse serum PAHSAs are not above SPE background with (**c**) or without a methanol prewash step **(b)**.

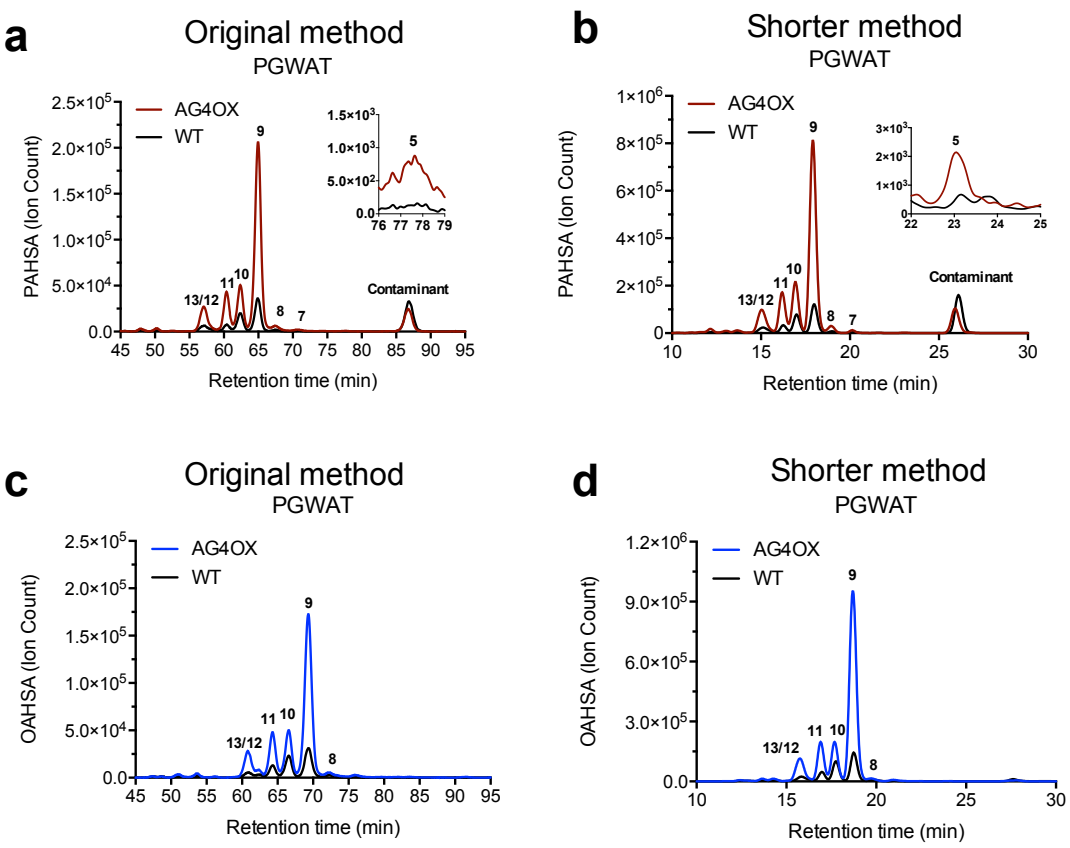

Figure 5.8. Analysis of OAHSAs and PAHSAs in PGWAT of WT and AG4OX with our original and shorter method. Extracted ion chromatograms comparing PGWAT PAHSAs in AG4OX and WT mice using the original (**a**) and shorter method (**b**). Extracted ion chromatograms analyzing OAHSAs in PGWAT WT and AG4OX mice in the original (**c**) and shorter method (**d**).

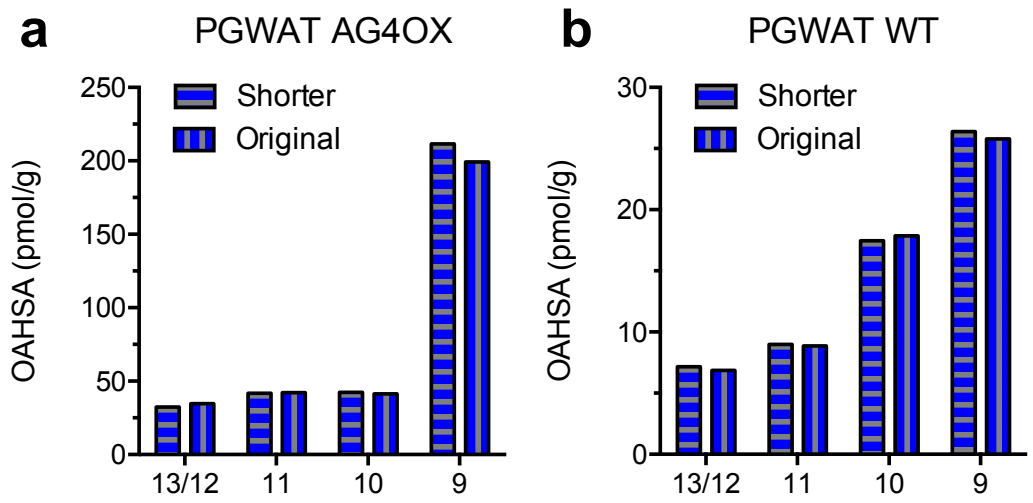

Figure 5.9. Quantitative comparison of WT and AG4OX PGWAT using the original versus the shorter method. Levels of 9-, 10, 11-, and 13/12-OAHSAs with the shorter and original methods for PGWAT AG4OX (**a**) and for PGWAT WT (**b**). OAHSA regiosomers quantified with the shorter method are depicted by bars with horizontal lines, and regiosomers measured on the original method are depicted by bars with vertical lines.

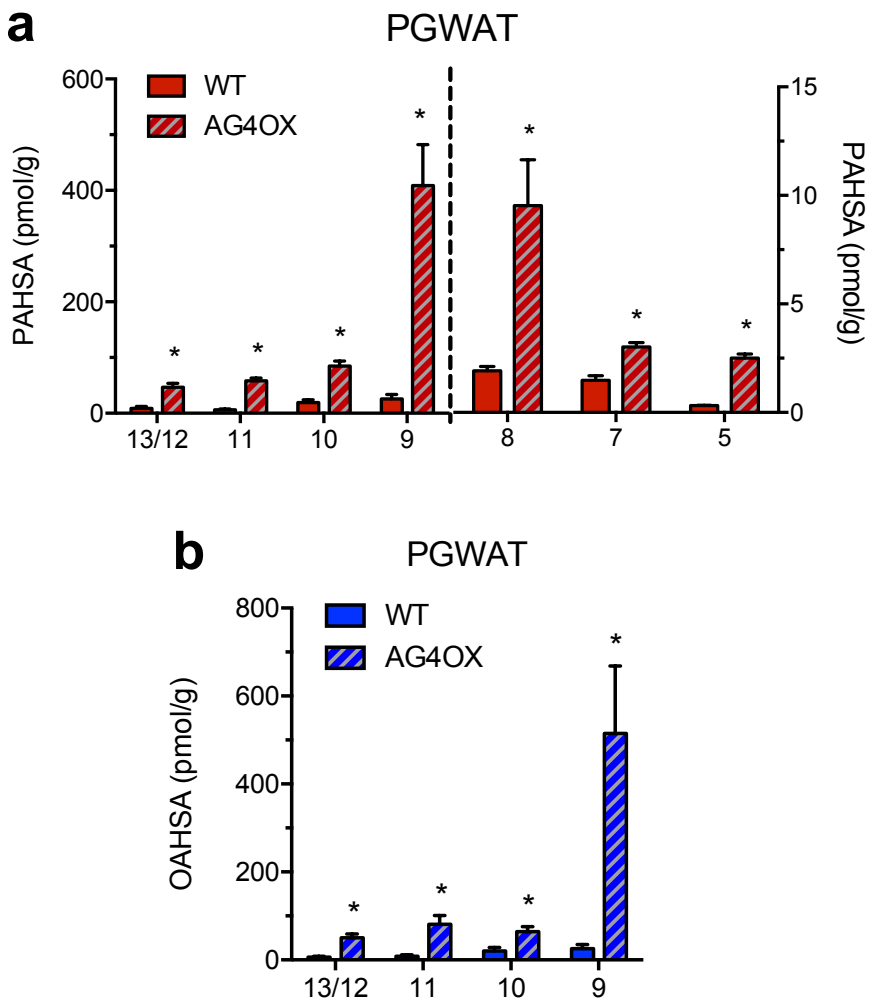

Figure 5.10. PAHSA and OAHSA quantification and distribution in AG4OX and WT PGWAT. Quantification of PAHSA (**a**) and OAHSA (**b**) isomers in WT and AG4OX PGWAT. Data are expressed as means ± SEM. Differences between groups was evaluated with Mann-Whitney test. n=3-5/group, *p<0.05.

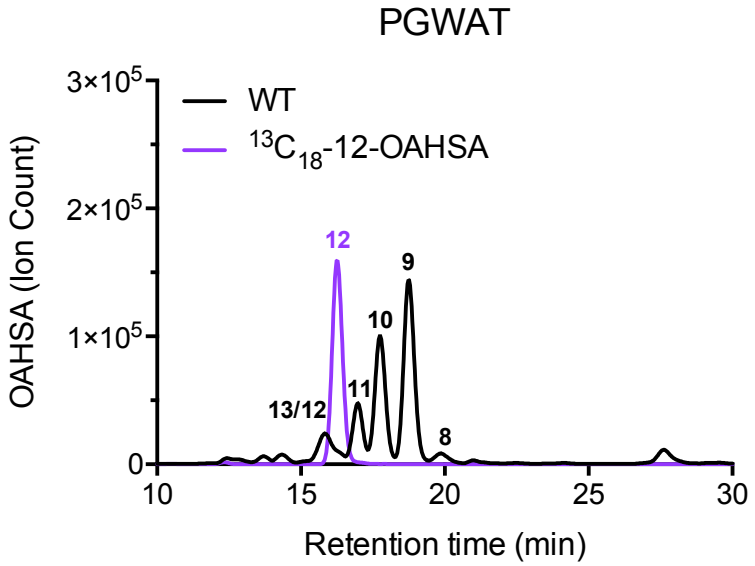

Figure 5.11. Overlay of $^{13}C_{18}$-12-OAHSA and WT PGWAT OAHSAs. Overlay of extracted ion chromatograms showing the internal standard $^{13}C_{18}$-12-OAHSA compared to WT PGWAT OAHSAs.

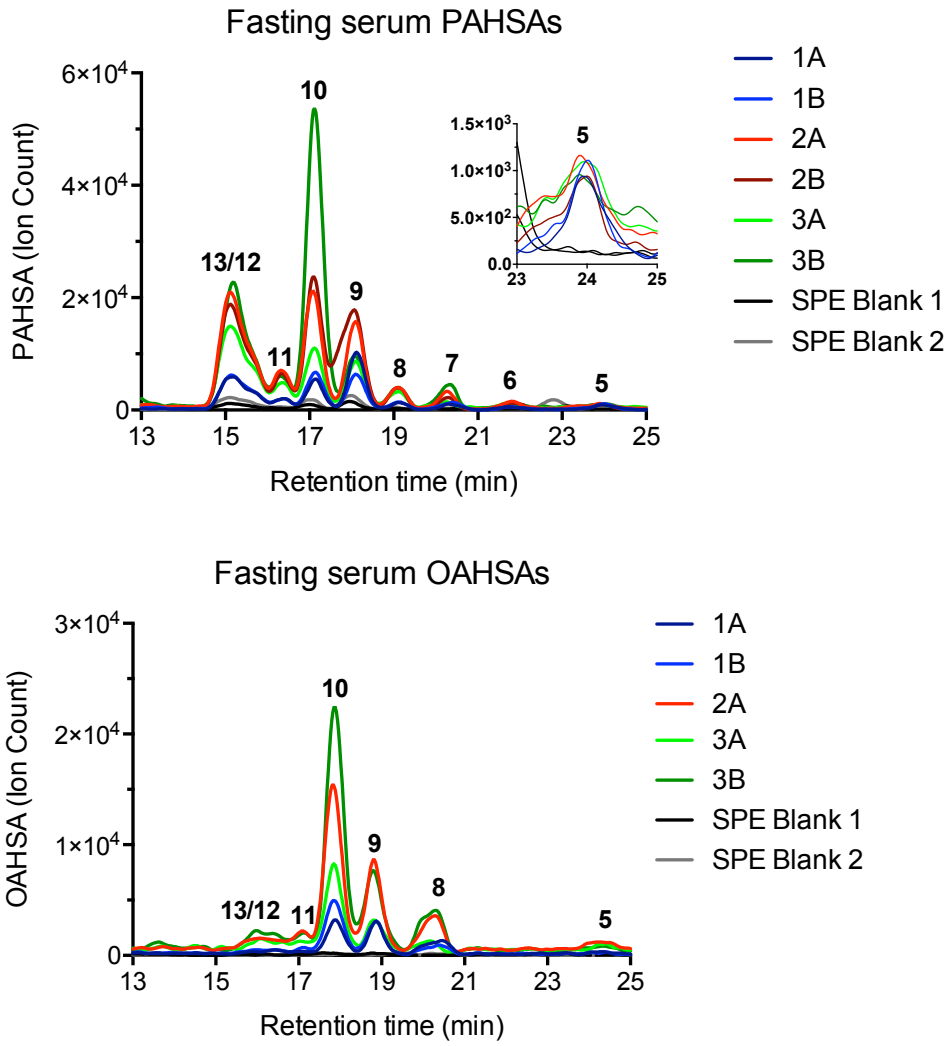

Figure 5.12. PAHSA and OAHSA regioisomers in fasting human plasma. Extracted ion chromatogram of PAHSAs (top trace) and OAHSAs (bottom trace).

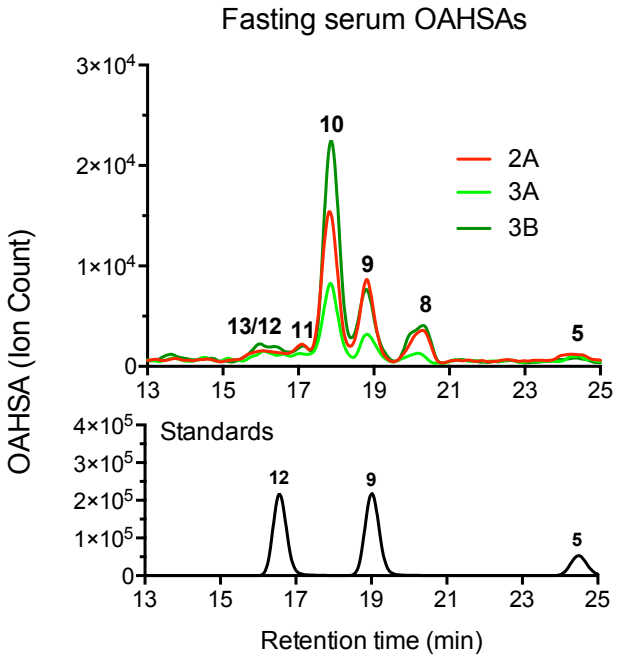

Figure 5.13. Comparison of human plasma OAHSAs with OAHSA standards. Extracted ion chromatograms showing plasma OAHSAs (top trace) and the 5-, 9-, and 12-OAHSA standards (bottom trace).

Table 5.1 MRM transitions for PAHSAs and OAHSAs and their respective standards. Quantifier ion is the fatty acid (FA), and the qualifier ions are the hydroxy fatty acid (HFA) and the HFA dehydration product (HFA-H_2O). The HFA-H_2O ion and the FA ion for OAHSA have the same m/z. The HFA ion and the FA ion for $^{13}C_{18}$-12-OAHSA have the same m/z. Q1 represents parent ion and Q3 represents daughter ions.

FAHFA	Q1 [M-H]$^-$	Q3 FA	Q3 HFA	Q3 HFA-H2O
PAHSA	537.5	255.2	299.3	281.2
$^{13}C_4$-9-PAHSA	541.5	259.2	299.3	281.2
OAHSA	563.5	281.2	299.3	-----
$^{13}C_{18}$-12-OAHSA	581.6	299.3	-----	281.2

Scheme 5.1. Synthesis of $^{13}C_{18}$-12-OAHSA**.** (**a**) A 250 mL round-bottom flask equipped with stir bas was charged with 12-hydroxystearic acid (TCI, >75%, 20 g, 66.7 mmol, 1 eq) and methanol (100 mL, 0.667 M), affording a clear solution. Concentrated sulfuric acid was added dropwise (3.55 mL, 66.7 mmol, 1 eq), giving a clear solution. A condenser was attached and the reaction was refluxed for 1 hour. Upon cooling to ambient temperature, solid sodium bicarbonate was added in portions until the pH was ~7-8. The mixture was vacuum filtered through celite and concentrated. The residue was taken up in ethyl acetate; washed with saturated aqueous sodium bicarbonate, water, and brine; dried (sodium sulfate); filtered; and concentrated. The crude white solid was recrystallized from hexanes, affording the desired product as a white solid (16.0 g, 76%). (**b**) A 10 mL round-bottom flask equipped with stir bar was flame-dried under vacuum, cooled to ambient temperature, flushed with nitrogen, sealed with a rubber septum, and maintained under a nitrogen atmosphere. Uniformly ^{13}C-labelled oleic acid (Cambridge Isotope Laboratories, 25 mg, 0.083 mmol, 1 eq) and dry DCM (2 mL, 0.042 M) were added via syringe, affording a clear, colorless solution. The reaction was cooled in an ice-water bath for 15 minutes before adding oxalyl chloride (0.03 mL, 0.35 mmol, 4.0 eq) dropwise via syringe. The solution remained clear, but yellowed slightly. The reaction was allowed to warm to ambient temperature and aged for 12 hours. The reaction was concentrated with the warming bath of the rotavap at ambient temperature. The crude amber oil was used in the next step without further purification. (**c**) A 10 mL round-bottom flask equipped with stir bar was flame-dried under vacuum, cooled to ambient temperature, flushed with nitrogen, sealed with a rubber septum, and maintained under a nitrogen atmosphere. The reaction vessel was charged with methyl 12-hydroxyoctadecanoate (25 mg, 0.081 mmol, 1 eq) and spurged with nitrogen. Dry DCM (1 mL, 0.041 M, 1/2 total volume) and pyridine (0.033 mL, 0.41 mmol, 5 eq) were added via syringe, affording a clear, slightly yellow solution. The flask was submerged in an ice-water bath and aged for 15 minutes before adding dropwise via syringe a solution of uniformly ^{13}C-labelled oleoyl chloride in dry DCM (1 mL, 1/2 total volume). The reaction was allowed to warm to ambient temperature and aged twelve hours before quenching with deionized water (2 mL). The biphasic mixture was vigorously stirred for 30 minutes before transferring to a separatory funnel. The aqueous layer was extracted with DCM (5 mL x 3). Combined organics were washed with 0.5 M aqueous HCl (5 mL), saturated aqueous sodium bicarbonate (5 mL), brine (5 mL), dried over sodium sulfate, filtered and concentrated. The residue was purified by column chromatography, eluting with hexanes:ethyl acetate (100:0 to 95:5) affording the desired product (28 mg) as a yellow oil in 60% yield over two steps. (**d**) Taking no precaution to maintain a dry, inert environment, a 4 mL vial equipped with “flea” stir bar was charged with 18-methoxy-18-oxooctadecan-7-yl uniformly ^{13}C-labelled-oleate (28 mg, 0.047 mmol, 1 eq) and THF (1 mL, 0.05 M), giving a clear, colorless solution. An aqueous solution of lithium hydroxide (0.094 mL, 1 M, 0.094 mmol, 2 eq) was added, giving a clear, colorless solution. The reaction was stirred until conversion was complete. The reaction was acidified with ice cold aqueous HCl until pH was ~1, and extracted with ethyl acetate (x3). Combined organics were washed with brine, dried (sodium sulfate), filtered and concentrated to give 12-OAHSA as a clear oil (26 mg, 95%).

a

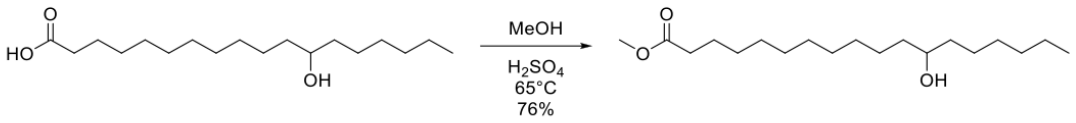
MeOH
H_2SO_4
65°C
76%

b

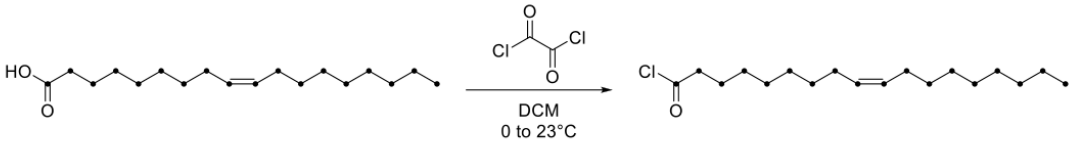
DCM
0 to 23°C

c

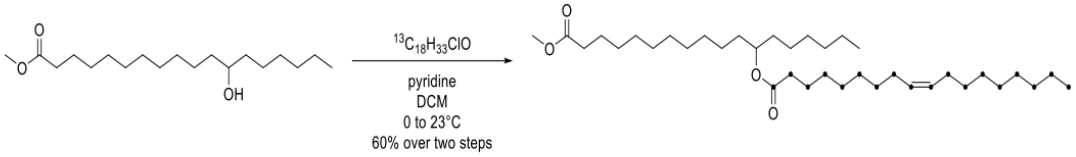
$^{13}C_{18}H_{33}ClO$
pyridine
DCM
0 to 23°C
60% over two steps

d

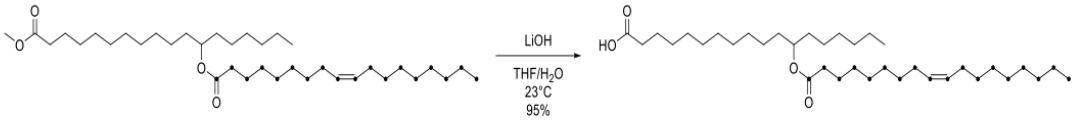
LiOH
THF/H_2O
23°C
95%

5.5 Experimental Section

Chemicals and standards. All PAHSAs, OAHSAs, and $^{13}C_4$-9-PAHSA were purchased from Cayman Chemical Company. The internal standard $^{13}C_{18}$-12-OAHSA was synthesized as described (**Scheme 5.1**)

Samples for FAHFA measurements. Male AG4OX mice and WT FVB littermate controls[16] at 40 weeks of age were used for FAHFA measurements. Mice were fed on chow diet (Lab Diet, 5008) ad libitum. Human plasma samples were prepared as previously described[17].

Lipid extraction. Lipid extraction was based on previous literature[11,18]. PGWAT (150 mg) Dounce homogenized on ice in a mixture of 1.5 mL PBS, 1.5 mL methanol, and 3 mL of chloroform. 5 pmol/sample of $^{13}C_4$-9-PAHSA and $^{13}C_{18}$-12-OAHSA and 1 pmol/sample of $^{13}C_{16}$-5-PAHSA were added to the chloroform prior to extraction. The mixture was then centrifuged at 2,200 g, 5 min, 4ºC to separate the organic (bottom) and aqueous phases. The organic phase was then transferred to a new vial and dried down under a gentle stream of nitrogen and stored at -80ºC. For blood samples, 200 µL of mouse serum or human plasma was added to 1.3 mL of PBS, 1.5 mL methanol and 3 mL chloroform with internal standard (1 pmol/sample of $^{13}C_4$-9-PAHSA, $^{13}C_{18}$-12-OAHSA, and $^{13}C_{16}$-5-PAHSA). The resulting mixture was then vortexed for 30 s and then centrifuged to separate the organic and aqueous phases. The organic phase was transferred, dried and stored following the same method for tissues.

Solid phase extraction (SPE). SPE was slightly modified from a previously reported method[11]. SPE was performed at room temperature using positive pressure (nitrogen) to push solvents though a Strata SI-1 Silica SPE cartridge (500 mg silica, 3 mL, Phenomenex, 8B-S012-HBJ-T). For the following steps, we recommend adding the elution solvents in aliquots of 2 mL. The SPE cartridge was first pre-washed with 6 mL of ethyl acetate and then conditioned with 6 mL hexane. Afterwards, extracted lipids, from the previous lipid extraction step, were reconstituted in 200 µL chloroform and then applied to the cartridge. Neutral lipids were eluted

using 6 mL 5% ethyl acetate in hexane, followed by elution of FAHFAs using 4 mL ethyl acetate. The FAHFA fraction was dried down under a gentle stream of nitrogen and stored at -80ºC.

Targeted LC/MS analysis of PAHSAs and OAHSAs. PAHSAs and OAHSAs were measured on a TSQ Quantiva LC/MS instrument using Multiple Reaction Monitoring (MRM) in negative ionization mode. The following MS source parameters were used: spray voltage, 3.5 kV; ion transfer tube temperature, 325ºC; vaporizer temperature, 275ºC; sheath gas, 2.7 L/min; aux gas, 5.0 L/min; and sweep gas, 1.5 L/min. An Acquity UPLC BEH C18 column (1.7 μm, 2.1 mm x 100 mm, Waters) was used for separation of FAHFAs. PAHSAs and OAHSAs were resolved with isocratic flow at 0.2 mL/min using 93:7 methanol:water with 5 mM ammonium acetate and 0.03% ammonium hydroxide over 30 minutes. The column was kept at a constant temperature of 25ºC. Each extracted and fractionated sample was reconstituted in 40 μL methanol and 10 μL was injected for analysis. Multiple reaction monitoring (MRM) was utilized using one quantifier and one or two qualifier transitions per FAHFA (**Table 5.1**). The collision energies (CE) for the MRM transitions are as follows: FA (29 V), HFA (28 V), and HFA-H2O (27 V).

5.6 Acknowledgements

Chapter 5, in full, is a reprint with minor changes as it appears in A Faster Protocol for Endogenous FAHFA Measurements, *Analytical Chemistry*, 2018. The dissertation author was the primary investigator and author of this paper. Other authors include Andrew T. Nelson, Tina Chang, Meric E. Ertunc, Mitchell P. Christy, Lena Ohlsson, Magnus Härröd, Barbara B. Kahn, Dionicio Siegel, and Alan Saghatelian.

5.7 References

1 Shepherd, P. R., Gnudi, L., Tozzo, E., Yang, H., Leach, F. & Kahn, B. B. Adipose cell hyperplasia and enhanced glucose disposal in transgenic mice overexpressing GLUT4 selectively in adipose tissue. *Journal of Biological Chemistry* 268, 22243-22246 (1993).

2 Gnudi, L., Tozzo, E., Shepherd, P. R., Bliss, J. L. & Kahn, B. B. High level overexpression of glucose transporter-4 driven by an adipose-specific promoter is maintained in transgenic mice on a high fat diet, but does not prevent impaired glucose tolerance. *Endocrinology* 136, 995-1002 (1995).

3 Tozzo, E., Shepherd, P. R., Gnudi, L. & Kahn, B. B. Transgenic GLUT-4 overexpression in fat enhances glucose metabolism: preferential effect on fatty acid synthesis. *Am J Physiol* 268, E956-964 (1995).

4 Tozzo, E., Gnudi, L. & Kahn, B. B. Amelioration of insulin resistance in streptozotocin diabetic mice by transgenic overexpression of GLUT4 driven by an adipose-specific promoter. *Endocrinology* 138, 1604-1611 (1997).

5 Herman, M. A., Peroni, O. D., Villoria, J., Schon, M. R., Abumrad, N. A., Bluher, M., Klein, S. & Kahn, B. B. A novel ChREBP isoform in adipose tissue regulates systemic glucose metabolism. *Nature* 484, 333-338 (2012).

6 Winzell, M. S. & Ahrén, B. The High-Fat Diet–Fed Mouse. *Diabetes* 53, S215-S219 (2004).

7 US Department of Health and Human Services. Centers for Disease Control and Prevention. National Diabetes Statistics Report: Estimates of Diabetes and Its Burden in the United States. (2014).

8 Yore, M. M., Syed, I., Moraes-Vieira, P. M., Zhang, T., Herman, M. A., Homan, E. A., Patel, R. T., Lee, J., Chen, S., Peroni, O. D., Dhaneshwar, A. S., Hammarstedt, A., Smith, U., McGraw, T. E., Saghatelian, A. & Kahn, B. B. Discovery of a class of endogenous mammalian lipids with anti-diabetic and anti-inflammatory effects. *Cell* 159, 318-332 (2014).

9 Kuda, O., Brezinova, M., Rombaldova, M., Slavikova, B., Posta, M., Beier, P., Janovska, P., Veleba, J., Kopecky, J. & Kudova, E. Docosahexaenoic Acid–Derived Fatty Acid Esters of Hydroxy Fatty Acids (FAHFAs) With Anti-inflammatory Properties. *Diabetes* 65, 2580-2590 (2016).

10 Lee, J., Moraes-Vieira, P. M., Castoldi, A., Aryal, P., Yee, E. U., Vickers, C., Parnas, O., Donaldson, C. J., Saghatelian, A. & Kahn, B. B. Branched Fatty Acid Esters of Hydroxy

Fatty Acids (FAHFAs) Protect against Colitis by Regulating Gut Innate and Adaptive Immune Responses. *J Biol Chem* 291, 22207-22217 (2016).

11 Zhang, T., Chen, S., Syed, I., Stahlman, M., Kolar, M. J., Homan, E. A., Chu, Q., Smith, U., Boren, J., Kahn, B. B. & Saghatelian, A. A LC-MS-based workflow for measurement of branched fatty acid esters of hydroxy fatty acids. *Nat Protoc* 11, 747-763 (2016).

12 Nelson, A. T., Kolar, M. J., Chu, Q., Syed, I., Kahn, B. B., Saghatelian, A. & Siegel, D. Stereochemistry of Endogenous Palmitic Acid Ester of 9-Hydroxystearic Acid and Relevance of Absolute Configuration to Regulation. *Journal of the American Chemical Society* 139, 4943-4947 (2017).

13 Eichelberger, J., Behymer, T., Budde, W. & Munch, J. Method 525.2, Determination Of Organic Compounds In Drinking Water By Liquid-Solid Extraction And Capillary Column Gas Chromatography. *Mass Spectrometry. National Eeposure Research Laboratory Office of Research and Development USEPA CINCINNATI, OHIO* 45268 (1995).

14 Junk, G. A., Avery, M. J. & Richard, J. J. Interferences in solid-phase extraction using C-18 bonded porous silica cartridges. *Analytical Chemistry* 60, 1347-1350 (1988).

15 Stiles, R., Yang, I., Lippincott, R. L., Murphy, E. & Buckley, B. Potential sources of background contaminants in solid phase extraction and microextraction. *J Sep Sci* 30, 1029-1036 (2007).

16 Shepherd, P. R., Gnudi, L., Tozzo, E., Yang, H., Leach, F. & Kahn, B. B. Adipose cell hyperplasia and enhanced glucose disposal in transgenic mice overexpressing GLUT4 selectively in adipose tissue. *J Biol Chem* 268, 22243-22246 (1993).

17 Ohlsson, L., Rosenquist, A., Rehfeld, J. F. & Harrod, M. Postprandial effects on plasma lipids and satiety hormones from intake of liposomes made from fractionated oat oil: two randomized crossover studies. *Food Nutr Res* 58 (2014).

18 Bligh, E. G. & Dyer, W. J. A rapid method of total lipid extraction and purification. *Can J Biochem Physiol* 37, 911-917 (1959).

Chapter 6:

LAHLAs, a novel class of anti-inflammatory FAHFAs

Abstract

Bioactive lipids are important contributors to physiology and different lipid classes mediate different biology. Prostaglandins, leukotrienes, and thromboxanes are all members of the eicosanoid family because they share an underlying structure of 20 carbons, yet modest structural differences between these lipids can elicit very different biological activities. Fatty acid esters of hydroxy fatty acids (FAHFAs) are a recently discovered class of bioactive endogenous mammalian lipids with anti-diabetic and anti-inflammatory activity. FAHFAs are classified into families based on the composition of fatty acid and hydroxy fatty acid. To date there have been over 20 FAHFA families reported but only two FAHFA families—palmitic acid esters of hydroxy stearic acids (PAHSAs) and docosahexaenoic acid esters of hydroxy linoleic acid (DHAHLA)—have been functionally characterized. Akin to other bioactive lipids, to fully appreciate the biological role of FAHFAs, additional members of this class of lipids should be functionally characterized to determine their bioactivity. Here we report the identification, structural elucidation, and functional characterization of linoleic acid esters of linoleic acid esters (LAHLAs). The structure of a known oat oil lipid led us to hypothesize that oat oil might contain FAHFAs, and analysis of a bioactive preparation of oat oil led to the identification of 13-LAHLA. Synthesis of 13-LAHLA validated our structural assignment and confirmed the presence of this lipid in oat oil as well in rodent tissues, indicating that this is also an endogenous lipid. Cellular assays revealed that 13-LAHLA can inhibit LPS induction of the cellular inflammatory response to down regulate the expression and secretion of cytokines and other important mediators of the immune response. These studies highlight the importance of characterizing additional FAHFAs, as they can reveal novel bioactive molecules which should be explored for biological activity.

6.1 Introduction

Inflammation is a protective response to pathogens and injury that includes many cell types and different classes of molecules including proteins and metabolites. Under normal conditions inflammation helps clear pathogens and can remove dead cells from injured tissue, and as these events occur the inflammation should subside. In the absence of resolution, however, a state of chronic inflammation emerges, and can lead to additional diseases including atherosclerosis and cancer.

One therapeutic option for treating inflammation target the biochemical pathways associated with the production of pro-inflammatory prostaglandins, highlighting the importance of lipid mediators in physiological pathways. The recent discovery of endogenous lipids with anti-diabetic and anti-inflammatory activity, fatty acid esters of hydroxy fatty acids (FAHFAs), indicate the existence of additional, uncharacterized lipid mediators of inflammation[1].

FAHFA families are comprised of different combinations of fatty acids and hydroxy fatty acids, such as palmitic acid esters of hydroxy stearic acids (PAHSAs) and oleic acid esters of HSAs (OAHSAs). Within each FAHFA family there also exists several (as many as eight) regioisomers that differ in the position of the linking ester with respect to the carboxylate. For example, in human and mouse fat, we observe the following regioisomers: 13-PAHSA, 12-PAHSA, 11-PAHSA, 10-PAHSA, 9-PAHSA, 8-PAHSA, and 5-PAHSA[1].

FAHFAs were discovered as a structurally novel class of upregulated lipids in a mouse model that is insulin sensitive and protected from diabetes even though these animals are obese. FAHFAs are also downregulated in humans that are insulin resistant but not diabetic, supporting a role for these lipids in human biology and disease[1]. Biological testing of PAHSAs revealed potent anti-diabetic and anti-inflammatory activities *in vivo*. Mechanistic studies revealed that FAHFAs regulate several cellular and physiological pathways, and that some of the biology is attributable to PAHSA acting as agonists for GPR120, a G-protein coupled

receptor[1]. Other ligands for GPR120 include the omega-3 fatty acids, which are essential fatty acids that are obtained only through diet[2]. Analysis of FAHFAs in a mouse model of colitis showed that anti-inflammatory activity of FAHFAs extends beyond metabolic models and further solidified a role for GPR120 in mediating PAHSA activity[3].

FAHFAs are endogenous metabolites in that we find their levels regulated by changes in biochemistry on mice with similar diets, indicating their endogenous regulation. At least three lipases—CEL, Aig1, and ADTRP—have been found to prefer FAHFAs as substrates *in vitro*, suggesting the existence of dedicated biochemical pathways for regulating these lipids[4,5]. For some FAHFAs, exogenous sources of FAHFAs or FAHFA precursors (fatty acids or hydroxy fatty acids (HFAs)) might contribute to their levels *in vivo*. Administration of omega-3 fatty acids to cells or mice, for example, results in the production of docosahexaenoic acid esters of hydroxy linoleic acids (DHAHLAs), which were shown to have potent anti-inflammatory activity in cellular assays[6]. The discovery of DHAHLAs from DHA also signaled the possibility that perhaps FAHFAs have a role in the activity of omega-3 fatty acids, and fish oils.

As a recently discovered class of lipids, there is still much more work that needs to be done to explore the biological and potential therapeutic impact of the FAHFAs. Including all the regioisomers, there are greater than 80 reported FAHFAs, yet only three of these have been synthesized and tested for their biological activity. To expedite the discovery of additional bioactive FAHFAs, we wondered whether there existed other, natural sources biologically active lipids that hinted at the presence of bioactive FAHFAs. Oat oil emerged as a potential source of bioactive FAHFAs because it has shown both anti-inflammatory and anti-diabetic activities[7,8], like FAHFAs, and an digalactosyldiacylglycerol (DGDG) lipid containing a FAHFA, linoleic acid ester of 15-hydroxy linoleic acid (15-LAHLA), has been identified[9]. We reasoned that this lipid could be a metabolic precursor of FAHFAs.

Separation of oat oil afforded a FAHFA-enriched fraction that was then tested for biological activity in an inflammatory assay. The FAHFA-enriched fraction showed a dose-

dependent decrease in the production of IL-6 from a macrophage cell line treated with lipopolysaccharide (LPS). While PAHSA levels are extremely low in oat oil, we found that oat oil has high levels of uncharacterized 15-, 13-, and 9-LAHLA. Plasma analysis from people fed oat oil revealed elevated levels of LAHLAs, which correlated with increases in the levels of the appetite regulating hormones GLP-1, PYY, and CCK[7].

Hydroxy linoleic acids are also known as hydroxyoctadecadienoic acids, or HODEs, which are endogenous mammalian lipids produced from the oxidation of linoleic acid by lipoxygenases. The presence of HODEs in tissues suggested that endogenous LAHLAs might exist and targeted lipidomic analysis of mouse and human tissues confirmed the presence of 13- and 9-LAHLA in white adipose tissue (WAT). Synthesis and testing of 13-LAHLA, which is found in oat oil and mammalian tissues, revealed this lipid to be a potent modulator of cytokine levels in LPS-treated macrophages.

6.2 Results and Discussion

Oat Oil and the FAHFA fraction from oat oil have anti-inflammatory activity

Because other FAHFAs have shown to have anti-inflammatory properties, we tested whether oat oil and FAHFA-enriched oat oil could modulate inflammation using an *in vitro* cell culture model. The experiment measures interleukin 6 (IL-6) release from a mouse macrophage cell line (RAW 264.7 cells) upon treatment with lipopolysaccharide (LPS). Previously, this assay had been used to demonstrate anti-inflammatory effects for 9-PAHSA and 13-DHALHA, as both of these lipids mitigated LPS-stimulated IL-6 release from RAW 264.7 cells[6]. We used this assay to test whether oat oil had any effect in this assay. We performed a dose-response by incubating different concentrations of oat oil (2-400 parts per million (ppm)) for 20 hours and then measured secreted IL-6 levels. For oat oil, suppression of LPS-stimulated IL-6 secretion was observed as low as 10 ppm (~15% inhibition) with a clear dose-response (**Figure 6.1b**).

To determine whether FAHFAs within oat oil might be responsible for this activity, we enriched FAHFAs using a previously established solid-phase extraction (SPE) protocol[10]. We performed a dose-response experiment with the FAHFA-enriched oat oil (2-400 parts per million (ppm)) for 20 hours and then measured secreted IL-6 levels. This fraction was more potent that the unenriched fraction with ~30% inhibition at 2 ppm and >90% inhibition at 100 ppm and (**Figure 6.1c**). To show that these effects were due to activity and not cytotoxicity, we performed a MTT cell viability assay (**Figure 6.2**). There was no observed death cellular death at the tested concentrations of oat oil and FAHFA-enriched oat oil.

These experiments positively identify oat oil as a source of lipid soluble molecules with the ability to modulate cellular inflammation but does not conclusively identify FAHFAs since other molecules might also be enriched in this fraction. For instance, previous studies have identified a natural product class called avenanthramides from oats with anti-inflammatory activity[11,12]. Thus, we still need to determine whether oat oil contains FAHFAs, and whether those FAHFAs have biological activity that are consistent with these observations.

LAHLAs a new FAHFA family are abundant in oat oil

Using our established targeted liquid chromatography mass spectrometry (LC-MS) method in multiple reaction monitoring (MRM) mode[10], we analyzed oat oil to determine if there were free FAHFAs after FAHFA-enrichment using SPE. FAHFAs are analyzed in negative ionization mode and yield three characterized product ions that that correspond to the free fatty acid (FFA), the hydroxy fatty acid (HFA), and the dehydration product of the hydroxy fatty acid. First, we looked for PAHSAs and OAHSAs, two families that are in high abundance in mouse adipose tissue. These experiments validated the existence of FAHFAs in oat oil as we could detected some PAHSA and OAHSA regioisomers; however, the levels of these lipids were very low (~ 1 pmol/mg in oat oil, which we thought would be too low to observe any biological activity.)

FAHFA metabolism in oats might favor different families and isomers, so we expanded our search to include other FAHFAs, including FAHFAs we had not observed in mammalian tissues. In particular, we were sure to include transitions for LAHLAs, which were reported as parts of the galactolipids. Specifically, we monitored the precursor-to-product ion transitions to the component linoleic acid (*m/z* 557.5 → 279.2, red) and hydroxy linoleic acid (*m/z* 557.5 → 295.2, black) to detect LAHLAs (**Figure 6.3a**). This analysis revealed the existence of three different LAHLA isomers in oat oil (**Figure 6.3b**) and MS2 data for all three isomers provided the signature ions (*m/z* 279.2, *m/z* 295.2, and *m/z* 277.2) expected for a LAHLA (**Figure 6.3c**).

Unlike the PAHSAs and OAHSAs, which are less than 1 pmol/mg, LAHLAs are much more abundant reaching concentrations of ~350 pmol/mg. We found no other FAHFAs in these samples that were as abundant as the LAHLAs and we focused our energy on the potential role of the LAHLAs.

LAHLAs are present in human plasma after oat oil ingestion

With the large abundance of LAHLAs present in oat and the beneficial metabolic effects seen from human subjects who ingest oat oil, we wanted to determine if these favorable effects could be due to FAHFAs. To investigate this, we measured plasma FAHFAs in people that had consumed oat oil and compared these samples to controls (no oat oil). Initial blood samples were taken after the subjects fasted overnight. Subsequent blood samples were taken at 1, 3, 5, and 7 hours post-ingestion of a controlled breakfast supplemented with either oat oil or yogurt (control).

Using LC-MS we did not observe any LAHLA peaks in the plasma of subjects when fasting overnight, however three peaks (retention time = 7.5, 8.5, and 9.3 min) were present at every time point after oat oil ingestion (**Figure 6.3e**). Although all three LAHLA peaks exist at each time point after the subject has ingested oat oil, the levels of these peaks vary. For example, over time, the 7.5 peak decreases while the 8.5 and 9.4 peaks increase. When

comparing the MRM of LAHLAs in subjects ingesting oat oil versus control, LAHLAs were much lower in plasma control subjects versus oat oil ingesting subjects, suggesting that oat oil is the source of these lipids or that oat oil is modulating endogenous LAHLA levels (**Figure 6.4**).

We also quantified the levels of PAHSAs and OAHSAs in the plasma of subjects ingesting oat oil versus the control food (**Figure 6.3f,h**). Plasma PAHSA and OAHSA levels were not changed in oat oil versus control subjects. By contrast, plasma LAHLA levels were increased in the plasma of oat oil treated subjects at every measured time point post-ingestion. The highest plasma concentration of LAHLAs (~ 40 nM) was measured at 7 hours post-ingestion which was ~45-fold higher than control treated subject plasma also at 7 hours.

As reported in the initial study, ingesting oat oil such lowers glycemia and increasing satiety hormones GLP-1 and PYY, and CCK at 7 hours post-ingestion[7]. LAHLA levels correlate with these beneficial effects. Since pure LAHLAs were not administered in these studies we can only speculate that LAHLAs might responsible for some of the beneficial effects; however, we feel that the data points to the LAHLAs as an interesting new family of FAHFAs that warrant further investigation.

Identification of the LAHLA regioisomers in oat oil

To be able to study these LAHLAs in greater detail, we needed to know which regioisomers were present and then synthesize pure version of these lipids for biological assays. The numbering nomenclature of FAHFAs is determined by the carbon of the hydroxy fatty acid where the ester is formed (starting from the carboxylate), such as 5-, 9-, and 13-PAHSA. As mentioned, we observed three LAHLA peaks, indicating the presence of at least three different LAHLA regioisomers. To identify the structures of these LAHLA isomers, we developed an approach based on the recently reported method for the structural elucidation of the 13-DHAHLA[6]. By performing an MS3 they were able to identify the family and regioisomer of

the 13-DHAHLA, with the MS3 spectra providing the information necessary to identify the regioisomer.

We did not have access to an instrument capable of MS3 measurements, so we performed a pseudo-MS3 instead. In this approach, we increased the source voltage of the mass spectrometer to induce the first fragmentation of the LAHLAs into LA and HLA, and then fragmented the HLA in the mass spectrometer to reveal the regioisomer position of the ester group (**Figure 6.5a**). Analysis of the oat oil samples using this approach led to HLA fragments that with the same exact retention times (6.0, 6.7, and 7.3 min) as the LAHLA peaks (**Figure 6.5b**). Pure 13-HLA (also known as 13-HODE) eluted much earlier in the gradient indicating that the HLA fragments we were detecting are product ions of the LAHLAs (data not shown).

The most abundant fragment ions of the HLA peaks at 6.0, 6.7 and 7.3 were used to determine where the position of the hydroxy group is on the HLA (**Figure 3c,d**). For example, using a MS2 scan range of *m/z* 100-250 the HLA fragmentation profile for the peak at 6.0 yields a major ion at *m/z* 223.1699 which is consistent with a calculated fragment of 15-HLA (*m/z* 223.1704). The peak at 6.7 min matches to 13-HLA with a product ion at *m/z* 195.1383 and the peak at 7.3 matches to 9-HLA with a product ion at *m/z* 171.1017. The 13- and 9-HLA fragment results are consistent with prior results using the standard MS3 approach[6].

The relative retention times of LAHLAs is consistent with what we observe for other FAHFAs: the farther away the ester is from the carboxylate the earlier the retention time (i.e., 15-LAHLA elutes first and 9-LAHLA elutes later). The large abundance of 15-LAHLA in oat oil is consistent with the high abundance of 15-HLA and 15-LAHLA-containing galactolipid (**Figure 6.1a and 6.3b**)[9,13]. The three LAHLA isomers in human plasma correspond to 15-, 13-, and 9-LAHLA (**Figure 6.3e**), but 13-LAHLA is the most abundant LAHLA at 3 hours (**Figure 6.3e**), suggesting that endogenous metabolism is also playing a role in shaping the levels of different LAHLA regioisomers.

LAHLAs are present in mouse and human adipose tissues

We have previously shown that PAHSAs are endogenous FAHFAs with the highest levels found in adipose tissue[1]. There exist multiple PAHSA regioisomers with 9-PAHSA being the most abundant PAHSA. Although PAHSAs are present in some foods, they can be synthesized endogenously. We explored if LAHLAs were also present in mouse adipose tissues as well. We examined subcutaneous white adipose tissue (SQWAT) of wild-type (WT) mice fed *ad libitum* for the presence of LAHLAs and observed that there were multiple LAHLA regioisomers present with 13-LAHLA being the most abundant regioisomer (**Figure 6.7a,b**). We also observed a similar finding with 13-LAHLA being the most abundant regioisomer in human white adipose tissue (**Fig 6.7c,d**). Additional studies will be needed to know whether 13-LAHLA is produced in tissues locally, but for now it is sufficient to know that 13-LAHLA can be found in mammalian tissues as a potential bioactive lipid. Because 13-LAHLA was the most abundant plasma lipid after three hours in subjects ingesting oat oil, and we could find evidence of 13-LAHLA in rodent and human adipose tissue but not 15-LAHLA, we decided to focus on 13-LAHLA since it would inform us about a bioactive lipid that is present in oat oil ***and*** in mammalian tissues.

Synthesis and characterization of 13-LAHLA

To determine if 13-LAHLA has direct effects on metabolism and inflammation, we first needed to synthesize 13-LAHLA (**Figure 6.6a**). The characteristic precursor-to-product ion transitions and the retention times were the same for the synthetic and natural 13-LAHLA indicating a structural match (**Figure 6.6b**). Using the synthetic 13-LAHLA, we validated the structure of the LAHLA isomers in oat oil and human plasma as 13-LAHLA (**Figure 6.6c**).

13-LAHLA exhibits anti-inflammatory effects *in vitro*

PAHSAs, specifically 9- and 5-PAHSA have been shown to have anti-inflammatory effects. PAHSAs have been shown to block LPS-stimulated dendritic cell activation and cytokine production[1]. In addition, these PAHSAs were protective against dextran sodium sulfate-induced colitis in mice[3]. *In vitro* data shows that PAHSAs exhibit their anti-inflammatory effects through GPR120, however, other anti-inflammatory signaling pathways may be involved[1].

Due to beneficial effects of PAHSAs, we wanted to know if LAHLAs are also bioactive which would be consistent with other FAHFAs and with our initial results with oat oil assays. We analyzed the effects of 9-PAHSA and 13-LAHLA on suppressing LPS-stimulated mRNA cytokine levels in RAW 264.7 macrophages. Both 9-PAHSA and 13-LAHLA at 10 μM significantly suppressed mRNA levels of IL-6 and IL-1β, with 13-LAHLA having a much greater effect (**Figure 6.8a,b**). In addition, 13-LAHLA (10 μM) also suppressed mRNA levels of iNOS and COX-2 in RAW 264.7 cells when co-stimulated with LPS for 20 hours (**Figure 6.8c,d**). These pro-inflammatory cytokines and downstream effectors of iNOS and COX-2 such as NO and prostaglandins, respectively, in activated macrophages play crucial roles in inflammatory diseases. We hypothesize that 13-LAHLA is interfering with the stimulatory signaling of LPS on nuclear factor kappa B (NF-κB) as this proinflammatory transcription factor modulates diverse transcriptional targets including IL-1β, IL-6, COX-2 and iNOS[14].

Synthesis of a non-hydrolyzable 13-LAHLA

To rule out the possibility that the effect of 13-LAHLA was not due to its hydrolytic products LA or 13-HLA (13-HODE), we synthesized a non-hydrolyzable 13-LAHLA derivative. We replaced the internal ester to an amide and call this compound 13-aza-LAHLA (**Figure 6.8e**). To test that 13-aza-LAHLA was protected from enzymatic hydrolysis, we performed an *in*

vitro substrate hydrolysis assay using either 13-LAHLA or 13-aza-LAHLA as a substrate for carboxyl ester lipase (CEL), our fastest reported FAHFA hydrolase (**Figure 6.8f**). 13-LAHLA was significantly hydrolyzed by CEL-transfected membrane proteome while 13-aza-LAHLA was protected from hydrolysis. We then sought to determine if changing the ester to an amide would affect activity. We tested 13-aza-LAHLA and 13-LAHLA for their ability to suppress IL-6 secretion in LPS-stimulated RAW 264.7 cells (**Figure 6.8g**). At 25 μM, 13-aza-LAHLA exhibited stronger inhibition of LPS-induced IL-6 secretion than 13-LAHLA. 9-PAHSA was used a positive control. This data shows that altering the ester to an amide of 13-LAHLA does not negatively affect its activity.

6.3 Conclusion

The presence of a DGDG-monoestolide, which contains a 15-LAHLA in its structure, led to the hypothesis that some of the biological activity of oat oil might be due to heretofore unidentified FAHFAs in the oat oil. The identification of the biologically active 13-LAHLA validated this hypothesis and revealed a novel FAHFA family with potent anti-inflammatory activity. Several questions about the mechanism of LAHLA activity remain, but our results suggest that this lipid, which is also found in mouse tissues, might have a central role in regulating cellular and physiological inflammation. Future studies should explore the regulation and role of 13-LAHLA *in vivo* as a mediator of inflammation.

6.4 Figures

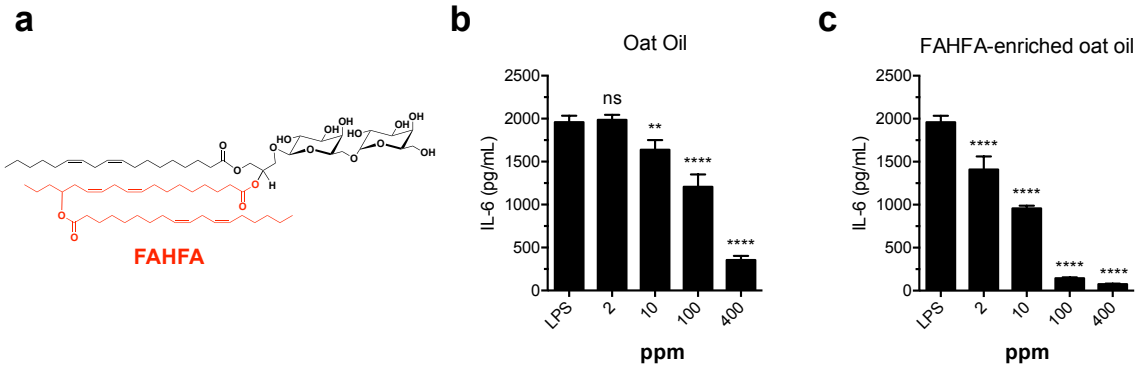

Figure 6.1. Anti-inflammatory effects of oat oil. (**a**) Structure of a highly abundant DGDG-monoestolide found in oat seed. The FAHFA moiety is highlighted in red. Oat oil (**b**) and FAHFA-enriched oat oil (**c**) effects on LPS-stimulated RAW 264.7 IL-6 secretion. 400, 100, 10, and 2 ppm of oat oil and FAHFA-enriched oat oil was co-treated with LPS for 20 hours and the media was removed for IL-6 analysis while the cells were then were tested viability. Data represents mean $\pm$ S.E.M. for three biological replicates. ****$P \leq 0.0001$; **$P \leq 0.01$; versus LPS by one-way ANOVA. ns, not significant.

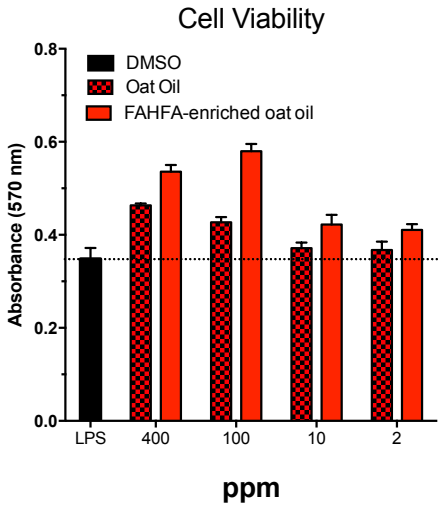

Figure 6.2. MTT cell viability assay for oat oil and FAHFA-enriched oat oil treatment. Corresponds to **Figure 6.1b,c**.

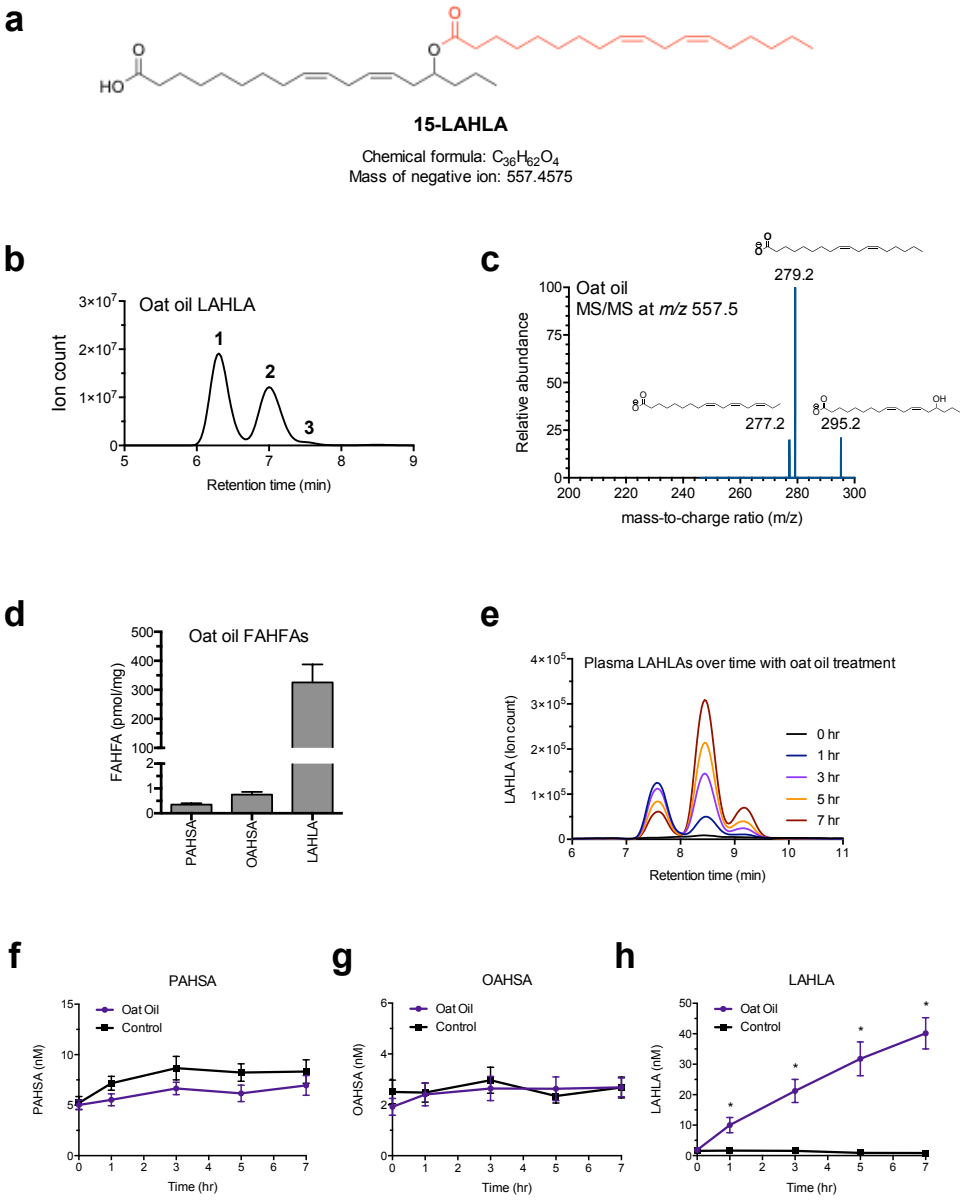

Figure 6.3. LAHLAs are present in oat oil and human plasma post-ingestion of oat oil. (**a**) Structure of 15-LAHLA showing the hydroxy linoleic acid (black) and linoleic acid (red). (**b**) MRM of LAHLAs in oil shows three peaks representing three different LAHLA regioisomers. FAHFAs were normalized to the internal standard $^{13}C_4$-9-PAHSA. Data represents mean ± S.D. (n = 2). (**c**) MS2 of expected LAHLA at *m/z* 557.5 yields three major fragments at *m/z* 279.2, *m/z* 295.2, and *m/z* 277.2. (**e**) Representative MRM chromatogram of LAHLAs in human plasma before and after ingesting oat oil. The three peaks represent three LAHLA regioisomers. (**f-h**) Levels of plasma FAHFAs in oat-oil versus control treated subjects over the time course of 7 hours. (**f**), PAHSA, palmitic acid ester of hydroxy stearic acid; (**g**) OAHSA, oleic acid ester of hydroxy stearic acid (**h**) LAHLA, linoleic acid ester of linoleic acid. Time 0 hours represents plasma FAHFAs when subjects fasted overnight. Data represents mean ± S.E.M. (n = 10-12). *$P \leq 0.05$ by two-sided Student's t-test for oat oil treated versus control treated.

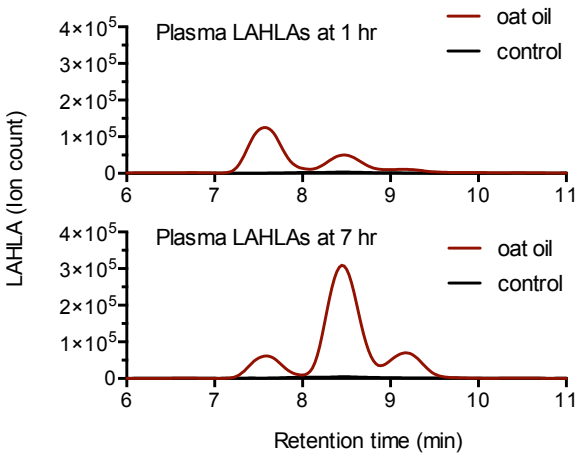

Figure 6.4. Plasma LAHLA chromatograms of oat oil treated and control treated subjects at 1 and 7 hours.

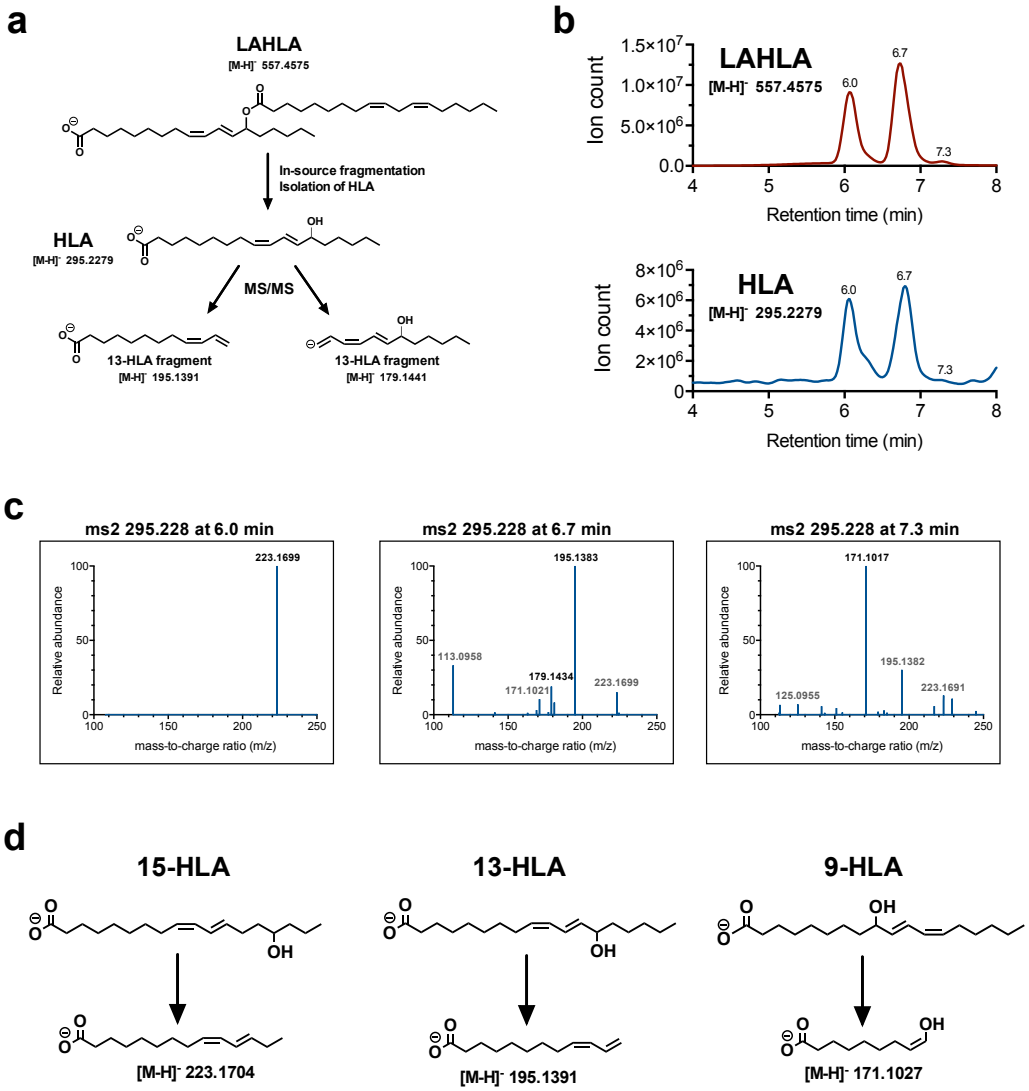

Figure 6.5. Identification of LAHLA regioisomers. (**a**) Schematic of a pseudo-MS3 approach to identify the hydroxy position of the LAHLA HLA. (**b**) Ion chromatogram of FAHFA-enriched oat oil with a source energy of 60 eV showing the presence of LAHLAs (*m/z* 557.4575) and HLA fragments from the LAHLAs (*m/z* 295.2279) which both have retention times of 6.0, 6.7 and 7.3 min. (**c**) MS2 of HLA resulting in different major fragments at 6.0, 6.7, and 7.3 min. Relative ion abundance of ions between a *m/z* 100 and a *m/z* 250 are shown. (**d**) Schematic of MS/MS fragments from 15-HLA, 13-HLA, and 9-HLA which correspond with the major fragments seen in (**c**).

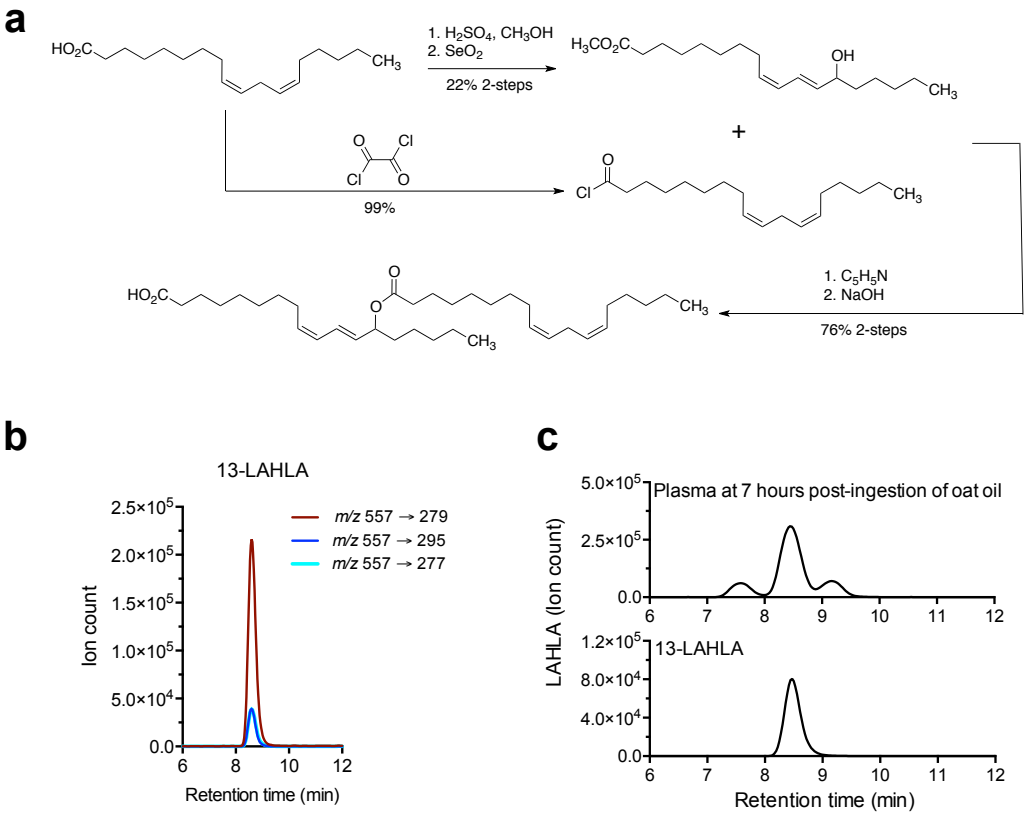

Figure 6.6. Synthesis and characterization of 13-LAHLA. (**a**) Synthesis of 13-LAHLA. (**b**) MRM of 13-LAHLA (*m/z* 557) showing relative ratios of the three LAHLA-specific transitions. (**c**) Chromatogram of LAHLA isomers in human plasma at 7 hour post-ingestion of oat oil (top trace) with 13-LAHLA (bottom trace) used as a retention time standard.

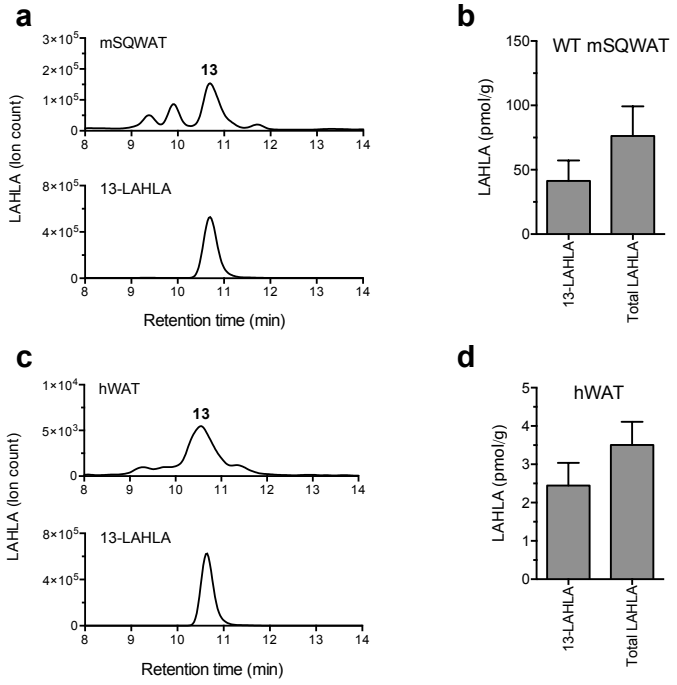

Figure 6.7. 13-LAHLA is present in mouse and human WAT. (**a**) Chromatogram of LAHLA isomers (*m/z* 557.5 → 279.5) in mouse SQWAT (top trace) with 13-LAHLA standard (bottom trace) for retention time alignment and isomer identification. (**b**) Quantification of 13-LAHLA and total LAHLA levels in mouse SQWAT. Data represents mean ± s.e.m. (n = 3). (**c**) Chromatogram of LAHLA isomers in human WAT (top trace) compared to 13-LAHLA standard (bottom trace). (**d**) Quantification of 13-LAHLA and total LAHLA in human WAT. Data represents mean ± s.e.m. (n = 3).

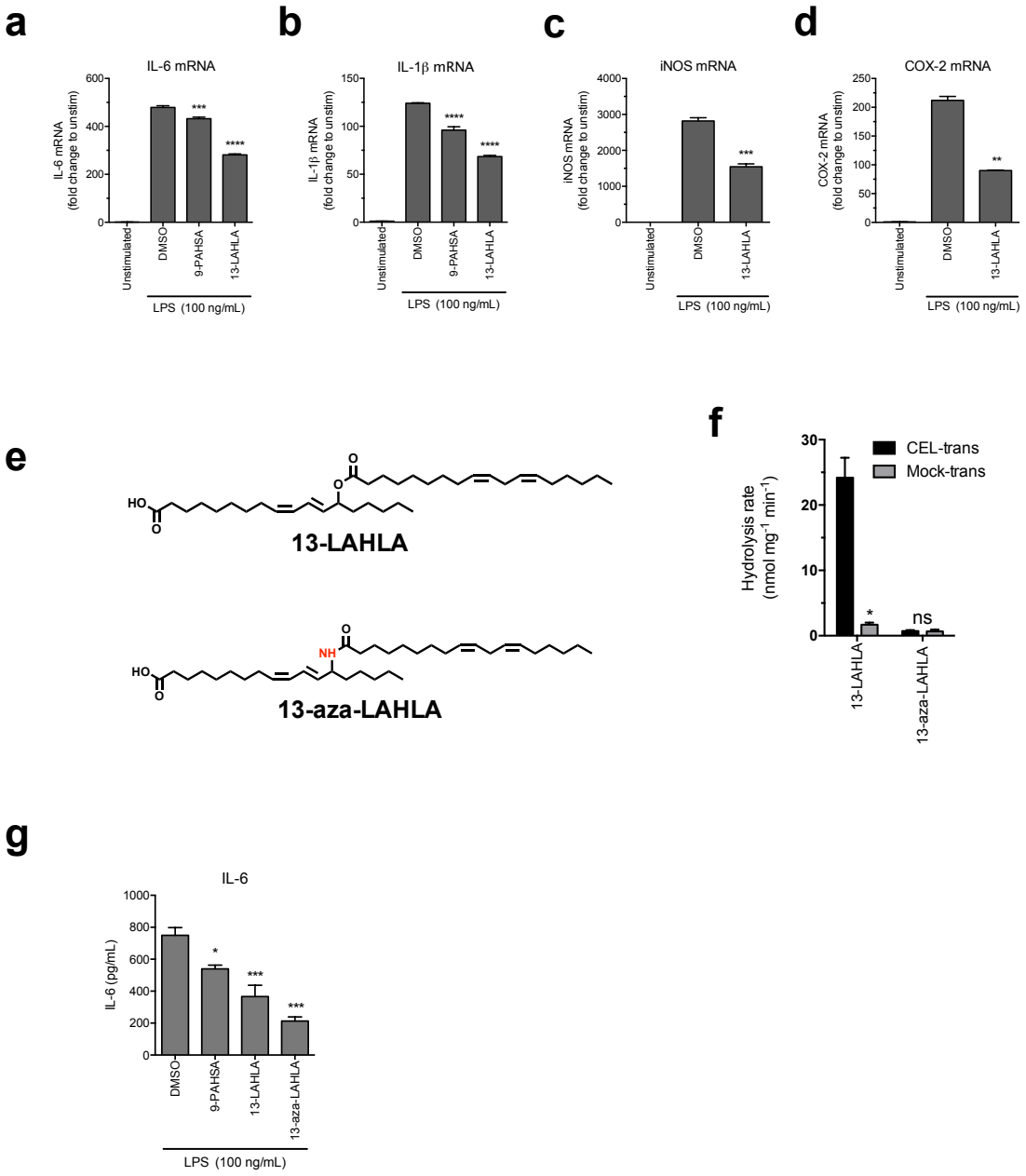

Figure 6.8. Anti-inflammatory effects of 13-LAHLA and 13-aza-LAHLA. (**a**) Effects of 9-PAHSA (10 μM) and 13-LAHLA (10 μM) on IL-6 and IL-1β mRNA levels in RAW 264.7 macrophages co-treated with LPS (100 ng/mL) for 20 hours. Data represents mean ± S.D. (n = 3-4). ***$P \leq 0.001$, ****$P \leq 0.0001$ by two-sided Student's t-test for FAHFA treated versus LPS treated alone. (**b**) Effects 13-LAHLA (10 μM) on iNOS and COX-2 mRNA levels in RAW 264.7 macrophages co-treated with LPS (100 ng/mL) for 20 hours. Data represents mean ± S.D. (n = 3-4). **$P \leq 0.01$, ***$P \leq 0.001$by two-sided Student's t-test for FAHFA treated versus LPS treated alone. (**c**) Structure of 13-LAHLA (top) and 13-aza-LAHLA (bottom) (**d**) *In vitro* substrate assay for 13-LAHLA and 13-aza-LAHLA using membrane proteomes of mock- and CEL-transfected HEK293T cells.

2.5 Experimental Section

Chemicals. 9-PAHSA was purchased from Cayman Chemical. 13-LAHLA and 13-aza-LAHLA were synthesized.

Mouse and human tissue for FAHFA measurements. Wild-type C57BL/6J mice were purchased from Jackson Laboratories. All animals were housed in groups on a 14-h light, 10-h dark schedule at the Salk. All animal care and experimental procedures were in accordance with the standing committee on the Use of Animals in Research and Teaching at Salk and Institutional Animal Care and Use Committee (IACUC), and the National Institutes of Health Guidelines for the Humane Treatment of Laboratory Animals. SQWAT was collected immediately after euthanasia and snap frozen using liquid nitrogen. Human adipose tissue from a 46 year-old African American female was purchased (BioreclamationIVT, Hicksville, NY). Human plasma samples were obtained and prepared as previously described[7]. An IRB letter of exemption for the deidentified human plasma samples used in this study is on file at the Salk Institute for Biological Sciences.

Lipid extraction and SPE. Lipid extraction of samples and solid-phase extraction was performed as previously described[10]. Briefly, WAT (150 mg) was dounce homogenized on ice in a mixture of PBS, methanol, and chloroform (1.5 mL/1.5 mL/3 mL). Five pmol of $^{13}C_4$-9-PAHSA was added to the chloroform prior to lipid extraction as an internal standard. The mixture was vortexed and then centrifuged at 2200 g for 5 min. The organic layer (bottom) was then transferred to a new vial, dried down, and then stored at -80°C for future use. The human plasma was prepared similarly, except no dounce homogenization was performed. SPE was performed at room temperature using a Strata SI-1 silica cartridge (500 mg silica, 3 mL , Phenomenex). The column was washed using 6 mL of ethyl acetate followed by column equilibration with 6 mL hexanes. The lipid extract from the prior step was then added to the equilibrated column and neutral lipids were removed using 6 mL of 95:5 hexanes:ethyl acetate

followed by the elution of FAHFAs with 4 mL ethyl acetate. This eluate was dried down and then subjected to LC-MS analysis.

Cell culture methods. RAW264.7 cells were cultured in RPMI 1640, supplemented with 10% FBS at 37 °C and 5% CO_2.

IL-6 ELISA and viability assay. RAW 264.7 cells were seeded using a 48-well plate (2.5 X 10^4 cells per well). The next day when cells were ~50% confluent, cells were co-treated with LPS (100 ng/mL) and compound (oat oil extract or FAHFA) in a total volume of 200 μL media for 20 hours at 37°C before the supernantants were collected. Secreted IL-6 was quantified using the mouse IL-6 ELISA MAX™ Deluxe Kits following the manufacturer's protocol (BioLegend). After the media was removed for IL-6 measurements, the remaining cells were assessed for their viability using the MTT assay according to the manufacturer's protocol (Calbiochem).

qT-PCR. RAW 264.7 cells (6-well plate, 60-70% confluent) were co-treated with FAHFA and LPS (100 ng/mL) or the equivalent amount of DMSO in cell media for 20 hours. Total RNA was isolated using a Purelink RNA Mini Kit (Thermo Fisher), according to the manufacturer's instructions. RNA from each replicate (2 μg) was reverse transcribed to double-stranded cDNA using the QuantiTect Reverse Transcription Kit (Qiagen). qRT-PCR was performed using a LightCycler 480 II (Roche), with SYBR Green qPCR Master Mix (Bimake). qRT-PCR reaction conditions were: 95 °C for 10 min; 35 x (95 °C for 15 s; 55 °C for 30 s; 72 °C for 30 s). The relative quantification of gene expression was calculated by using the $2^{-\Delta\Delta Ct}$ approximation method. The primers used in this study are were GAPDH, iNOS1[15], COX2[15], IL-6[6], and IL-1B[6] (IL-1B and IL-6 primer sequences were obtained through personal communication). GAPDH forward 5'-AGG TCG GTG TGA ACG GAT TTG-3', GAPDH reverse 5'-TGT AGA CCA TGT AGT TGA GGT CA-3'; COX2 forward 5'-GGA GAG ACT ATC AAG ATA GT-3', COX2 reverse: 5'-GGA GAG ACT ATC AAG ATA GT-3', iNOS forward 5'-AAT GGC AAC ATC AGG TCG GCC

ATC ACT-3', iNOS reverse 5'-GCT GTG TGT CAC AGA AGT CTC GAA CTC-3'; IL-6 forward 5'- AAC CAC GGC CTT CCC TAC TT-3', IL-6 reverse 5'- GCC ATT GCA CAA CTC TTT TCT C-3'; IL-1B forward 5'- ACC TGG GCT GTC CTG ATG AGA G-3', IL-1B reverse 5'-CCA CGG GAA AGA CAC AGG TAG C-3'.

13-LAHLA and 13-aza-LAHLA hydrolysis assay and analysis. The hydrolysis assay was performed as previously described[4,5]. Briefly, mouse CEL- or mock- transfected membrane proteomes (20 μg) from HEK293T cells were incubated with 100 μM 13-LAHLA or 13-aza-LAHLA in PBS (200 μL) at 37 °C while being shaken. After 15 minutes, the reaction was stopped by the addition of a 2:1 $CHCl_3$:MeOH mixture (400 μL). C17:1 free fatty acid (500 pmol) and 9-hydroxyheptadecanoic acid (9-HHDA, 50 pmol) was premixed with the $CHCl_3$/MeOH mixture as an internal standard. The mixture was vortexed and centrifuged at 2200g for 5 min and the bottom layer was collected and dried under a stream of nitrogen. The extract was then resolubilized in 100 μL of MeOH and 10 μL was injected onto a Q Exactive LC-MS instrument. To measure the rate of hydrolysis of 13-LAHLA and 13-aza-LAHLA, we measured free linoleic acid (*m/z* 279.23) and normalized this to the C17:1 (FFA) (*m/z* 267.23) internal standard and divided this by the amount of protein used (20 μg) and reaction time (15 min).

Targeted LC-MS analysis of FAHFAs. FAHFAs were measured on a TSQ Quantiva LC-MS instrument using multiple reaction monitoring (MRM) in negative ionization mode as previously described[10]. Resolution of FAHFAs was achieved using an Acquity UPLC BEH C18 column (1.7 μm, 2.1 mm X 100 mm, Waters) with a flow rate of 0.2 mL/min with a 93:7 (MeOH: H_2O) mobile phase with 5 mM ammonium acetate and 0.03% ammonium hydroxide. LAHLAs were analyzed by monitoring the following precursor-to-product ion transitions, *m/z* 557.5 → 279.2 and *m/z* 557.5 → 295.2, which correspond to the parent LAHLA to linoleic acid and LAHLA to hydroxy linoleic acid, respectively.

Pseudo-MS3 for analysis of LAHLA regioisomers. Oat oil (5 μL) was dissolved in 2:1 CHCl3:MeOH (400 μL) and then 5 μL was subjected to LC-MS analysis. LC separation was achieved using a Gemini 5U C-18 column (Phenomenex). Resolution of LAHLAs was achieved using using an Acquity UPLC BEH C18 column (1.7 μm, 2.1 mm X 100 mm, Waters) with a flow rate of 0.2 mL/min with a 93:7 (MeOH: H_2O) mobile phase with 5 mM ammonium acetate and 0.03% ammonium hydroxide. MS analysis was performed using a Thermo Scientific Q Exactive Plus fitted with a heated electrospray ionization source. To facilitate in-source fragmentation, the in-source CID was set to 60.0 eV. To attain MS2 data of HLA, the *m/z* of the negative HLA ion *m/z* 295.227 was added to the inclusion list to of masses to be fragmented.

6.6 References

1 Yore, M. M., Syed, I., Moraes-Vieira, P. M., Zhang, T., Herman, M. A., Homan, E. A., Patel, R. T., Lee, J., Chen, S. & Peroni, O. D. Discovery of a class of endogenous mammalian lipids with anti-diabetic and anti-inflammatory effects. *Cell* **159**, 318-332 (2014).

2 Talukdar, S., Bae, E. J., Imamura, T., Morinaga, H., Fan, W., Li, P., Lu, W. J., Watkins, S. M. & Olefsky, J. M. GPR120 is an omega-3 fatty acid receptor mediating potent anti-inflammatory and insulin-sensitizing effects. *Cell* **142**, 687-698 (2010).

3 Lee, J., Moraes-Vieira, P. M., Castoldi, A., Aryal, P., Yee, E. U., Vickers, C., Parnas, O., Donaldson, C. J., Saghatelian, A. & Kahn, B. B. Branched fatty acid esters of hydroxy fatty acids (FAHFAs) protect against colitis by regulating gut innate and adaptive immune responses. *Journal of Biological Chemistry* **291**, 22207-22217 (2016).

4 Kolar, M. J., Kamat, S. S., Parsons, W. H., Homan, E. A., Maher, T., Peroni, O. D., Syed, I., Fjeld, K., Molven, A., Kahn, B. B., Cravatt, B. F. & Saghatelian, A. Branched Fatty Acid Esters of Hydroxy Fatty Acids Are Preferred Substrates of the MODY8 Protein Carboxyl Ester Lipase. *Biochemistry* **55**, 4636-4641 (2016).

5 Parsons, W. H., Kolar, M. J., Kamat, S. S., Cognetta, A. B., 3rd, Hulce, J. J., Saez, E., Kahn, B. B., Saghatelian, A. & Cravatt, B. F. AIG1 and ADTRP are atypical integral membrane hydrolases that degrade bioactive FAHFAs. *Nat Chem Biol* **12**, 367-372 (2016).

6 Kuda, O., Brezinova, M., Rombaldova, M., Slavikova, B., Posta, M., Beier, P., Janovska, P., Veleba, J., Kopecky, J., Jr., Kudova, E., Pelikanova, T. & Kopecky, J. Docosahexaenoic Acid-Derived Fatty Acid Esters of Hydroxy Fatty Acids (FAHFAs) With Anti-inflammatory Properties. *Diabetes* **65**, 2580-2590 (2016).

7 Ohlsson, L., Rosenquist, A., Rehfeld, J. F. & Harrod, M. Postprandial effects on plasma lipids and satiety hormones from intake of liposomes made from fractionated oat oil: two randomized crossover studies. *Food Nutr Res* **58** (2014).

8 Chon, S. H., Tannahill, R., Yao, X., Southall, M. D. & Pappas, A. Keratinocyte differentiation and upregulation of ceramide synthesis induced by an oat lipid extract via the activation of PPAR pathways. *Exp Dermatol* **24**, 290-295 (2015).

9 Hamberg, M., Liepinsh, E., Otting, G. & Griffiths, W. Isolation and structure of a new galactolipid from oat seeds. *Lipids* **33**, 355-363 (1998).

10 Kolar, M. J., Nelson, A. T., Chang, T., Ertunc, M. E., Christy, M. P., Ohlsson, L., Harrod, M., Kahn, B. B., Siegel, D. & Saghatelian, A. Faster Protocol for Endogenous Fatty Acid Esters of Hydroxy Fatty Acid (FAHFA) Measurements. *Anal Chem* (2018).

11 Chen, C.-Y. O., Milbury, P. E., Collins, F. W. & Blumberg, J. B. Avenanthramides are bioavailable and have antioxidant activity in humans after acute consumption of an enriched mixture from oats. *The Journal of nutrition* **137**, 1375-1382 (2007).

12 Sur, R., Nigam, A., Grote, D., Liebel, F. & Southall, M. D. Avenanthramides, polyphenols from oats, exhibit anti-inflammatory and anti-itch activity. *Archives of dermatological research* **300**, 569 (2008).

13 Hamberg, M. & Hamberg, G. 15 (R)-Hydroxylinoleic acid, an oxylipin from oat seeds. *Phytochemistry* **42**, 729-732 (1996).

14 Baud, V. & Karin, M. Is NF-κB a good target for cancer therapy? Hopes and pitfalls. *Nature reviews Drug discovery* **8**, 33 (2009).

15 Kim, J.-B., Han, A.-R., Park, E.-Y., Kim, J.-Y., Cho, W., Lee, J., Seo, E.-K. & Lee, K.-T. Inhibition of LPS-induced iNOS, COX-2 and cytokines expression by poncirin through the NF-κB inactivation in RAW 264.7 macrophage cells. *Biological and Pharmaceutical Bulletin* **30**, 2345-2351 (2007).